LBL-19099 c.2

Lawrence Berkeley Laboratory
UNIVERSITY OF CALIFORNIA

RECEIVED
LAWRENCE
BERKELEY LABORATORY
MAR 26 1985
LIBRARY AND
DOCUMENTS SECTION

Materials & Molecular Research Division

ELECTRON ENERGY LOSS SPECTROSCOPY OF ADSORBATES ON Ni AND Cr SURFACES

A.G. Baca
(Ph.D. Thesis)

February 1985

TWO-WEEK LOAN COPY
This is a Library Circulating Copy which may be borrowed for two weeks.

LBL-19099 c.2

Prepared for the U.S. Department of Energy under Contract DE-AC03-76SF00098

DISCLAIMER

This document was prepared as an account of work sponsored by the United States Government. While this document is believed to contain correct information, neither the United States Government nor any agency thereof, nor the Regents of the University of California, nor any of their employees, makes any warranty, express or implied, or assumes any legal responsibility for the accuracy, completeness, or usefulness of any information, apparatus, product, or process disclosed, or represents that its use would not infringe privately owned rights. Reference herein to any specific commercial product, process, or service by its trade name, trademark, manufacturer, or otherwise, does not necessarily constitute or imply its endorsement, recommendation, or favoring by the United States Government or any agency thereof, or the Regents of the University of California. The views and opinions of authors expressed herein do not necessarily state or reflect those of the United States Government or any agency thereof or the Regents of the University of California.

LBL-19099

Electron Energy Loss Spectroscopy of Adsorbates on Ni and Cr Surfaces

Albert George Baca
(Ph.D. Thesis)

Materials and Molecular Research Division
Lawrence Berkeley Laboratory
and
Department of Chemistry
University of California
Berkeley, California 94720

February 1985

This work was supported by the Director, Office of Energy Research, Office of Basic Energy Sciences, Chemical Sciences Division of the U.S. Department of Energy under Contract No. DE-AC03-76SF00098.

TABLE OF CONTENTS

ABSTRACT..... vi

I. INTRODUCTION..... 1

A. Background of Surface Vibrational Spectroscopy..... 2

B. Theoretical Background..... 5

C. Properties of Ni and Cr Surfaces..... 8

References..... 12

Figure Captions..... 15

Figures..... 16

II. EXPERIMENTAL..... 18

A. The EEL Spectrometer..... 18

B. Sample Preparation and Characterization..... 20

References..... 24

Figure Captions..... 25

Figures 26

III. ADSORPTION OF H_2S ON Ni(100)..... 29

A. Introduction..... 29

B. Experimental..... 30

C. Results..... 31

1. Coverage Dependence at 110 K..... 31

2. Temperature Dependence..... 34

D. Discussion..... 35

E. Summary..... 40

References..... 41

Table..... 43

Figure Captions..... 44

Figures..... 46

IV. CH_3NH_2 ADSORPTION ON Ni(100), Ni(111), Cr(100), AND Cr(111)..... 55

A. Introduction..... 55

B. Experimental..... 56

C. Results..... 57

1. Ni Surfaces..... 57

2. Cr Surfaces..... 59

3. Other Results..... 61

D. Discussion..... 62

1. Mode Assignments and Molecular Orientation..... 62

2. Surface Composition..... 64

3. Linewidths..... 65

4. Intensity Differences..... 67

5. Comparison Between Ni and Cr Surfaces..... 70

E. Summary..... 71

References..... 72

Tables..... 76

Figure Captions..... 80

Figures..... 82

V. THE INITIAL OXIDATION OF Cr(100)..... 88

A. Introduction..... 88

B. Experimental..... 89

C. Results..... 90

D. Discussion..... 96

E. Summary..... 101

References..... 102

Figure Captions..... 104

Figures..... 106

VI. DISSOCIATIVE ADSORPTION OF CO AND O_2 ON Cr(100), Cr(110), AND Cr(111) IN THE TEMPERATURE RANGE 300-1175 K..... 112

A. Introduction..... 112

B. Experimental..... 113

C. Oxygen Adsorption..... 114

1. O/Cr(110)..... 114

2. O/Cr(111)..... 115

D. CO Adsorption..... 116

1. CO/Cr(100)..... 116

2. CO/Cr(110)..... 117

3. CO/Cr(111)..... 119

4. Comparison Between Surfaces..... 120

E. Discussion..... 120

1. Site Assignments..... 120

2. Cr(110) LEED Patterns..... 123

F. Summary..... 125

References..... 127

Table..... 129

Figure Captions..... 131

Figures..... 133

ELECTRON ENERGY LOSS SPECTROSCOPY OF ADSORBATES ON Ni AND Cr SURFACES

Albert George Baca

Materials and Molecular Research Division
Lawrence Berkeley Laboratory
and
Department of Chemistry
University of California
Berkeley, California 94720

ABSTRACT

Electron energy loss spectroscopy (EELS), a probe of the vibrations of adsorbate-covered surfaces, is a powerful tool in the determination of the chemical identity of surface species. Adsorption studies have been carried out on single crystal surfaces of Ni and Cr using EELS, low energy electron diffraction, and Auger electron spectroscopy.

H_2S adsorption has been studied on Ni(100) at temperatures between 110-295 K. At 110 K and low coverages, H_2S dissociates to S_{ads} + H_{ads}. At higher coverages two distinct molecular species, H_2S with C_{2v} symmetry and either HS or H_2S with C_s symmetry, coexist with H_{ads} and S_{ads}, and a H-Ni stretching frequency of 650 cm^{-1} suggests a 4-fold hollow site for H_{ads}. The molecular species dissociate at ~ 170 K and H_2 desorbs at 220 K.

Adsorbed CH_3NH_2 has been studied on Ni(100), Ni(111), Cr(100), and Cr(111) at 300 K. Molecular adsorption occurs on all four surfaces with bonding through the nitrogen lone pair, although a substantial amount of dissociation also occurs on the chromium surfaces. The CN stretch is anomalously broad on Ni(100) and Ni(111) but not detectably broadened on Cr(100), indicating a strong sensitivity of this

bond to interactions with the Ni surfaces. Striking EELS intensity differences are attributed partly to impact scattering and partly to intrinsic differences in the interaction of CH_3NH_2 with the different surfaces. A model explaining the linewidth and intensity differences is proposed.

Dissociative chemisorption of O_2 and CO has been characterized on Cr(100), Cr(110), and Cr(111). No evidence of molecular CO was observed on any of the surfaces studied at 300 K and above. Dissociated CO and O give very similar EEL spectra on all surfaces. Site assignments based on EELS frequencies are given. A (6x1) LEED pattern is observed after an 825 K anneal for a 0.75 L exposure of CO/Cr(110) and a model consistent with the EELS data and the LEED pattern is presented.

Based on a sequence of O_2 exposures at 300 K and after 625 K and 1175 K anneals, a model of the initial oxidation of Cr(100) is proposed. Subsurface oxygen in interstitial sites with Cr atoms maintaining bulk positions is proposed to act as a nucleus for subsequent oxide growth. Oxide growth at 300 K is proposed to occur primarily through domain expansion, while frequent creation of new domains is observed at 625 K. At elevated temperatures competition between domain growth and diffusion into the bulk is observed.

David A. Shirley

I. INTRODUCTION

The termination of a three-dimensional crystalline metal along a certain plane leaves a surface which is not the thermodynamically favored state. Such a surface, termed clean, is very reactive towards molecules if the metal is valently unsaturated. Single crystal surfaces are most commonly studied in order to limit the number and type of interactions at given sites of the surface, and in this way, to systematically study different kinds of surfaces. Understanding surfaces prepared by the interaction of clean metals with gaseous molecules under a variety of conditions has been the goal of surface scientists for more than a decade now. A great variety of surfaces has been produced. Whether one studies ordered atomic or molecular overlayers, disordered but single site overlayers, or mixtures of surface species depends in large part on the experimental techniques available. The methods used in carrying out this work are ideally suited to the latter types of studies.

The emphasis of this thesis will be the determination of the chemical identity of surface species which form as a result of the interaction of a known quantity of gas molecules with clean well-ordered transition metal surfaces. High resolution electron energy loss spectroscopy (EELS) is used in conjunction with low energy electron diffraction (LEED) and Auger electron spectroscopy. EELS allows one to determine the vibrational spectra of adsorbates in the surface layer. These spectra, when interpreted by methods described in this chapter, can be used to identify surface species, give

qualitative information about their orientation, and determine adsorption sites in favorable cases.

A. BACKGROUND OF SURFACE VIBRATIONAL SPECTROSCOPY

Among the many techniques available for the study of molecules on surfaces, vibrational spectroscopy is one of the most powerful. Vibrational spectroscopy has been used to study gas, liquid, and condensed phase samples for more than half a century now. Each molecule has a unique vibrational spectrum and a wide body of information is available for comparison with surface species. This makes the chemical identification of surface species very straightforward. Perhaps most importantly, vibrational frequencies in molecules of interest are generally well separated from those of substrates of interest, and the surface signal can be easily isolated. The majority of surface vibrational studies have been carried out using infrared spectroscopy (IRS) and EELS, separately described below.

Surface spectroscopic methods must be sensitive to the small quantity of adsorbates on surfaces relative to the large amount of substrate. The first vibrational experiments on surfaces were carried out using IRS to study CO adsorbed on silica-supported transition metals.[1] Transmission IRS was used and high surface area materials were necessary to detect the surface signal. There have been a number of improvements made in the last two decades to make IRS more surface sensitive and capable of studying adsorption on single crystal

surfaces. Greenler showed that at grazing incidence, infrared reflection absorption spectroscopy (IRRAS) is more than an order of magnitude more surface sensitive than conventional IRS.[2] Even in IRRAS, only a very small percentage of photons are absorbed, and they are detected by measuring a small change in the reflected beam. Recent improvements in the experimental technique enhance this small signal and have allowed the study of submonolayer quantities of adsorbed molecules. These improvements include some combination of the use of Fourier Transform IR (FTIR) spectroscopy, polarization modulation, and wavelength modulation.[3-10] More recently the techniques of direct IR absorption by measuring the temperature rise of absorbing surfaces[11] and IR emission[12] have shown success.

In spite of these improvements in sensitivity, the vast majority of surface IR studies continue to focus on simple, highly absorbing molecules such as CO. The high resolution of IRS ($\leqslant 5\ cm^{-1}$) allows the study of vibrational lifetimes[7] and dipole-dipole coupling in CO molecules,[3] as discerned by spectra of mixtures of ^{12}CO and ^{13}CO, which at present cannot be studied by EELS. The principal drawbacks of IRS are the lack of sensitivity compared to EELS ano the difficulty in scanning the entire spectral region at once.

The idea of using the electron as a probe of surface vibrational structure is very appealing because its strong interactions with matter insure that it is sensitive primarily to the first few atomic layers of the surface. In the EELS experiment, incident electrons may interact with the sample and lose energy to a molecular vibrational

mode. The electrons that are scattered away from the sample and reach the detector are energy analyzed. Typically 1-5 scattered electrons in a thousand lose a small fraction of their energy to a vibrational mode. Two conditions must be fulfilled in order to have a successful experiment. First, the resolution of the electron energy analyzer must be great enough to measure small energy losses and closely spaced vibrational peaks. Second, the background of imperfectly analyzed elastically (no energy loss) scattered electrons must be kept low enough that the inelastically scattered electrons are not obscured.

The initial application of EELS at surfaces dates to Propst and Piper in 1967,[13] and a resolution of ~ 200 cm^{-1} was employed. Improvements in the design of Ibach and coworkers[14] brought the resolution down to ~ 80 cm^{-1} where it reached a plateau for a number of years. Recently, a number of groups[15-22] have built spectrometers with a resolution of 30-50 cm^{-1}. This resolution is still almost a factor of ten worse than what has been attained by surface IR. However, many vibrational modes are broadened beyond 30-50 cm^{-1} (see Chapters IV-VI), and even this resolution is very useful.

The principal advantages of EELS are the ease in scanning the entire spectral range from ~ 300-4000 cm^{-1} and the high surface sensitivity to even moderately weak oscillators (see Chapters III and IV). To date, EELS has proven to be particularly useful in studying the adsorption of larger molecules, the observation of intermediates to decomposition reactions (often identified in the presence of other

surface species), and in studying the interaction between co-adsorbed atoms or molecules.

Other vibrational spectroscopies used at present play only a minor role, although some of them show promise of becoming important techniques. Inelastic tunneling spectroscopy[23] attains a resolution intermediate to IRS and EELS, but is limited to studies at surfaces interfacing a metal and a thin metal oxide. Surface enhanced Raman spectroscopy[24] offers a high sensitivity and resolution but is limited to atomically roughened surfaces. Recently, surface Raman spectroscopy without enhancement has been reported for submonolayer coverages by using optical multichannel detection.[25] Raman spectroscopy has different selection rules than either IRS or EELS and would offer complementary information. Other techniques that show promise are inelastic atom scattering[26] and surface photoacoustic spectroscopy.[27]

B. THEORETICAL BACKGROUND

The purpose of this section is to present some results from the theory of EELS which are referred to in the interpretation of data in Chapters III-VI. The complete theory is quite involved and has been treated by Ibach and Mills.[28] As most chemists and physicists are more familiar with infrared spectroscopy, frequent comparisons and similarities to IRS will be pointed out.

There are two types of scattering mechanisms in EELS. The first is a long range mechanism in which the oscillating electric field

produced by surface vibrations interacts with the incident electron. This is known as dipole scattering since the dipole fields of the surface oscillations are able to interact at long range. The theory was mainly developed by Mills and coworkers[29-31] and was further refined in Ibach and Mills.[28] A semiclassical approach was found sufficient to explain the essential features of dipole scattering. The Schroedinger equation was solved by the methods of perturbation theory for the differential scattering cross section, $d^2S/d\Omega(\hat{k}_s)d\hbar\omega$, where the oscillating electrostatic potential used in the Schroedinger equation was derived by classical methods, i.e., by neglecting the microscopic structure of the surface. The model of the surface used is illustrated in Fig. 1. For the typical case where $\hbar\omega << E_i$ the following result was obtained.

$$\frac{d^2S}{d\Omega(\hat{k}_s)d\hbar\omega} \quad \frac{|R_i|^2}{k_i E_i \cos\theta_i} \times \frac{1}{[(\theta_i-\theta_s)^2 + (\hbar\omega/2E_i)^2]^2} \tag{1}$$

where k_i is the magnitude of the incident electron's wavevector, E_i is the incident energy, θ_i the angle of incidence from the normal, and $|R_i|^2$ is the reflection coefficient of the elastically scattered electron. The proportionality factor includes other more complex geometric factors and a factor including the transition probability.

Several important points should be noted in expression (1). The inelastic scattering cross section is proportional to the elastically scattered intensity. Smaller impact energies (as long as E_i remains

large compared to $\hbar\omega$) and angles close to grazing incidence are favored. Finally and most importantly, scattering is sharply peaked in the specular direction, $\theta_s \sim \theta_i$.

Impact scattering is a generic term which includes any mechanism that is not the long range dipole scattering. This could include negative ion resonances such as those observed in the gas phase, or scattering from the higher multipole fields generated during the vibration. The first process has been observed on surfaces for physisorbed samples at low temperatures.[32] The angular distribution in impact scattering is practically flat compared to dipole scattering.[33]

The selection rules for dipole scattering in EELS from metal surfaces are the same as for IRS; vibrations which produce a change in dipole moment normal to the surface can be observed. This comes about because of the long range nature of the process. As seen in Fig. 2, the parallel dipoles are screened by the image charges generated in the metal surface. For atoms and simple molecules, such as those in Chapters III, V, and VI, application of the selection rule is straightforward. The normal modes are easily enumerated and separated into parallel and nonparallel vibrations. For more complex molecules, another variation of the selection rule which involves the application of group theory is more convenient.

The transition matrix element in dipole scattering is

$$\langle f|\mu_z|i\rangle \qquad (2)$$

where μ_z is the dipole moment perpendicular to the surface. The initial vibrational state always belongs to the totally symmetric representation. The product of the final vibrational state (the v=1 state has the symmetry of the normal mode) and μ_z must contain the totally symmetric representation for the matrix element to be nonzero. The possible symmetries on a surface are strongly affected by the symmetry breaking discontinuity of the surface-vacuum interface. Ibach and Mills have shown that for the symmetry point groups possible on surfaces, μ_z belongs to the totally symmetric representation for every case.[28] This provides another equivalent manifestation of the surface selection rule. Only the totally symmetric normal modes will be active in dipole scattering. For the analysis of the data in Chapter IV, the group theoretical approach was found to be more useful.

In impact scattering, non-totally symmetric vibrations can be observed both in the specular direction and away from it. By making both specular and non-specular EELS measurements, one can identify the totally symmetric vibrations and learn something about the molecular orientation. In IRS only the totally symmetric modes are observed and information about the orientation is also obtained.

C. PROPERTIES OF Ni AND Cr SURFACES

The primary emphasis of this thesis has been to choose interesting systems that can be addressed by vibrational spectroscopy. A definitive comparison between Ni and Cr surfaces is not my intent, but

a meaningful comparison does result because the same molecule has been studied on a number of different surfaces of the same metal for O_2, CO (by other workers on the Ni surfaces), and CH_3NH_2 adsorption. Some of the properties of the two metals are summarized below.

Nickel surfaces are among the most widely studied because of their technological importance. The Fisher-Tropsch reaction (hydrogenation of CO over metal catalysts) uses Ni as a catalyst. The importance of Ni as a catalyst stems from the fact that its surfaces are reactive but not indiscriminately so. Both CO and NH_3 adsorb molecularly up to their desorption temperatures on Ni surfaces.[34-37] The CO bond can be weakened on Ni surfaces by the presence of coadsorbed alkali atoms.[38]

The desorption temperature of NH_3 can be raised and azimuthal ordering can be induced by coadsorbed O.[34] Hydrocarbons tend to adsorb molecularly at liquid nitrogen temperatures and decompose at varying temperatures above and below room temperature.[39] Most of the reactive and dissociative behavior of the above compounds occurs above room temperature and many possibilities exist for surface modifications to produce <u>selective</u> chemistry on Ni surfaces.

Chromium metal is thought to derive its technological importance from the extreme stability of its oxide and its ability to resist corrosion. Almost no molecular adsorption studies have been carried out on Cr surfaces, and Cr is used much less in catalysis than Ni. I suspect that this is because of the reputation Cr has for being extremely and indiscriminately reactive. This reputation is primarily

due to the greater reactivity of the group V-VII transition metals toward CO and NH_3, as very little other adsorption studies have been carried out on these metals.

This thesis presents a first attempt to characterize molecular adsorption on Cr surfaces. This is done for CO and O_2 adsorption (Chapters V and VI) and compared to previously published work on Ni surfaces. A comparison of the adsorption of CH_3NH_2 on Ni and Cr surfaces is presented in Chapter IV. Five structurally different surfaces have been chosen, three Cr surfaces and two Ni surfaces. Adsorption on structurally different surfaces of the same metal allow one to determine similarities intrinsic to a metal and make a comparison between different metals more meaningful.

The rest of this thesis is organized as follows. In Chapter II, the experimental procedures are given, and a high resolution EEL spectrometer, crucial to the success of this thesis, is described. In Chapter III, the system H_2S/Ni(100) is investigated between 110 K and 295 K. It is at the same time a model system in which a dissociative reaction can be completely observed and a system of potential technological importance. In Chapter IV, the study of CH_3NH_2 on four surfaces of Ni and Cr attempts to bridge the gap between lone pair donors and hydrocarbon molecules. Interesting intensity variations and linewidth differences are explained by a model of adsorption. In Chapters V-VI, the dissociative adsorption of CO and O_2 on three surfaces of Cr is presented. The mechanism of the oxidation of Cr(100) (Chapter V) is uncovered and presented in

more detail than previously known. The most meaningful comparison between Ni and Cr surfaces results from the material in Chapters IV and VI.

REFERENCES

1. R.P. Eischens, W.A. Pliskin, and S.A. Francis, J. Chem. Phys. 22, 1786 (1954).

2. R.G. Greenler, J. Chem. Phys. 44, 310 (1966).

3. A. Crossley and D.A. King, Surf. Sci. 68, 528 (1977).

4. M.D. Baker and M.A. Chesters, in Vibrations at Surfaces, ed. R. Caudano et al., (Plenum Press, New York, 1982).

5. H. Pfnür, D. Menzel, F.M. Hoffmann, A. Ortega, and A.M. Bradshaw, Surf. Sci. 93, 431 (1980); A. Ortega, F.M. Hoffmann, and A.M. Bradshaw, Surf. Sci. 119, 73 (1982).

6. W.G. Golden, D.S. Dunn, and J. Overend, J. Catal. 71, 395 (1981).

7. R. Ryberg in Vibrations at Surfaces, ed. R. Caudano et al., (Plenum Press, New York, 1982).

8. P. Hollins and J. Pritchard, in Vibrational Spectroscopy of Adsorbates, ed. R.F. Willis, (Springer, New York, 1981).

9. J.C. Campuzano and R.G. Greenler, Surf. Sci. 83, 301 (1979).

10. M. Kawai, T. Onishi, and K. Tamaru, Appl. Surf. Sci. 8, 361 (1981).

11. R.B. Bailey, T. Iri, and P.L. Richards, Surf. Sci. 100, 626 (1980).

12. S. Chiang, R.G. Tobin, and P.L. Richards, Proceedings of the 1982 third International Conference on Vibrations at Surfaces, J. Electron Spectrosc. Related Ph. 29, 113 (1983).

13. F.M. Propst and T.C. Piper, J. Vac. Sci. Technol. 4, 53 (1967).

14. H. Froitzheim, H. Ibach, and S. Lehwald, Rev. Sci. Instr. 46,

1325 (1975).

15. H. Ibach and D. Bruchmann, Phys. Rev. Lett. 44, 36 (1980).

16. S. Andersson and P.-A. Karlsson, and M. Persson, Phys. Rev. Lett. 51, 2378 (1983).

17. L.L. Kesmodel, J. Vac. Sci. Technol. A 1, 1456 (1983).

18. J.E. Demuth, K. Christmann, and P.N. Sanda, Chem. Phys. Lett. 76, 196 (1980).

19. C. Nyberg and C.G. Tengstal, Proceedings of the 1982 third International Conference on Vibrations at Surfaces, J. Electron Spectrosc. Related Ph. 29, 191 (1983).

20. P.A. Thiry, J. Ghijsen, J.J. Pireaux, and R. Caudano, ibid., p. 193.

21. N.R. Avery, A.B. Anton, B.H. Toby, and W.H. Weinberg, ibid., p. 233.

22. B.E. Koel and G.A. Somorjai, ibid., p. 287.

23. T. Wolfram, ed., Inelastic Electron Tunneling Spectroscopy (Springer-Verlag, New York, 1978).

24. R.K. Chang and T.E. Furtak, eds., Surface Enhanced Raman Scattering (Plenum, New York, 1982).

25. A. Campion, J.K. Brown, and V.M. Grizzle, Surf. Sci. 115, L153 (1982).

26. G. Brusdeylins, R.B. Doak, and J.P. Toennis, Phys. Rev. Lett. 44, 1417 (1980).

27. F. Träger, T.J. Chuang, and H. Coufal, Proceedings of the 1982 third International Conference on Vibrations at Surfaces, J.

Electron Spectrosc. Related Ph. 30, 19 (1983).

28. H. Ibach and D.L. Mills, Electron Energy Loss Spectroscopy and Surface Vibrations (Academic Press, New York, 1982).

29. V. Roundy and D.L. Mills, Phys. Rev. B 5, 1347 (1972).

30. E. Evans and D.L. Mills, Phys. Rev. B 5, 4126 (1972); ibid. 7, 853 (1973).

31. D.L. Mills, Surf. Sci. 48, 59 (1975).

32. J.E. Demuth, D. Schmeisser, and Ph. Avouris, Phys. Rev. Lett. 47, 1166 (1981).

33. W. Ho, R.F. Willis, and E.W. Plummer, Phys. Rev. Lett. 40, 1463, (1978).

34. F.P. Netzer and T.E. Madey, Surf. Sci. 119, 422 (1982).

35. G.B. Fisher and G.E. Mitchell, Proceedings of the 1982 third International Conference on Vibrations at Surfaces, J. Electron Spectrosc. Related Ph. 29, 253 (1983).

36. E.G. Keim, F. Labohm, O.L.J. Gijzeman, G.A. Bootsma, and J.W. Geus, Surf. Sci. 112, 52 (1981) and references therein.

37. Z. Murayama, I. Kojima, E. Miyazaki, and I. Yasumori, Surf. Sci. 118, L281 (1982).

38. M.P. Kiskinova, Surf. Sci. 111, 584 (1981).

39. S. Lehwald and H. Ibach, Surf. Sci. 89, 425 (1979).

FIGURE CAPTIONS

Figure 1. The model of the surface used for a semiclassical calculation of dipole scattering (see ref. 28, Chapter 3).

Figure 2. A dipole above a classical conductor is reinforced by its image for a perpendicular orientation and screened by its image for a parallel orientation.

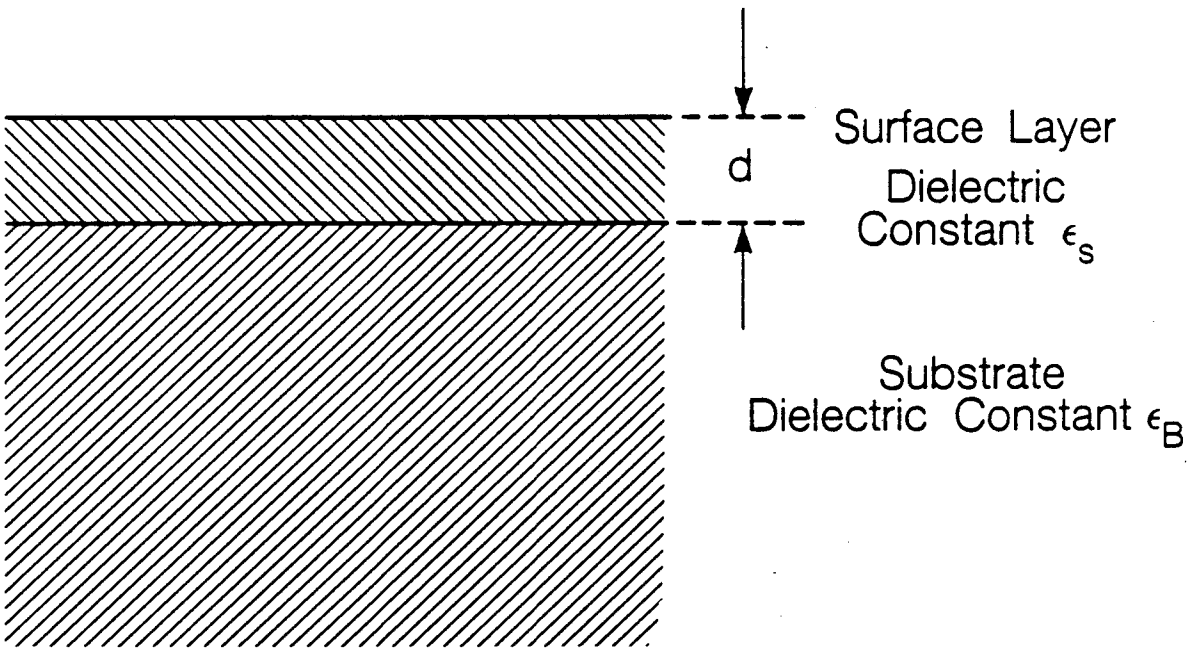

XBL 851-768

Figure 1

IMAGE MODEL

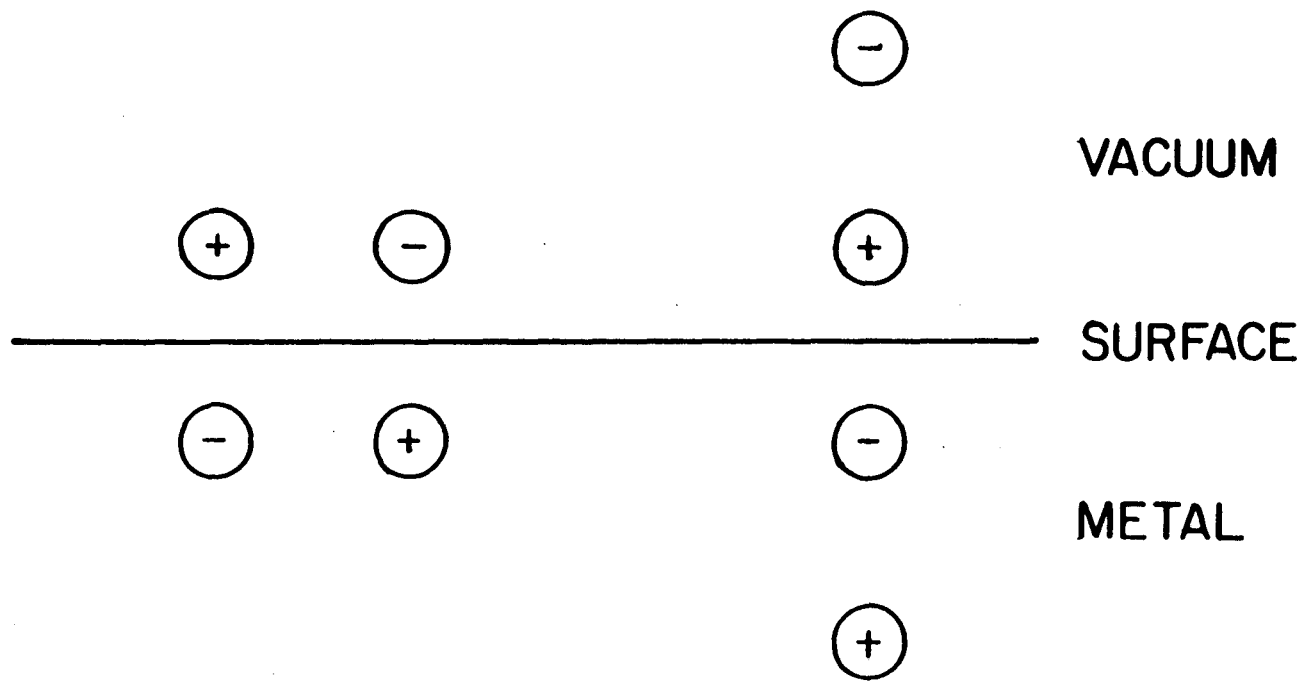

XBL 812-8138

Figure 2

II EXPERIMENTAL

The experimental aspects of this thesis will be described in this chapter. LEED, Auger, and EELS measurements have all been necessary to produce the material presented in the following chapters, but the EELS measurements have provided the most novel results. The EEL spectrometer has been previously documented[1] and will be briefly described in section A, while methods of sample preparation common to all of the work presented in this thesis will be described in section B. Additional, specific experimental details can be found in each chapter.

A. THE EEL SPECTROMETER

As a historical note, the EELS project was initiated by Danny Rosenblatt before I joined the group in 1979. The project turned out to be of such magnitude that I was able to participate in many aspects of design, assembly, and testing before the project was complete in the fall of 1982. All aspects of the design and performance of the spectrometer have been documented in Rosenblatt's thesis,[1] and only those aspects necessary for an understanding of the experiment will be described here.

A schematic of the experimental geometry is shown in Fig. 1. The monoenergetic source of electrons, known as the "electron monochromator", is detailed in Fig. 2. It consists of a hairpin tungsten filament, a three element asymmetric lens which focuses electrons produced by the filament onto the entrance aperture of the pre-

monochromator, two sets of hemispherical dispersing elements, entrance and exit slits or apertures, and a three element asymmetric "zoom" lens which transports electrons from the exit slit of the monochromator and focuses them onto the sample. The purpose of the electron monochromator is to produce a monoenergetic beam of electrons which is low in background of stray electrons. The latter requirement is important because typically one in one thousand or less electrons lose energy to vibrational modes and the spectrometer background must be lower than that, especially near the elastic peak. The use of two sets of hemispheres serves to reduce the spectrometer background, as the large number of electrons with the wrong energy which are rejected by the premonochromator are not likely to traverse the monochromator. The reason for choosing hemispheres as the electrostatic dispersing elements over the more popular cylindrical devices is because of the 2x greater theoretical resolution of hemispheres,[2-4] although no claims as to the superiority of one spectrometer design or the other are made here. A comparison between these two types of spectrometers is made elsewhere.[1,5]

Monoenergetic electrons incident on the sample can interact with vibrational modes through any of the mechanisms described in Chapter I and be scattered into the electron energy analyzer, shown in Fig. 3. The analyzer operates in an analagous manner as the monochromator. A three element asymmetric zoom lens focuses electrons onto the analyzer entrance slit. The angular acceptance is physically limited to $\pm 7^{\circ}$ but is usually much less because of the laws of electron optics.[3]

Electrons passing through the hemispheres of the analyzer are energy analyzed by electrostatic deflection. Electrons with the correct energy pass through the exit slit and are detected with a spiraltron electron multiplier using pulse counting methods. Count rates of the elastic peak varied between 5-500 KHz, depending on the state of the sample. The instrumental resolution, customarily defined as the full width at half maximum (FWHM) of the elastic peak, ranged between 40-55 cm^{-1} for all experiments.

In order to use the selection rules of EELS described in Chapter I, either the sample, the monochromator, or the analyzer must be rotatable. In this spectrometer, both the sample and the analyzer are rotatable, allowing the freedom of independently varying the angles of incidence and detection. Other parameters such as the electron impact (incident) energies and angles of incidence are for the most part chosen to maximize the count rate and are reported with the data.

Finally, a highly stable, low noise power supply[6] provides voltages for all the electron optic elements and the spectrometer is computer controlled.

B. SAMPLE PREPARATION AND CHARACTERIZATION

Of interest are the means for producing an ultra high vacuum (UHV) and the techniques for characterizing a sample. The chamber is pumped by a 220 l/s triode ion pump, a titanium sublimation pump, and a liquid helium-cooled cryopump (Air Products). A base pressure of $\sim 1.5\times10^{-10}$ Torr can be reached after a bakeout to 475 K.

The samples used in this thesis come from high purity stock of single crystalline Ni and Cr. The crystals were oriented and cut to within 1° of a desired plane, polished, and etched by standard methods.[7,8] The crystals were then ready to be cleaned by means of UHV techniques.

Both Ni and Cr crystals were pre-cleaned in a similar way to rid them of bulk impurities. Ar ion sputtering with ~ $5x10^{-5}$ Torr of Ar was carried out while a crystal was cycled between temperatures of 300 K and 1075 K for Ni (1175 K for Cr). Approximately three weeks of this treatment were required for the Cr crystals and somewhat less time for the Ni crystals. The main impurities were found to be C, N, and O in the case of Cr, while S and C were the principal contaminants of bulk Ni. Once the crystals were sufficiently pre-cleaned, only brief periods (2-4 hours) of Ar ion sputtering were required to return the crystals to a state of cleanliness after an experiment. Slight variations of the cleaning procedure pertinent to individual experiments are described in the appropriate chapters. The liquid helium-cooled cryopump, a recent addition to the chamber, was found to be most useful in returning the vacuum chamber quickly to its base pressure after a brief period of sputtering, thus minimizing contamination of the freshly cleaned sample.

LEED and Auger were used to characterize the clean surfaces as well as provide supplementary information to EELS measurements. The observation of diffraction spots verifies that the correct single crystalline surface has been prepared. An Auger spectrum indicates

whether impurities on the clean surface are below acceptable limits. Both LEED and Auger measurements were made using a retarding field analyzer (RFA or LEED optics). The sensitivity of such a system for Auger is not as great as that of a cylindrical mirror analyzer, and impurity levels must be kept below detectable limits of the RFA in order to assure oneself of a clean surface. The cleanliness of the surface was verified in most instances with an EEL spectrum. LEED was also used to characterize the interesting overlayer structures observed in Chapters V-VI, while Auger was used to quantify the atomic constituents of interesting adlayers and was especially useful for studying the oxidation of Cr(100). Both LEED and Auger are potentially destructive of molecular adsorbates and all measurements were made after EEL spectra were collected.

Exposure of the single crystalline metal surfaces to the adsorbate gas was made by both ambient dosing and effusive beam dosing. With ambient dosing, exposures are reported in langmuirs (L: 1 L = 1×10^{-6} Torr-sec). For effusive beam dosing, a calibration in langmuirs was often desirable in order to make a comparison with the results of other workers. This was possible because the stability of the sample manipulator (Vacuum Generators) was great enough that reproducible distances to the beam doser were obtained. A calibration with Auger was then used if deemed desirable. If not, an arbitrary relative scale of exposures was used. Sample heating was carried out by resistive heating of the sample plate in some experiments and electron beam heating in others. Liquid nitrogen cooling (with modified Vacuum

Generators coils) was used when sample temperatures below 300 K were needed.

REFERENCES

1. D.H. Rosenblatt, Ph.D. thesis, University of California, Berkeley, 1982 (LBL-14774, unpublished).
2. D. Roy, A. Delage, and J.D. Carette, J. Phys. E 8, 109 (1975).
3. C.E. Kuyatt and J.A. Simpson, Rev. Sci. Instrum. 38, 103 (1967).
4. S. Lehwald, H. Ibach, and H. Steininger, Surf. Sci. 117, 342 (1982).
5. D. Roy and J.D. Carette, in Electron Spectroscopy for Surface Analysis, edited by H. Ibach, (Springer-Verlag, New York, 1977).
6. J.E. Katz, P.W. Davies, J.E. Crowell, and G.A. Somorjai, Rev. Sci. Instrum. 53, 785 (1982).
7. S.D. Kevan, Ph.D. thesis, University of California, Berkeley, 1982 (LBL-11017, unpublished).
8. R.F. Davis, Ph.D. thesis, University of California, Berkeley, 1982 (LBL-13511, unpublished).

FIGURE CAPTIONS

Figure 1. A schematic of the experimental geometry. A beam of monoenergetic electrons is incident upon the sample. Those electrons that are scattered from the sample are energy analyzed. Angles of incidence and scattering, θ_i and θ_s, are measured with respect to the surface normal. $\theta_i = \theta_s$ defines the specular direction.

Figure 2. A cross-sectional illustration of the electron monochromator.

Figure 3. A cross-sectional illustration of the electron energy analyzer.

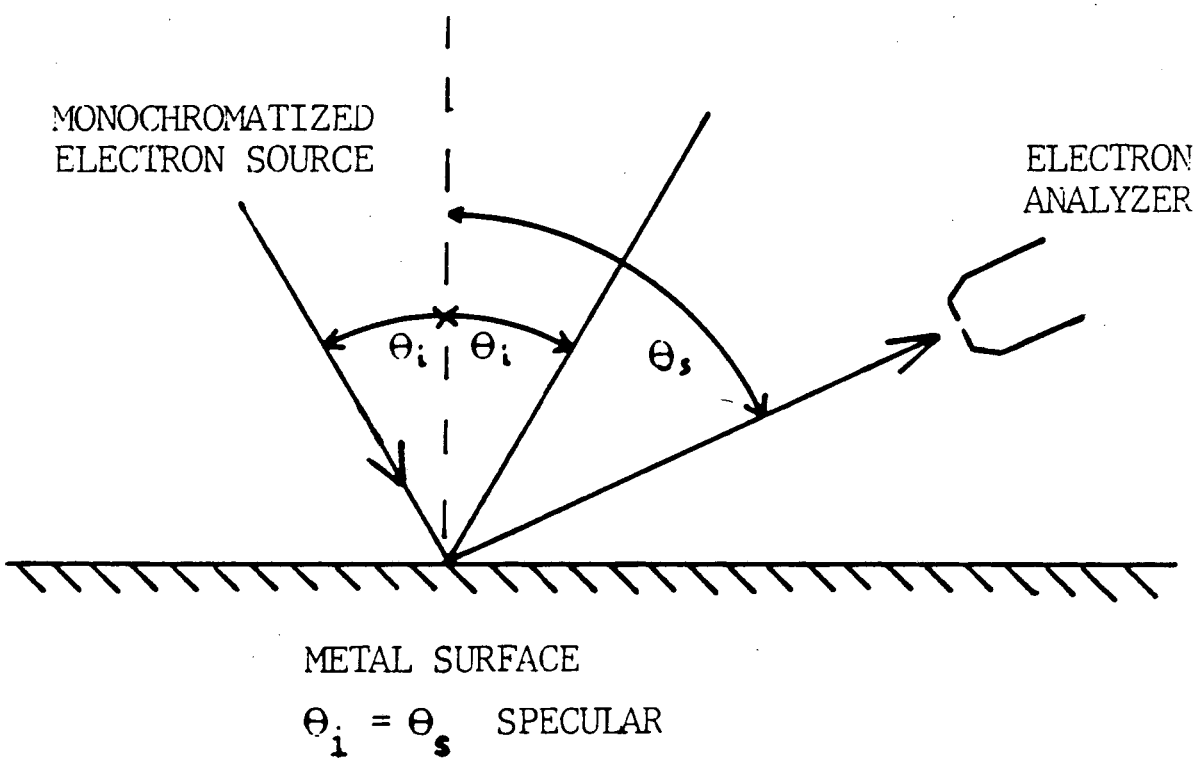

XBL 812-8140

Figure 1

EELS ELECTRON MONOCHROMATOR

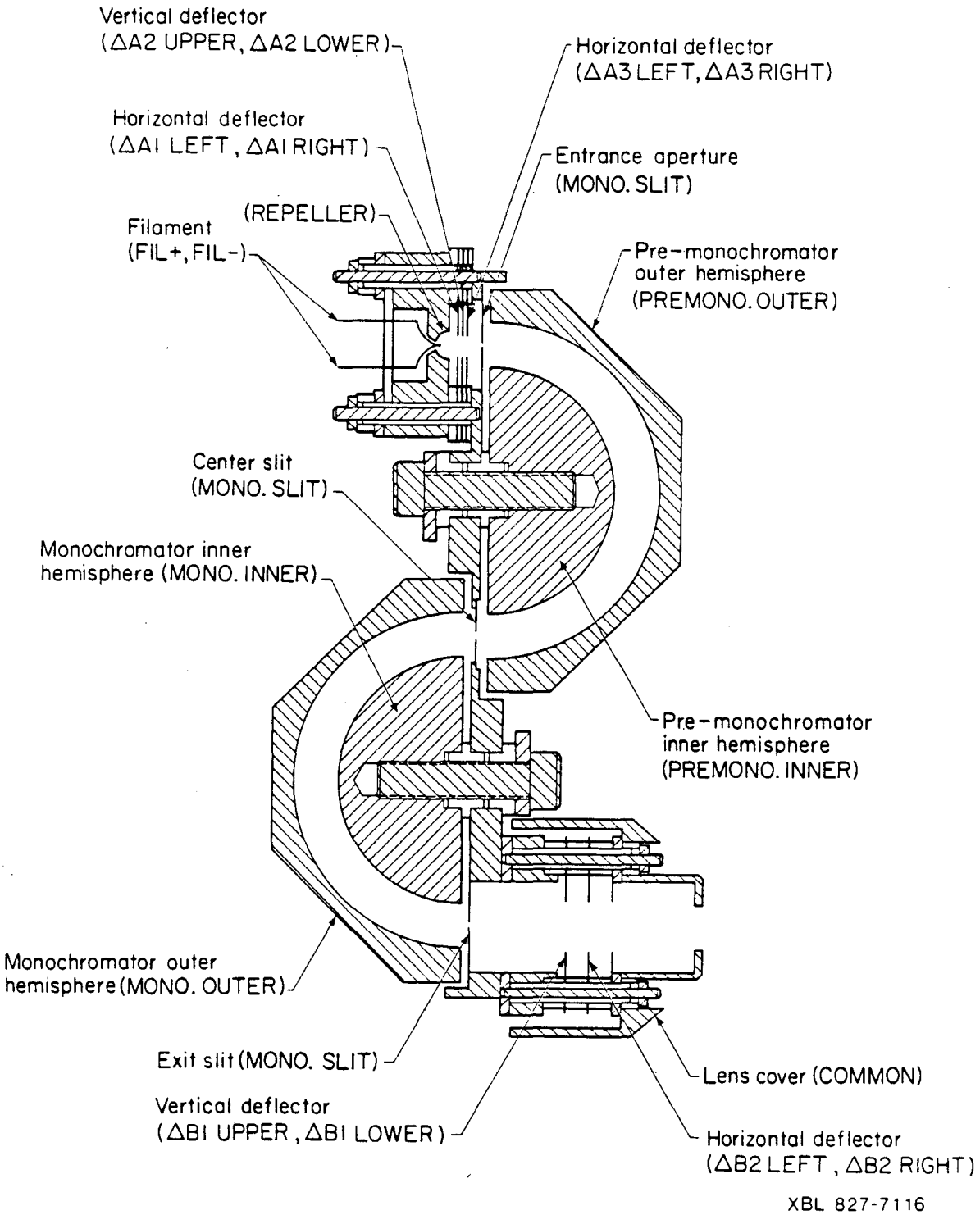

Figure 2

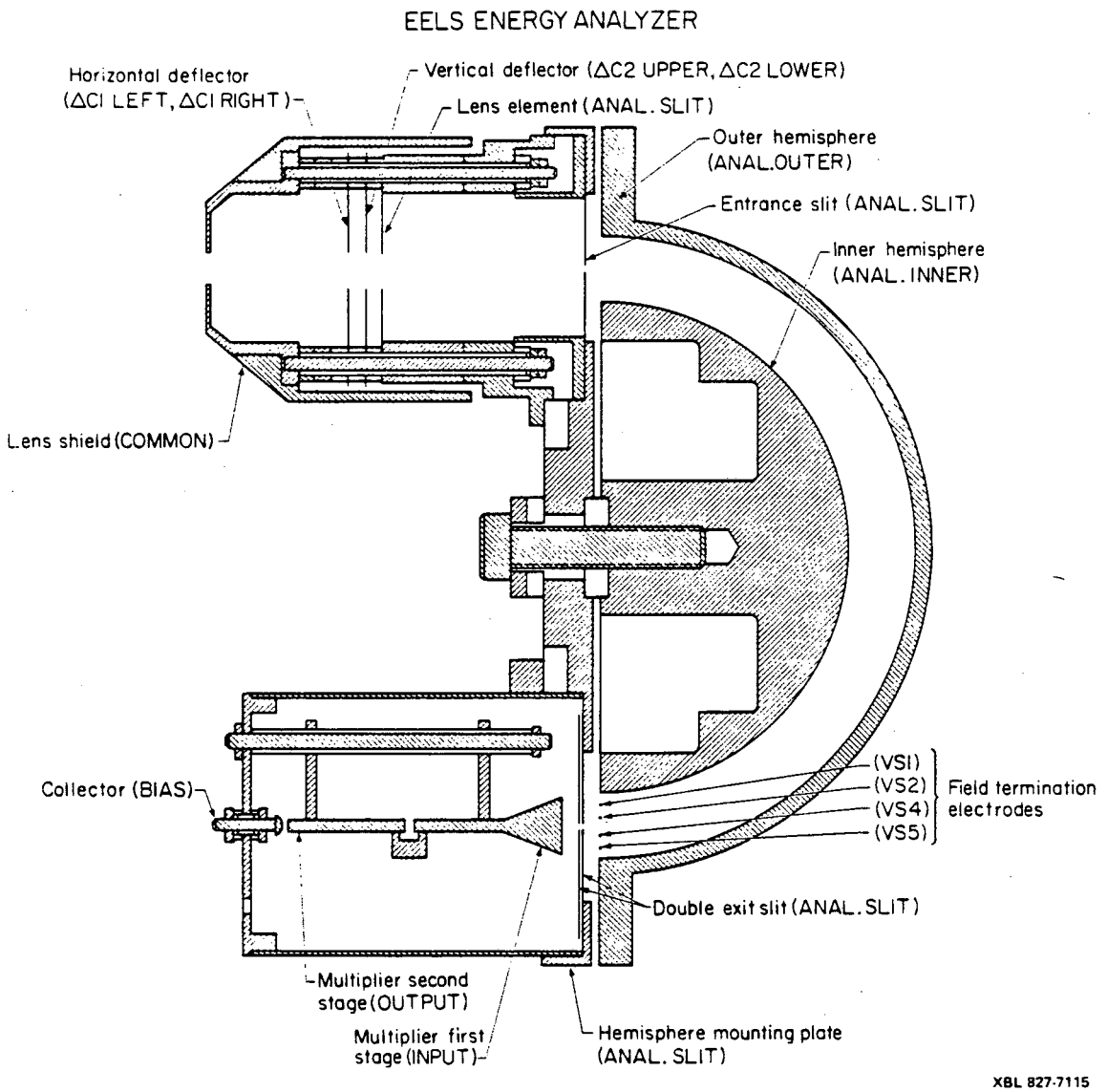
EELS ENERGY ANALYZER
Horizontal deflector (ΔC1 LEFT, ΔC1 RIGHT)
Vertical deflector (ΔC2 UPPER, ΔC2 LOWER)
Lens element (ANAL. SLIT)
Outer hemisphere (ANAL.OUTER)
Entrance slit (ANAL. SLIT)
Inner hemisphere (ANAL. INNER)
Lens shield (COMMON)
Collector (BIAS)
(VS1)
(VS2)
(VS4)
(VS5)
Field termination electrodes
Double exit slit (ANAL. SLIT)
Multiplier second stage (OUTPUT)
Multiplier first stage (INPUT)
Hemisphere mounting plate (ANAL. SLIT)
XBL 827-7115

Figure 3

III. ADSORPTION OF H_2S ON Ni(100)*

A. INTRODUCTION

The role of sulfur-containing compounds in atmospheric pollution and the related necessity of removing sulfur from coal and petroleum products hardly need stressing. In addition, many reactions transforming coal and petroleum products into more valuable chemicals use catalysts of rare or costly materials that are eventually poisoned by sulfur. The need for understanding the chemistry of sulfur on metal surfaces and its relation to the above problems is widely understood, and a lot of effort is being expended in this area. However, the vast majority of the work so far has dealt with atomic sulfur on various metal surfaces.[1] Little work has been done on the adsorption and subsequent reactions of molecular sulfur-containing compounds which are more relevant to the actual process of sulfur extraction. It is generally necessary to carry out such studies at low temperatures in order to observe stable molecular adsorption on a time scale of a surface measurement. These studies include spectroscopic[2-4] and nonspectroscopic studies on W,[5] Ag,[5] Ni,[6] and Pb.[7] The spectroscopic studies all used ultraviolet photoelectron spectroscopy (UPS) as the primary tool which identifies molecular and atomic species on the surface. Fisher studied the coverage dependence of H_2S/Ru(110)[2] at 80 K. Bhattacharaya[3] found a small amount of molecular HS on W(100) at room temperature. On polycrystalline Ni, Brundle and Carley[4] found that at 120 K molecular adsorption was occurring, though some degree of dissociation was considered possible.

A fairly complete characterization of the adsorption and decomposition reactions of H_2S on Ni(100) is reported here. EELS has been used to characterize the coverage dependence of this system at 110 K and the temperature dependence of the high coverage sample. Like the abovementioned UPS studies, EELS has proven to be very useful for identifying both molecular and atomic species. In addition, direct spectroscopic information for hydrogen adsorption is reported, which gives qualitative structural information.

B. EXPERIMENTAL

The crystal was cleaned by the methods described in Chapter II. Carbon, oxygen, and sulfur impurity levels were less than detection limits of retarding field Auger spectroscopy, and no impurities other than small amounts of CO in some EEL spectra were observed. Spectroscopic grade H_2S obtained from Matheson was directed at the liquid nitrogen cooled (110 K minimum achievable temperature) surface by means of an effusive beam. A one second exposure to the effusive beam corresponds to ~ .05-.1 L. The D_2S used (98% D) was obtained from Stohler Isotopes. Purity was checked *in situ* by means of a residual gas analyzer (Inficon IQ200) during exposures. Recording the time of exposure for reproducible sample coordinates at a given chamber pressure (1.0×10^{-9} torr of H_2S) was found to give adequately reproducible exposures. LEED and Auger measurements of an overlayer of H_2S were taken after an EEL spectrum. These corresponded well to LEED and Auger measurements obtained for freshly

prepared, equivalent exposure samples. Resistive heating was used, and temperature measurements were made by means of a chromel-alumel thermocouple attached to the sample plate near the Ni(100) crystal. The electron impact energy was nominally 1.60 eV. All EEL spectra were collected in the specular direction with an incident angle of 55° from the normal and at a temperature of 110 K.

C. RESULTS

1. Coverage Dependence at 110 K

When H_2S is exposed to the clean Ni(100) surface at 110 K, a saturation coverage is attained. Further exposure to H_2S leads to no further increase in the S Auger signal, as well as no further change in a c(2x2) LEED pattern observed under these conditions. The c(2x2) LEED pattern is of poor quality with very faint and diffuse c(2x2) spots and a high background of scattered electrons between diffraction spots. At 110 K it appears that the degree of order is not very great. The Auger spectra show the same dependence of the S(LMM) intensity for a 110 K exposure as that shown by a room temperature exposure followed by a 470 K anneal. This and the c(2x2) LEED pattern indicate a saturation coverage of 1/2 monolayer is reached at 110 K with an exposure of ~ 3-6 L.

The EEL spectrum of H_2S and D_2S at saturation coverage is shown in Fig. 1. The frequency shifts upon deuteration of the loss peaks at 2515, 1170, 650, and 480 cm^{-1} indicate that these features involve primarily hydrogen motion, although the shifts of the 1170 and

650 cm^{-1} peaks, which should occur near 830 and 460 cm^{-1} (near the arrows in Fig. 1), are not readily discernible due to the uneven background of the D_2S spectra. A comparison of these spectra to gas phase H_2S and D_2S is given in Table 1. The gas phase spectra show three vibrational modes: symmetric (ν_1) and asymmetric (ν_3) stretches, and an SH_2 (SD_2) deformation or "scissoring" mode (ν_2). The observation of ν_1 and ν_2 indicates the presence of molecular H_2S, the surface frequencies being downshifted by ~ 100 cm^{-1}. The ν_3 mode on the surface is dipole inactive (absent in the specular direction). This is expected if the molecular symmetry is C_{2v} or C_s with a mirror plane normal to the surface bisecting the H atoms. The aspect of molecular symmetry and our assignment will be addressed more fully in section D.

Coverage dependent spectra at 110 K are shown in Fig. 2. The spectra show a trend of decreasing dissociative adsorption as the coverage is increased. At the lowest exposure of 12 seconds, H_2S is dissociated on the Ni(100) surface. The S-Ni stretch at 350 cm^{-1} agrees well with the value Andersson has reported for S/Ni(100) at room temperature.[8] The broad shoulder centered at 570 cm^{-1} is identified as a H-Ni stretch. Evidence supporting this by a comparison to 1 L of H/Ni(100) is shown in Fig. 3.

A small amount of CO adsorbed from the residual gas of the chamber during the 60-90 minutes required to collect a spectrum is seen in the 12 second exposure in Fig. 2. Its intensity is comparable to other features in the spectrum because of the large dipole deriva-

tive of CO. It is not seen in the higher coverage spectra for the following reasons. Each spectrum was obtained after exposure to a freshly cleaned surface, i.e., impurities do not build up from one exposure to the next. At the higher coverages less sites are available for CO and other impurities to adsorb during the time it takes to collect a spectrum. In addition, less time is required to collect a spectrum at higher coverages.

At higher exposures of H_2S gas four additional features appear in the loss spectrum at 480, 650, 1170, and 2510 cm^{-1}, the latter two previously attributed to H_2S. The likely candidates responsible for the high coverage spectrum are H_2S and a mixture of H_2S and HS. The loss at 480 cm^{-1} has a different coverage dependence than the 1170 and 2510 cm^{-1} losses as seen in Fig. 4. This could result from a different chemical identity of the 480 cm^{-1} feature (HS) or a different molecular orientation of H_2S (C_s vs. C_{2v}) at different coverages. These possibilities are discussed at length in section D. For the present, it suffices to note that two different species are observed. It should also be noted that EELS intensities depend not only on the number of dipole oscillators and oscillator strength but also on the degree of surface order, which in general changes with coverage. However, if the 480, 1170, and 2510 cm^{-1} losses are due to one species, one would not expect any intensity ratio differences vs. coverage due to the degree of order.

2. Temperature Dependence

The temperature dependence of the high coverage spectrum from 0-1000 cm^{-1} is shown in Figs. 5 and 6. The spectra were recorded by annealing to the indicated temperature for five minutes and cooling back down to 110 K before collecting the spectrum. The feature at 480 cm^{-1} is seen to disappear by 170 K while the feature at 650 cm^{-1} persists until 220 K. This is interpreted as the dissociation of H_2S (or HS) and the desorption of hydrogen, respectively. It is only observed that hydrogen leaves the surface; however, Fisher's thermal desorption data confirm this interpretation.[9] A complete spectrum from 0-2800 cm^{-1}, taken after a 150 K anneal, shows the disappearance of the 1170 and 2510 cm^{-1} features as well, which indicates that the two different molecular species have approximately the same temperature dependence.

Further evidence for assigning the 650 cm^{-1} feature to a H-Ni stretch is given in Fig. 7. The spectrum obtained by annealing a saturation coverage of H_2S to 170 K, lowest trace, is compared with a spectrum generated by adding 5 L of H_2 to the S/Ni(100) surface at 110 K, middle trace, and a spectrum of 1 L of H_2 adsorbed on Ni(100). The loss features in the range 570-650 cm^{-1} are thus correlated to surface hydrogen.

A sample with fewer surface species was prepared by carrying out the following experiment. A c(2x2) S/Ni(100) overlayer annealed to 470 K (equivalent to annealing a saturation coverage of H_2S at 110 K to 470 K as LEED and Auger show) was cooled to 110 K and further

exposed to a large amount of H_2S (25 times saturation coverage). The count rate of the elastic peak of the resulting surface was reduced by a factor of 10, even after extensive retuning, indicating that some change on the surface had taken place. The spectrum collected under these conditions is shown in Fig. 8. Two features at 1210 and 2520 cm^{-1} can be assigned to H_2S, and no feature is seen at 480 cm^{-1}. This is further evidence that two molecular species exist on the surface at different coverages, and that the higher coverage species (H_2S, C_{2v} symmetry) can be isolated as the only molecular species.

D. DISCUSSION

One can think of three possibilities for H_2S orientation on Ni(100) as shown in Fig. 9. However, only (a) and (b) are consistent with the absence of an asymmetric SH_2 stretch at ~ 2600 cm^{-1}. The orientation with C_{2v} symmetry has only two vibrational modes that are dipole allowed, i.e. that have a change in dipole moment perpendicular to the surface. These are the SH_2 symmetric stretch and scissor modes. Other possible normal modes are the SH_2 rock, wag, and twist. The rocking mode becomes dipole active for orientation (c), which has already been ruled out, while the wag is dipole active for orientation (b). The data show three modes with the same or similar temperature dependence at 480, 1170, and 2510 cm^{-1}, which could be a mixture of orientations (a) and (b). Alternatively we have the possibility of two molecular surface species; H_2S in

C_{2v} symmetry, having modes at 1170 and 2510 cm^{-1}, and SH with modes at 480 and 2510 cm^{-1}. Our data allow either possibility. However, the results of two previous workers[2,10] may tend to favor SH. Fisher observed SH at intermediate coverages on Ru(110) by means of difference spectra in UPS and comparison with the UPS spectra of H_3SiSH.[11] Interestingly, he observed dissociation of H_2S at low coverages and molecular H_2S at high coverages, much as in the present work. Fisher and Sexton[10] identified an OH species on Pt(1$\bar{1}$1) in the presence of co-adsorbed O using EELS by exposing a surface containing O to H_2O at 110 K and heating to 155 K. Their assignment did not have the alternate possibility that exists here because there was <u>no</u> H_2O simultaneously present under the conditions they observed OH. However, a striking similarity is observed between this work and OH/Pt(111). The loss observed at 1015 cm^{-1} due to the OH bend is much stronger than any other feature in the spectrum. On Ni(100) the loss at 480 cm^{-1} is correspondingly more intense than all other features. To our knowledge there are no vibrational data for inorganic compounds of HS or H_2S bonded to transition metals available for comparison. The closest possibility is $(CH_3)_3SiSH$,[12] which contains no mention of an SH bend. Since there is no basis of comparison for assigning the 480 cm^{-1} mode to an HS bend, or an SH_2 wag, only indirect evidence remains; the fact that the coverage dependences on Ru(110) and Ni(100) at liquid nitrogen temperatures are nearly identical if HS is the intermediate species on Ni(100), and the observation that the intensity ratio of the OH bend to the OH stretch

on Pt(111) is similar to that of the presumed HS bend to the HS stretch (and H_2S symmetric stretch) on Ni(100).

It is interesting to note the similarities between H_2S adsorption on Ru(110) and the present work. In both cases there is complete dissociative adsorption at low temperatures and low coverages, with hydrogen remaining on the surface. At higher coverages on Ru(110) first HS then H_2S was observed at 80 K, similar to what is observed here. The Ru(110) surface is much more open than the more densely packed Ni(100) surface. In order to dissociate H_2S an activation barrier must be overcome by some means such as a large amplitude vibrational motion which will bring hydrogens in close proximity to the metal surface. It is easy to imagine such a mechanism to be surface structure sensitive. In fact, the great similarities between H_2S/Ru(110) and H_2S/Ni(100) suggest that a mechanism for dissociation is not surface structure dependent but electronic structure dependent. This is consistent with Fisher's observation that large changes in the work function as a function of coverage occur up to the point where molecular species began to adsorb and then gradually level off.

Free surface hydrogen can take part in a variety of interesting processes including bond-forming reactions, modification of surface electronic properties, etc. For example, in the case of bond forming reactions, the activation energy for bond formation should depend critically on the hydrogen site. Yet structural information which could shed light on these processes is difficult to come by. Current

structural measurements are not applicable to hydrogen because it is a Z=1 element. Qualitative structural information that can be obtained by vibrational spectroscopy is difficult to come by for hydrogen when there are several surface species present because M-H stretching frequencies are both very weak and lie in a region where there are many other modes present; e.g. for hydrocarbons there are many CH_x bending modes in the range 600-1500 cm^{-1}. Even in cases where hydrogen is known to be on the surface at temperatures below the desorption threshold, such as methoxy on Ni(111)[13] where there is only one methoxy frequency at 1020 cm^{-1} in the range 600-1500 cm^{-1}, surface hydrogen is not observed by EELS. The present case is a fortunate example where a H-Ni stretch at 650 cm^{-1} can be discerned in the presence of three other surface species. The low frequency for the H-Ni stretch suggests that H lies in a 4-fold hollow site. For inorganic complexes, metal-hydrogen (M-H) stretching frequencies greater than 1600 cm^{-1} have been found by many workers to result from linear M-H bonds, and frequencies in the range 800-1300 cm^{-1} correspond to bridge sites.[14,15] Although there is not yet a wide body of information available on surfaces, data from inorganic complexes give a good qualitative guide. Since the 650 cm^{-1} frequency on Ni(100) lies below the accepted range for a bridge site, an assignment of a 4-fold hollow site can be made for H on Ni(100). In addition, data by Andersson[16] for H/Ni(100) and a theoretical study by Upton and Goddard[17] on a $Ni_{20}H$ cluster support such a conclusion. However, the situation is not so simple. The

site designations atop, bridge, 3-fold, and 4-fold hollows are more appropriate for larger atoms where hard sphere radii designations are valid. Were a hard sphere radius appropriate for hydrogen, the hydrogen would either fit solidly in the 4-fold hollow ($r_H > \sim .51$Å) site or have the possibility of bonding atop to the atom below or in a 3-fold site with the atom below and two of the surface Ni atoms ($r_H < \sim .51$Å). However, a hard sphere model is inappropriate for a proton with its surrounding electron density largely blending into the surface. In addition, sites intermediate to bridge and 3-fold have been reported for H/Ni(100).[18,19] It follows that while the 650 cm^{-1} H-Ni stretch indicates a high degree of coordination, probably 4-fold, this does not unambiguously determine the hydrogen site. The nature of this site is changing, as evidenced by the narrowing and upward shift of the H-Ni frequency (Fig. 6). What is causing this change is unclear.

V. SUMMARY

A fairly complete characterization of the adsorption and decomposition of H_2S on the Ni(100) surface has been carried out. The reaction steps listed below indicate species that have been

$$H_2S\ (gas) \xrightarrow[\text{Ni(100) 110 K}]{\text{low coverages}} S_{ads} + H_{ads}$$

$$H_2S\ (gas) \xrightarrow[\text{Ni(100) 110 K}]{\text{intermediate coverages}} \begin{bmatrix} HS \\ H_2S\ (C_s) \end{bmatrix} + \begin{bmatrix} H_2\ (gas) \\ H_{ads} \end{bmatrix}$$

$$H_2S\ (gas) \xrightarrow[\text{Ni(100) 110 K}]{\text{high coverages}} H_2S\ (C_{2v})$$

$$\begin{bmatrix} H_2S \\ HS \end{bmatrix} \xrightarrow[\text{170 K}]{\text{Ni(100)}} S_{ads} + \begin{bmatrix} H_{ads} \\ H_2\ (gas) \end{bmatrix}$$

$$H_{ads} \xrightarrow[\text{220 K}]{\text{Ni(100)}} H_2\ (gas)$$

identified using EELS under various conditions of coverage and temperature. Future experiments using HDS would be useful in determining the identity of the intermediate coverage species. Adsorbed hydrogen is observed in the presence of three other surface species. Desorption of H_2 is inferred from the disappearance of the H-Ni stretch and is confirmed by the thermal desorption data of Fisher.[9]

REFERENCES

*This chapter is based on experiments performed in collaboration with M.A. Schulz and D.A. Shirley and is published in J. Chem. Phys. 81, xxxx (1984).

1. Gabor A. Somorjai, Chemistry in Two Dimensions: Surfaces, (Cornell University Press, Ithaca, 1981) pp. 253-262. Thirteen references of S on metal surface are listed in this reference. Much work has been done since then.
2. G.B. Fisher, Surface Science 87, 215 (1979).
3. A.K. Bhattacharaya, L.J. Clarke, and L. Morales de la Garza, Chem. Soc. Faraday Trans. 1, 77, 2223 (1981).
4. C.R. Brundle and A.F. Carley, JCS Faraday Disc. 60, 51 (1975).
5. M. Saleh, C. Kemball, and M.W. Roberts, JCS Faraday Soc. Trans. 57, 1771 (1961).
6. E. Bechtold, L. Weisberg, and J.H. Block, Z. Phisik. Chem. NF 97, 97 (1975).
7. G.B. Saleh, B.R. Wells, and M.R. Roberts, Trans. Faraday Soc. 60, 1865 (1964).
8. S. Andersson, Proceedings of the 1978 International Conference on Vibrations in Adsorbed Layers, KFA reports - Julich, Conf. 26, 103 (1978); S. Andersson, Surface Science 79, 385 (1979).
9. G.B. Fisher, private communication.
10. G.B. Fisher and B.A. Sexton, Phys. Rev. Lett. 44, 683 (1980).
11. S. Craddock and R.A. Whiteford, JCS Faraday Trans. II 68, 281 (1972).

12. Von H. Kriegsman, Z. Anorg. Allgem. Chem. 294, 8, (1958).

13. J.E. Demuth and H. Ibach, Chem. Phys. Lett. 60, 395 (1979).

14. H.D. Kaesz and R.B. Saillant, Chem. Rev. 72, 231 (1972).

15. U.A. Jayasooriya, M.A. Chesters, M.W. Howard, S.F.A. Kettle, D.B. Powell, and N. Sheppard, Surface Science 93, 526 (1980).

16. S. Andersson, Chem. Phys. Lett. 55, 185 (1978).

17. T.H. Upton and W.A. Goddard, III, Phys. Rev. Lett. 42, 472 (1979).

18. T. Engel and K.H. Rieder, Surface Science 109, 140 (1981).

19. L. Ollé and A.M. Baró, Surface Science 137, 607 (1984).

Table 1. A comparison of gas phase H_2S and D_2S to surface spectra.

	$\nu_1(cm^{-1})$	$\nu_2(cm^{-1})$	$\nu_3(cm^{-1})$
H_2S (gas)	2611[a]	1290[b]	2684[b]
H_2S (surface)	2510	1170	-
D_2S (gas)	1892[a]	934[c]	1999[c]
D_2S (surface)	1830	-	-

a) G.M. Murphy and J.E. Vance, J. Chem. Phys. 6, 426 (1938).

b) A.D. Sprague and H.H. Nielsen, J. Chem. Phys. 5, 85 (1937); C.R. Bailey, J.W. Thompson, and J.B. Hale, ibid. 4, 625 (1936).

c) C.R. Bailey, J.W. Thompson, and J.B. Hale, J. Chem. Phys. 4, 625 (1936); A.H. Nielsen and H.H. Nielsen, ibid. 5, 277 (1937).

FIGURE CAPTIONS

Figure 1. The EEL spectra for a saturation coverage of H_2S and D_2S on Ni(100) at 110 K. The arrows point to $\omega/\sqrt{2}$ for a given frequency ω in the H_2S spectrum. $E_i = E_s = 55°$, $E_o = 1.6$ eV.

Figure 2. Coverage-dependent spectra for H_2S/Ni(100) at 110 K. The number of seconds of exposure to an effusive beam of H_2S is listed at the right of each trace. 1 second ~ .05-.1 L. $E_i = E_s = 55°$, $E_o = 1.6$ eV.

Figure 3. Comparison of the lowest exposure (12 sec) of H_2S/Ni(100) at 110 K to an exposure of 1 L of H_2 on Ni(100) at 110 K. $E_i = E_s = 55°$, $E_o = 1.6$ eV.

Figure 4. Intensity vs. H_2S exposure for the 480 cm^{-1} (+), 1170 cm^{-1} (∇), and 2510 cm^{-1} (o) peaks.

Figure 5. Temperature dependence of a saturation coverage of H_2S/Ni(100) from 110-170 K. Each spectrum was obtained after annealing to the given temperature for 5 minutes and then cooling back down to 110 K. $E_i = E_s = 55°$, $E_o = 1.6$ eV.

Figure 6. Temperature dependence of a saturation coverage of H_2S/Ni(100) from 200-295 K. Each spectrum was obtained after annealing to the given temperature for 5 minutes and then cooling back down to 110 K. $E_i = E_s = 55°$, $E_o = 1.6$ eV.

Figure 7. A comparison of the following surfaces: a surface obtained by annealing a saturation coverage of H_2S/Ni(100) to 170 K (lowest trace), a surface of 1/2 monolayer of S/Ni(100) cooled to 110 K to which 5 L of H_2 has been added (middle trace), and 1 L of H_2 on Ni(100) at 110 K (upper trace). $E_i = E_s = 55°$, $E_0 = 1.6$ eV.

Figure 8. A comparison of a surface to which a very large exposure (25x saturation) has been added to c(2x2) S/Ni(100) at 110 K. $E_i = E_s = 55°$, $E_0 = 1.6$ eV.

Figure 9. Three possible orientations of H_2S/Ni(100), (a) C_{2v} symmetry; (b) C_s symmetry with a mirror plane bisecting the H atoms; and (c) C_s symmetry with a symmetry plane containing the H_2S molecule.

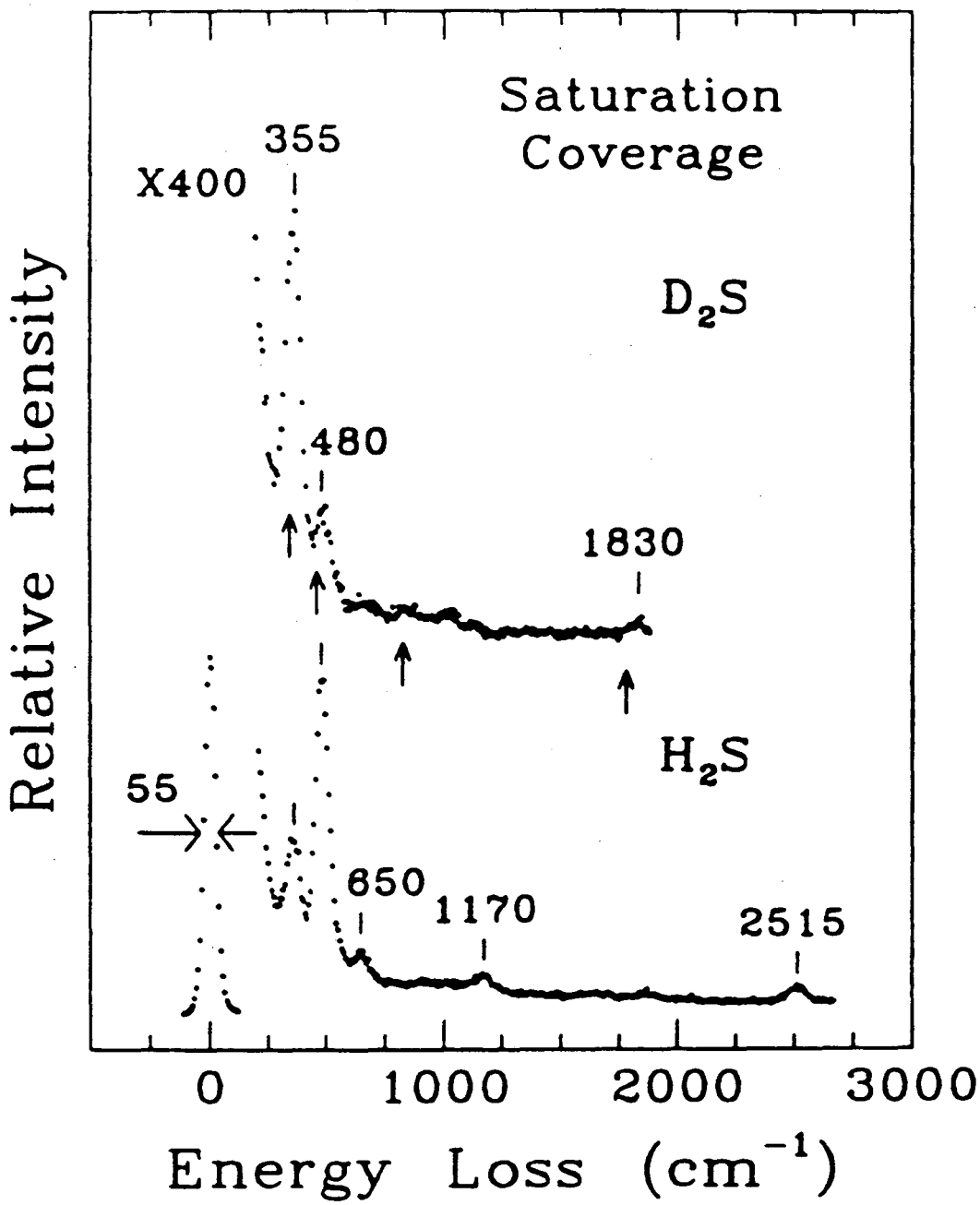

XBL 847-2642

Figure 1

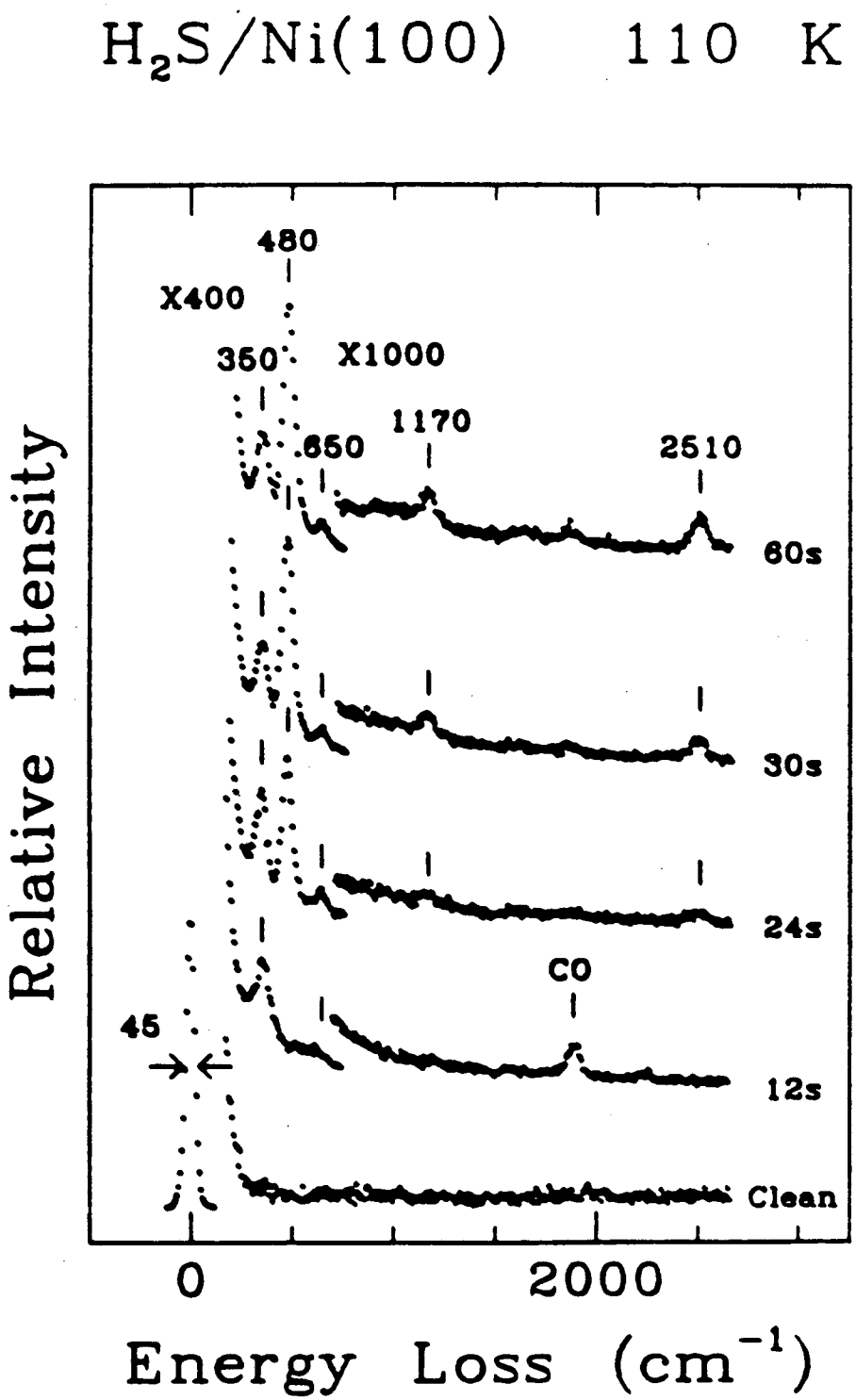

XBL 847-2639

Figure 2

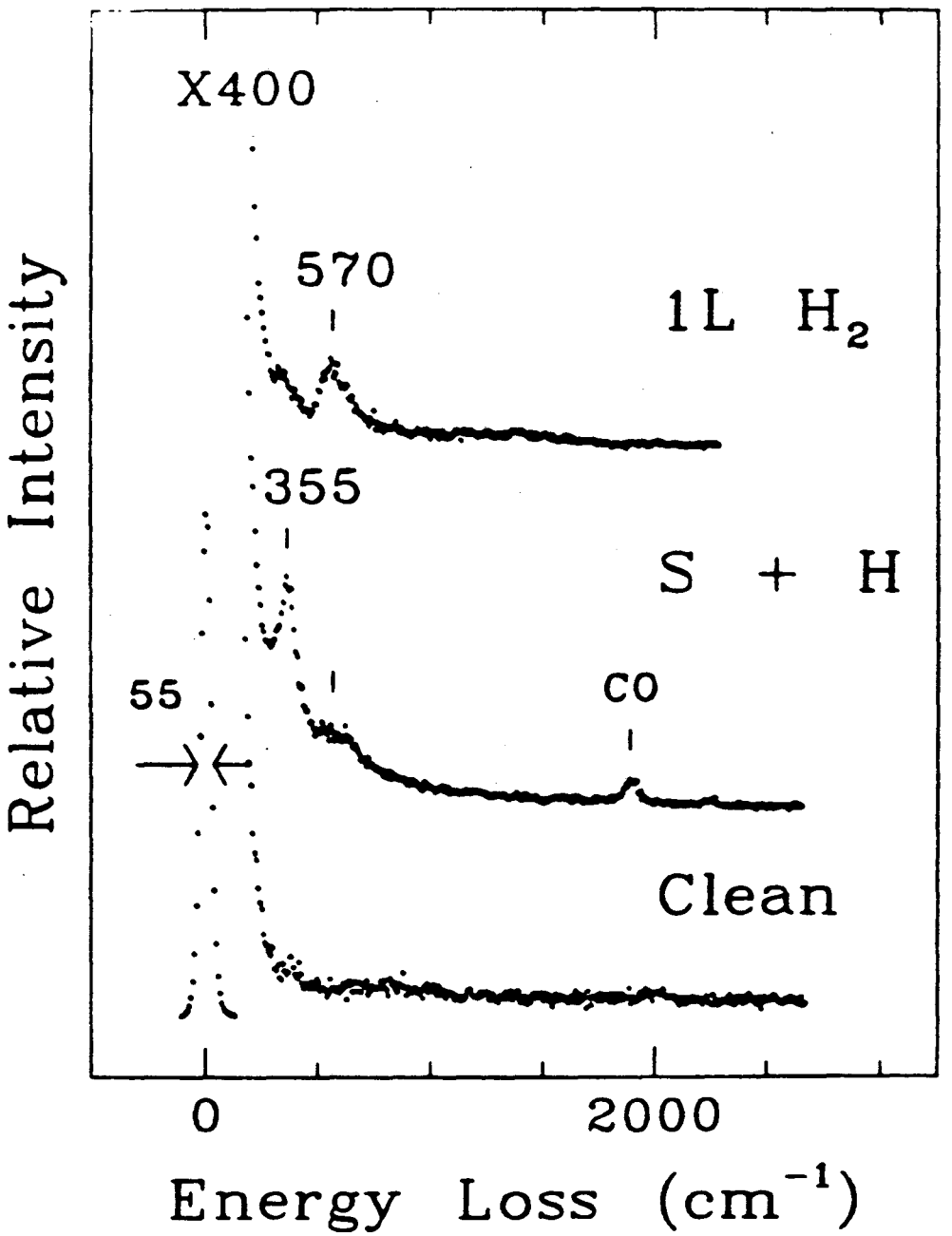

XBL 847-2641

Figure 3

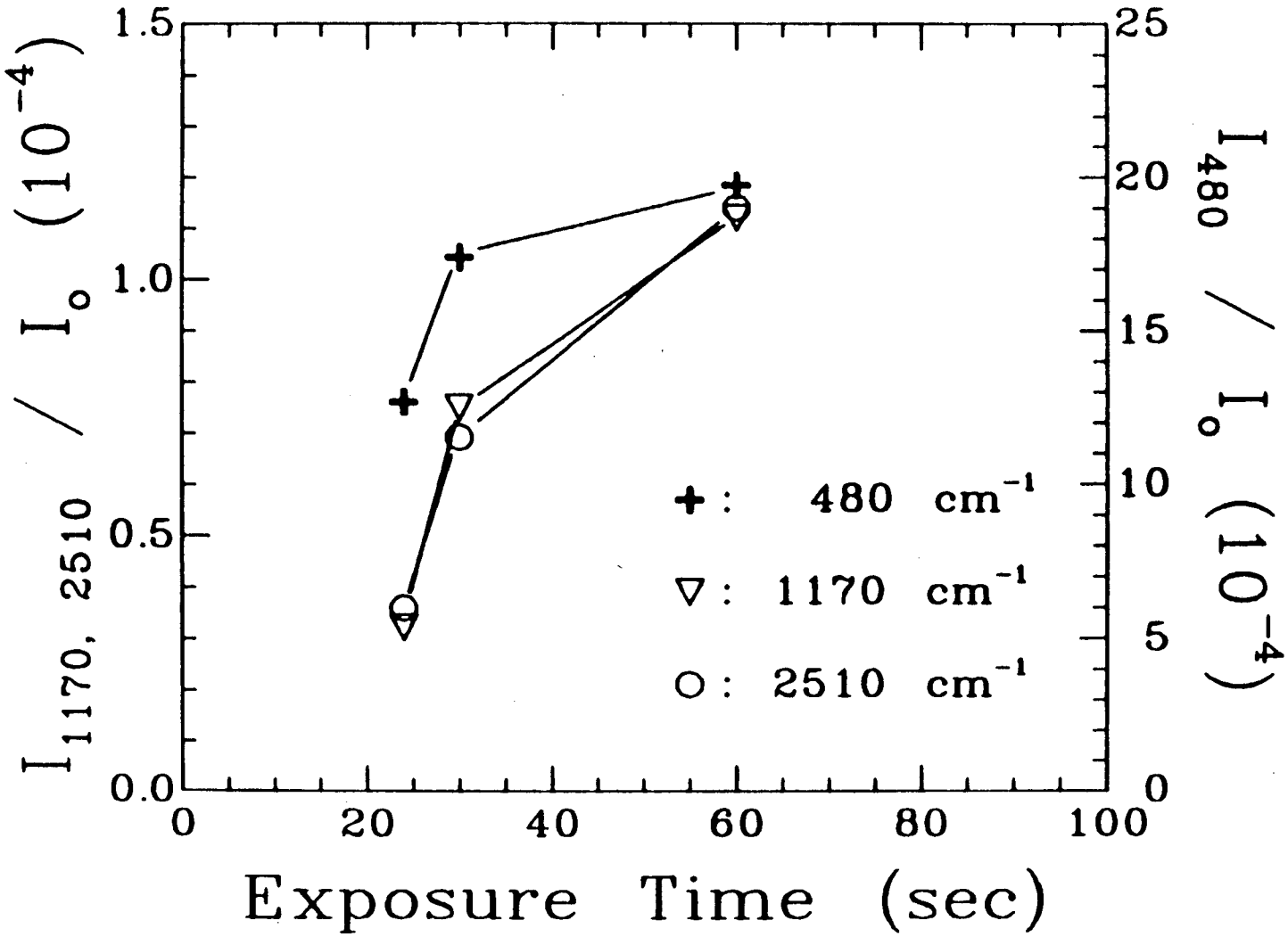

Figure 4

XBL 847-2646

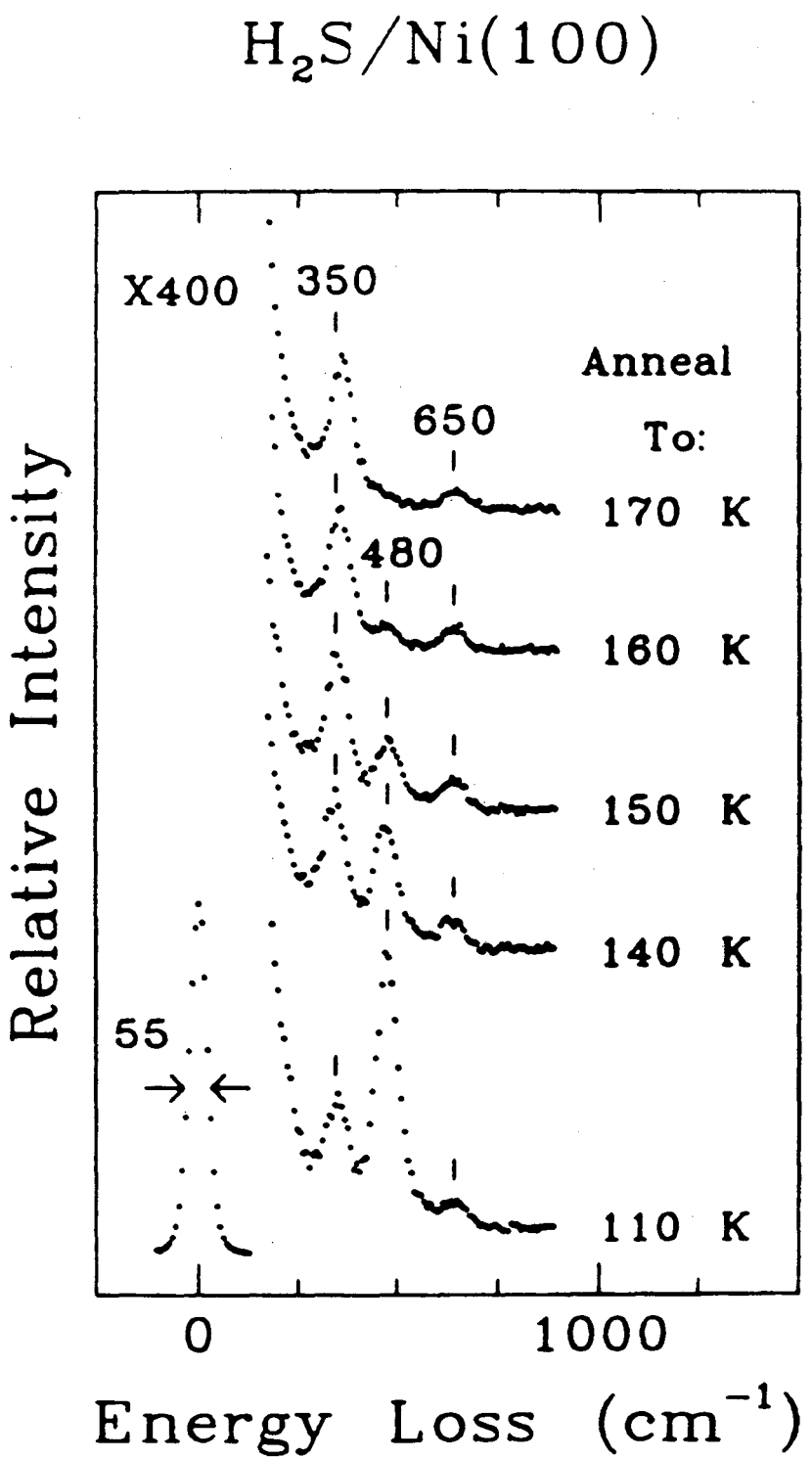

Figure 5

XBL 847-2645

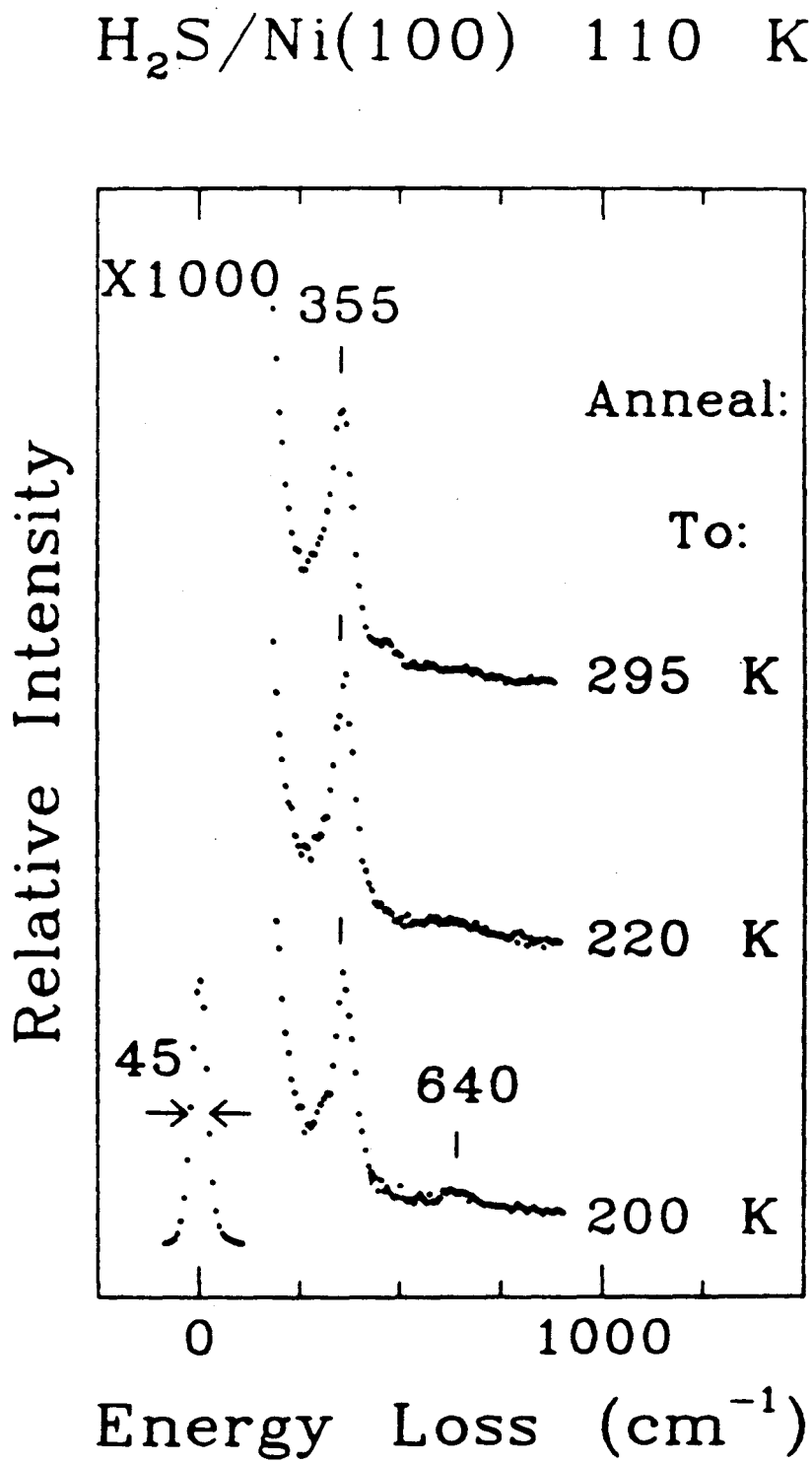

XBL 847-2644

Figure 6

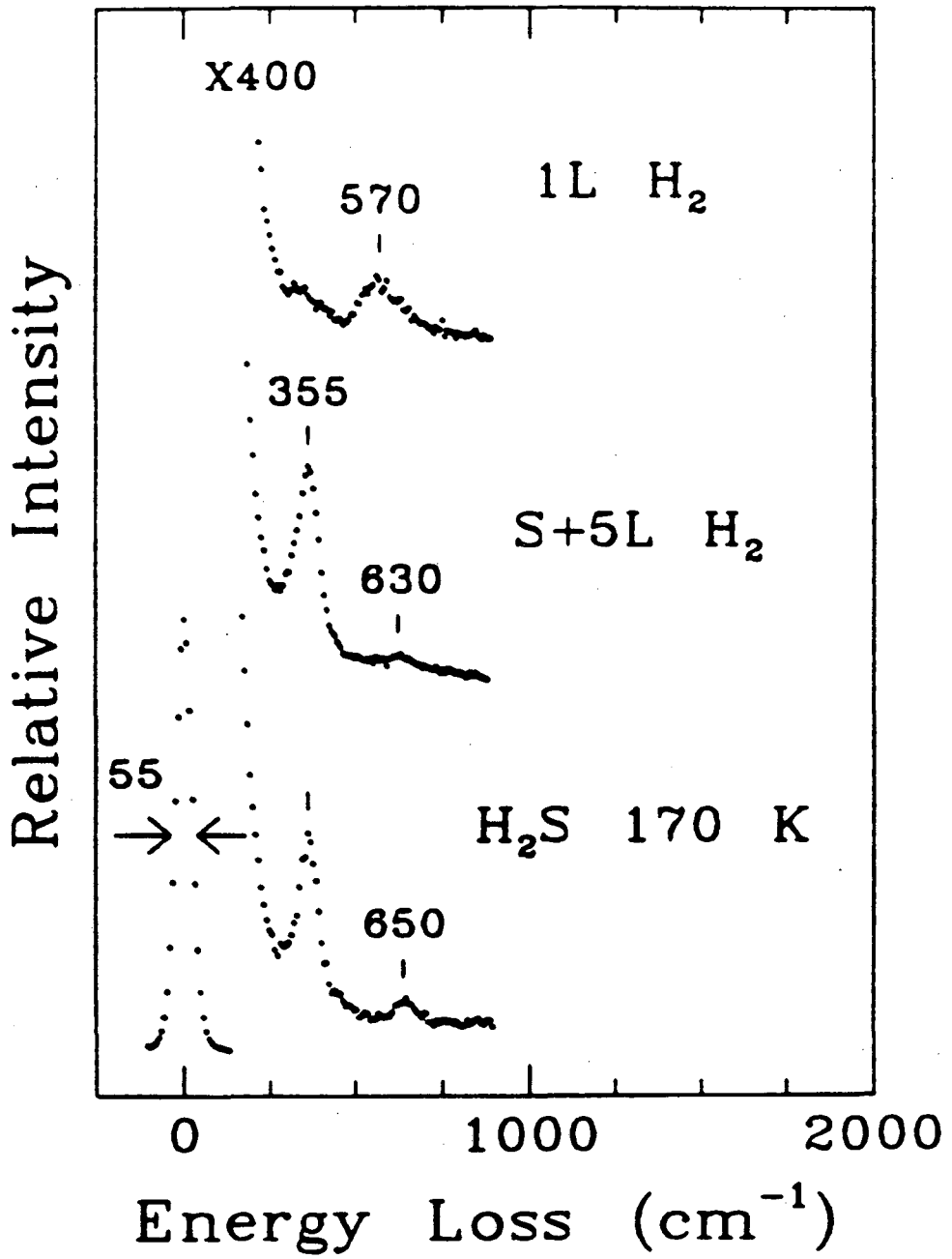

XBL 847-2640

Figure 7

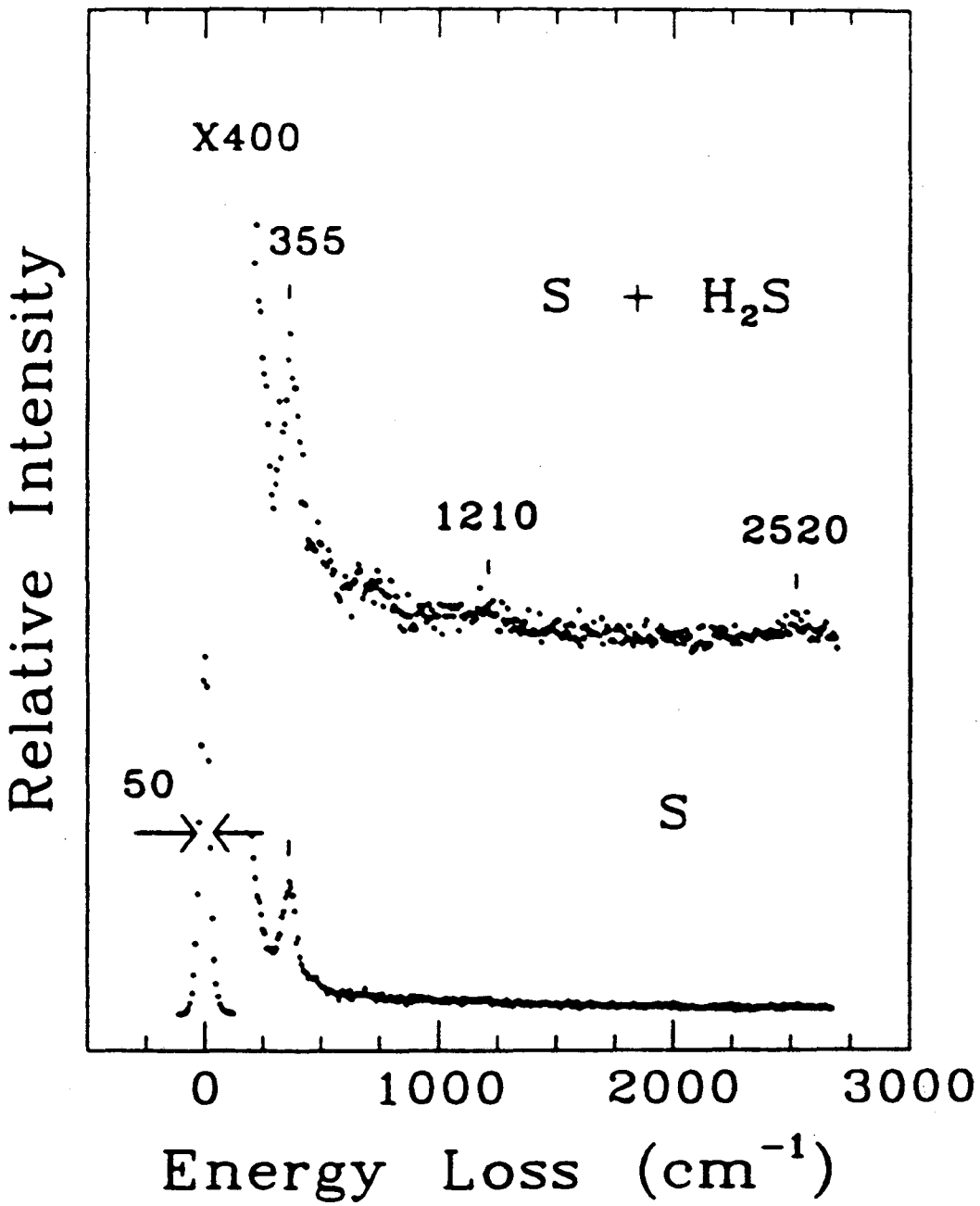

XBL 847-2643

Figure 8

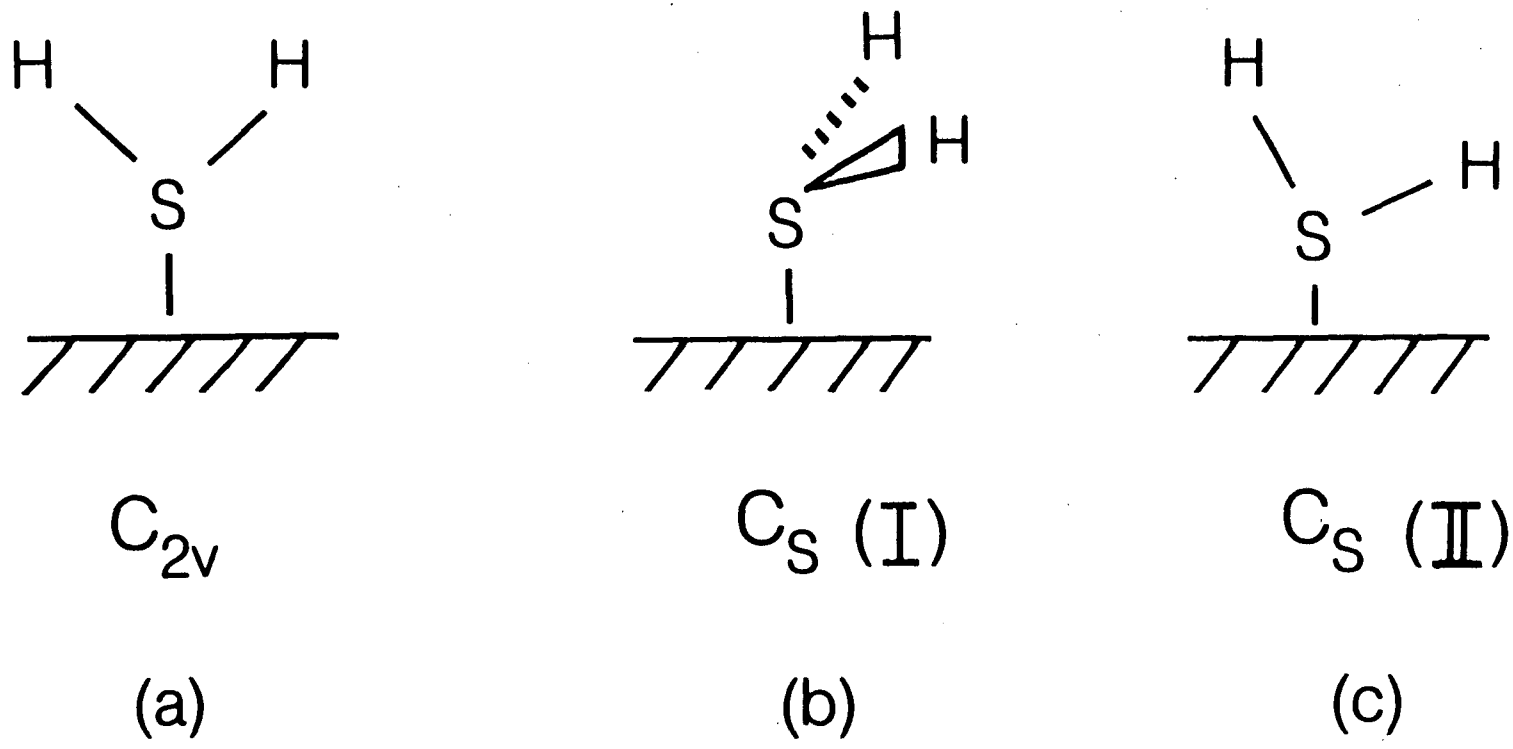

XBL 846 8474

Figure 9

IV. CH_3NH_2 ADSORPTION ON Ni(100), Ni(111), Cr(100), AND Cr(111)*

A. INTRODUCTION

A molecule can bond to a surface in such a way that no bonds are broken in the process. Two ways for this to occur are through an existing lone pair of electrons in the molecule of interest or through a rehybridization of a π-bonded system. Examples of the former have received much attention, especially the prototype systems CO and NH_3 adsorbed on transition metal surfaces. Adsorption energies tend to be weak (8-17 kcal/mole for NH_3[1-4] and 13-40 kcal/mole for CO[5-13]), making desorption competitive with decomposition on most transition metal surfaces. Molecules such as these provide a known type of interaction, which allow one to examine trends across the Periodic Table. Examples of π-bonded systems are simple olefins such as ethylene and acetylene, which tend to adsorb more strongly. Their chemistry with transition metals is more reactive. Dissociative chemistry with the formation of new surface species and/or molecular rearrangements on the surface is more common than thermal desorption of the parent compound. By attaching a hydrocarbon tail to a lone pair donating group, one can try to bridge the gap between these two types of behavior. Associative interactions in the hydrocarbon group should raise the adsorption energy of the molecule, allowing one to change the decomposition/desorption characteristics.

With these ideas in mind, a study of the adsorption of CH_3NH_2 on surfaces of nickel and chromium is presented. These metal surfaces

were chosen to provide a comparison between the right and left members of the transition metal series. The interaction of CO with transition metals shows progressively more dissociative behavior as one goes left and down across the Periodic Table.[14] The comparison between Ni and Cr is particularly illuminating because Cr is the most reactive metal yet studied. At 300 K, CO is completely dissociated on the structurally different low index surfaces of Cr at all coverages (see Chapter VI and reference 15). On Ni there is no dissociation at steps[16] or on the flat low index surfaces up to the desorption temperature of 450 K.[17] The study of CH_3NH_2 on these metal surfaces should strengthen this comparison. Structurally different surfaces have been chosen for each metal to separate differences due to structural and electronic properties.

There have been no previous studies on the adsorption of CH_3NH_2 on clean, well characterized transition metal surfaces. The only previous works were done on either dispersed particles[18] or poorly characterized surfaces.[19,20]

B. EXPERIMENTAL

Both the Ni and Cr crystals were precleaned by the methods of Chapter II. Between experiments, CH_3NH_2 was cleaned from both samples in the same way. First, the sample was sputtered to remove all but residual amounts of carbon. The sample was then exposed to a small amount of oxygen followed by flashing the crystal (1075 K for Ni, 1175 K for Cr) using an electron beam heater. The Ni surfaces

were then clean. The Cr surfaces required a brief period of sputtering to remove the oxygen. Surface cleanliness was monitored by Auger spectroscopy. The impact energy for the EEL spectra was chosen to optimize the signal, and for these studies ranged between 2.0-2.5 eV. The scattering geometry will be indicated separately for each measurement.

Methylamine was prepared by hydrolyzing $CH_3NH_2 \cdot HCl$ (Aldrich, 99+% pure) and liberating gaseous CH_3NH_2 from the solution by adding NaOH. The CH_3NH_2 was then purified by several freeze-pump-thaw cycles. It was introduced into an ultra high vacuum (UHV) chamber (base pressure 2×10^{-10} Torr) by means of an effusive beam doser which could be directed at the sample. Its purity was checked by saturating the UHV chamber with methylamine and waiting to detect the parent ion $CH_3NH_2^+$ with a residual gas analyzer (Inficon IQ200).

C. RESULTS

1. Nickel Surfaces

Figure 1 shows the EEL spectra of CH_3NH_2 on Ni(100) and Ni(111). Exposing methylamine to both surfaces leaves a saturation coverage after which no major changes, other than a gradual decrease in the total signal, are observed in the spectra with further exposure. An assignment of the spectra and a comparison with gas phase IR and Raman spectra as well as matrix isolated CH_3NH_2 and cis-$[Pt(CH_3NH_2)_2Cl_2]$ are made in Table 1. Seven peaks in each

spectrum can be correlated with the A' normal modes of molecular CH_3NH_2. The other normal modes of CH_3NH_2 can also be accounted for. Modes that occur in the regions 1400-1500 cm^{-1}, 2900-3000 cm^{-1}, and 3200-3300 cm^{-1} could be too close to be separately resolved or they could be forbidden by the surface selection rule. This aspect will be discussed further in section D.

For spectra on both surfaces, an extra feature could be attributed to a CO impurity. Such features are commonly present in EEL spectra reported in the literature because CO has a large dynamic dipole moment and is often present in the residual gas of vacuum chambers. In the CH_3NH_2 spectra, CO probably also comes from the walls of the beam doser. Long purging times to get rid of this source of CO were used at first but were discontinued after degradation in the performance of the EEL spectrometer was noticed. In any case, the amount of CO present on the surface is much less than the proportionate intensity of its loss feature compared to those of CH_3NH_2, because of the much larger dynamic dipole moment of CO.

On both Ni(100) and Ni(111), the spectra can be adequately accounted for by the presence of molecular CH_3NH_2. There are also some differences in the spectra. Shifts in peak positions of the internal modes for the chemisorbed molecule from gas phase values are expected, as are differences in these shifts on surfaces with different geometric structures and electronic properties. For example, the C-N stretch occurs at 1010 cm^{-1} on Ni(111) and 1030 cm^{-1} on Ni(100), compared with 1044 cm^{-1} in the gas phase.[21-23]

In fact, there are slight variations in the peak positions of all the normal modes of CH_3NH_2 on the two Ni surfaces.

2. Chromium Surfaces

The EEL spectra of CH_3NH_2 on Cr(111) and Cr(100) are shown in Fig. 2. Again, the spectra shown are for saturation coverage at room temperature. The essential features of the spectra are qualitatively the same as for nickel. Six peaks in the spectra, those near 1000, 1185, 1465, 1595, 2940, and 3300 cm^{-1}, have energies only slightly different from peaks on the nickel surfaces, and are assigned to internal normal modes of molecular methylamine. A seventh peak in the nickel spectra, the NH_2 wag, ν_9, may be obscured in the chromium spectra by two very intense features at ~ 500 cm^{-1} which are not present in the nickel spectra. These intense features are very similar to peaks observed for dissociated CO on the two Cr surfaces (see Chapter VI).

A comparison of CH_3NH_2/Cr(100), a c(2x2) N/Cr(100) surface (~ 1/2 monolayer), and 2 L of CO/Cr(100) (saturation coverage), all at 300 K, is shown in Fig. 3. The Cr-N stretch at 560 cm^{-1} is weaker in intensity than the peak at 520 cm^{-1} in the spectrum of dissociated CO (Cr-C and Cr-O stretches). Auger spectra taken after both EEL spectra were collected show no traces of oxygen. The peak at 510 cm^{-1} in the CH_3NH_2/Cr(100) spectrum can be assigned as a Cr-C stretch, and such an intense peak can only come from a substantial quantity of dissociated methylamine on Cr(100).

Comparison to the 2 L exposure of CO shows that the Cr-C and Cr-O stretches of dissociated CO are nearly degenerate in frequency. A similar conclusion can be reached for Cr(111) based on the broad feature centered at ~ 500 cm^{-1}.

There is a peak at ~ 2000 cm^{-1} on Cr(111) which is not observed on any of the other surfaces. This may be due to a small amount of molecular CO. It is shown in Chapter VI that no amount of dissociated CO passivates the Cr surfaces sufficiently to allow the subsequent adsorption of molecular CO at 300 K on these surfaces. It is conceivable that the combination of carbon, nitrogen, and CH_3NH_2 on Cr(111) stabilizes the adsorption of CO from the residual gas in the vacuum chamber. The peak at ~ 2000 cm^{-1} may also be due to an overtone of the CN stretch.

Like the companion spectra on the nickel surfaces, there are shifts in the peak positions of the normal modes of CH_3NH_2 adsorbed on the Cr surfaces when compared to gas phase values and values on the Ni surfaces. There are also intensity and linewidth differences which will be discussed in section D. It should be noted that some peaks, such as those at 1000, 1185, 1465, and 1595 cm^{-1} on Cr(100), 730 and 1195 cm^{-1} on Ni(111), and 1220 and 1572 cm^{-1} on Ni(100), have widths equal to the instrumental resolution of ~ 50 cm^{-1}, while most of the other peaks are 80 cm^{-1} or broader at the FWHM.

3. Other Results

For much of the discussion that follows, it will be important to establish that methylamine exists on the surfaces studied as approximately one monolayer at 300 K. Auger spectra collected after EELS measurements showed the presence of approximately one monolayer of carbon and nitrogen on all four surfaces. Since high energy electrons (2 KeV) in the fluxes used (50 μA, 5-10 minutes) could desorb and/or dissociate CH_3NH_2 molecules that may have been in an "ice" multilayer, these measurements are not relied on. Instead, a comparison is made with the results of other workers that use thermal desorption spectroscopy in conjunction with EELS or another spectroscopic technique to distinguish between adsorption of a monolayer, a second adsorbed layer where it is possible to determine this, and a multilayer. Table 2 shows the boiling point and the desorption temperatures of a multilayer and a second layer for a number of hydrogen containing polar molecules. The results indicate that, for compounds with a wide range of boiling points, the desorption temperatures of a multilayer and a second layer are well below room temperature under UHV conditions. The same conclusion can be reached for CH_3NH_2 adsorbed on transition metal surfaces. It should also be noted that the EELS data for adsorbed CH_3NH_2 in Table 1 are in clear disagreement with those of solid crystalline CH_3NH_2 and that EEL spectra for disordered multilayers show unresolvable features in qualitative contrast to the spectra in Figs. 1-2 for several cases where the data are of comparable

complexity.[24-26]

Finally, an attempt to collect spectra of the deuterated compounds CH_3ND_2, CD_3NH_2, and CD_3ND_2 was made in order to comfirm the assignments of Table 1. It was not successful due to isotopic mixing upon interaction of the deuterated methylamine with residual hydrogen on the walls of the beam doser and/or the main UHV chamber.

D. DISCUSSION

1. Mode Assignments and Molecular Orientation

Mode assignments of the spectra in Figs. 1-2 are given in Table 1. Values for the peaks in the bending region 700-1600 cm^{-1} were determined by visual inspection. The good agreement with gas phase and matrix isolated CH_3NH_2 makes the assignment of the modes ν_4 and ν_{7-9} straightforward. The breadth of the peak at ~ 1465 cm^{-1} makes the assignment of ν_5, ν_6, and ν_{12} ambiguous. The A" modes ν_{13-15} will not be discussed because results from high resolution IR are ambiguous about the assignment of these modes.[27-29] Values for the NH_2 stretches were determined by least squares fitting, but this was not attempted for the CH_3 stretching region near ~ 2900 cm^{-1} because of its complexity. The gas phase values for ν_2, ν_3 and ν_{11} are listed in Figs. 1-2 and Table 1 as a guide for the reader.

Gas phase CH_3NH_2 belongs to the C_s symmetry point group. Nine of the fifteen vibrational normal modes belong to the totally

symmetric representation, A', while six other normal modes belong to the A" representation. CH_3NH_2 can also adsorb on the surface with C_s symmetry if the plane containing the CN bond and bisecting the NH_2 group is perpendicular to the surface, or it could have a lower symmetry of C_1. For the case of C_s symmetry, the surface selection rule requires that only the nine A' modes be dipole allowed.[30] That is, for spectra collected in the specular direction, these nine A' modes should be the most intense. Seven peaks are observed which can be accounted for by eight or nine A' modes and two or three A" modes. In section 4, it is shown that the three A" modes ν_{10-12} have contributions from impact scattering. If they derive <u>all</u> of their intensity from impact scattering, the symmetry of surface CH_3NH_2 is C_s, and if not, the symmetry is C_1. In either case, the good agreement of our spectra with gas phase[21-23] and matrix isolated CH_3NH_2[27] supports the assignment of <u>molecular</u> CH_3NH_2 on all four of the surfaces.

Evidence also exists for bonding through the nitrogen lone pair. If CH_3NH_2 were bonded side-on instead of through the nitrogen lone pair, one would expect the methyl group to come in close proximity to the surface. This would allow formation of a three-centered M-H-C bond which would significantly weaken the C-H bond and lower the activation barrier to dissociation. Two examples of this effect have been reported in the literature. In the first case, the methyl group of toluene shows enhanced dissociation when compared with the phenyl hydrogens of toluene and benzene on Ni(100) and Ni(111).[31] In the

second example, spectroscopic evidence for C-H bond weakening was found using EELS for C_6H_{12} adsorbed on Ni(111) and Pt(111).[32] In addition to the expected CH stretch at ~ 2900 cm^{-1}, a very broad and intense feature at ~ 2600 cm^{-1}, indicative of a weakened CH bond, was observed. The lack of such a feature in Figures 1 or 2 supports a model in which the adsorbed CH_3NH_2 bonds to the surface through the lone pair, not a surprising conclusion, as this is the commonly accepted orientation for adsorbed ammonia.[3,4,33-39] The lone pair should be directed approximately perpendicular to the surface in order to keep the hydrogens away from the surface. Small variations of the angle of the lone pair will be discussed in section 4.

Careful examination of the CH_3 stretching region shows a very broad peak which is asymmetric to lower values. Spectra between 2500 and 3500 cm^{-1} are shown in Fig. 4. They are plotted on a logarithmic scale to facilitate comparison of peak shapes. The asymmetry of the ~ 2900 cm^{-1} peak cannot be accounted for by three gaussian peaks near the gas phase values and must be attributed to a small amount of hydrogen bonding, but not of the type discussed in the previous paragraph. It is also possible that lifetime broadening may contribute to this line shape.

2. Surface Composition

The question of molecular fragmentation cannot be addressed definitively because of the complexity of the spectra, but there is

little if any evidence for molecular fragments on Cr(100) and Ni(111), while there may be some on Ni(100) and Cr(111). Even substantial quantities of NH_2, NH, or CH_2 might not be able to be detected because peaks attributable to them would probably fall in a region of the spectrum where there are already peaks, although one cannot be completely sure of this because surface NH and NH_2 have yet to be identified by vibrational spectroscopy, and peaks due to CH_2 previously observed on Ru(001)[40] and Ni(111)[41] are very weak. Surface CH has been identified on a number of surfaces including Ni(111)[41] and Ni(100)[42] and has vibrational frequencies at ~ 790 cm^{-1} and ~ 3000 cm^{-1}, almost independent of the surface. As CH is very stable on both Ni(111)[41] and Ni(100)[42] at 300 K, one would expect decomposition of CH_3NH_2 on these surfaces to leave CH. From examination of the region near 790 cm^{-1} in Fig. 1, it can be seen that little or no CH is present on our Ni(111) sample, while there may be some on Ni(100). No evidence of CH is seen on either of the Cr surfaces, although, as mentioned previously, evidence for a large quantity of carbon is observed. The peak at ~ 1300 cm^{-1} on Cr(111) may be due to either a molecular fragment that cannot be identified or surface hydrogen.

3. Linewidths

There are enough differences in the linewidths of the internal modes of CH_3NH_2 on the four different surfaces to warrant a discussion. The broad linewidths on Cr(111) can be explained by the

availability of many inequivalent sites on this very open surface. The broad peak at ~ 500 cm^{-1} is evidence for a variety of adsorption sites of atoms (see Chapter VI). A distribution of such sites for CH_3NH_2 should inhomogeneously broaden its internal modes. On the other surfaces, the presence of some narrow lines indicates that selective broadening mechanisms are operative.

On Ni(111), the modes at 1010, 1485, 1570, ~ 2960, and ~ 3300 cm^{-1} are broad. The latter two are broad on all surfaces because symmetric and asymmetric modes overlap. The non-dipole modes ν_{10} and ν_{11}, which would normally have no intensity for spectra collected in the specular direction, contribute to these widths because of contributions from impact scattering. The three A' modes ν_4, ν_5, and ν_6 overlap and make the peaks at 1485 and 1570 cm^{-1} broad and unresolvable. The CN stretch at 1010 cm^{-1} is both separately resolved and broad, unlike the peaks at 730 cm^{-1} and 1195 cm^{-1}, which have the instrumental FWHM. By repeating the above analysis for the Ni(100) and Cr(100) surfaces, it appears that the only peak that is anomalously broad is the CN stretch, assuming that ν_9 on Ni(100) at 770 cm^{-1} is broad because of overlap with the CH bend if the CH fragment exists on Ni(100). It could also be that ν_9 is anomalously broad on Ni(100) only.

The CN stretch is broader than instrumental resolution on Cr(111), Ni(100), and Ni(111), but narrow on Cr(100). On Ni(100) and Ni(111), other peaks in the spectrum are narrow. An explanation of these facts necessarily involves an interaction of the CN bond with

the Ni surfaces and a lesser one for the CH_3 and NH_2 groups. Such an interaction is seen to be plausible by considering the orientation of CH_3NH_2 proposed in section IV A and shown in Fig. 5(a). The CN bond is almost parallel to the surface; a range of CN bond angles could cause differing interactions which inhomogeneously broaden the CN stretch, while keeping hydrogens in the CH_3 and NH_2 groups far enough above the surface to avoid interactions that would be observed with our resolution. Reasons for the different bond angles could be the dynamics of the CN bend or a distribution of slightly different sites, perhaps due to an incommensurate CH_3NH_2 overlayer. Incommensurate overlayers on Ni,[43] Pd,[44] Pt,[45] Co,[46] Rh,[47] and Ru,[48] have been observed for high coverages of CO and are to be expected when associative interactions become competitive with weak lone pair donor interactions.

These ideas are consistent with intensity differences that will be discussed in the next section, and the model will be further developed there.

4. Intensity Differences

There are striking intensity differences between the spectra on the two surfaces. Some of these differences can probably be attributed to the scattering mechanisms of EELS. Impact scattering makes a contribution to the intensities of some of the modes. The angular distribution of impact scattering is relatively flat,[49] and its intensity is proportional to the incident electron current.

Dipole scattering, on the other hand, is strongly peaked in the specular direction, and the intensity of inelastic features is proportional to the elastically scattered intensity. Any mechanism which lowers the elastic intensity, such as collection at angles other than specular or a decrease in surface order, will lower the intensity of dipole allowed inelastic features but will not change the intensity of the impact scattering features, provided that the incident electron current remains the same. A relative increase in the impact excited peaks is then observed.

Spectra that show enhancement of impact scattering in two ways are shown in Fig. 6. The Ni(100) surface has been exposed to 20 times the saturation exposure of CH_3NH_2, which has the effect of marginally increasing the coverage and inducing disorder, as evidenced by a fivefold decrease in the count rate of the elastic peak. The spectrum on the Ni(111) surface was collected 15° off specular. When these spectra are compared to those in Fig. 1, a relative increase in the peaks at ~ 1450 cm^{-1}, ~ 2950 cm^{-1}, and ~ 3300 cm^{-1} is seen, which is attributed to the contribution of impact scattering to these peaks.

The remaining intensity differences between the two surfaces are due to intrinsic differences of the interaction of CH_3NH_2 with the Ni surfaces. The most significant of these differences involves ν_8, the CN stretch at ~ 1010 cm^{-1}. On Ni(100), its intensity is approximately a factor of three lower than on Ni(111) in the spectra of Fig. 1. The other peaks in the Ni spectra show lesser intrinsic

intensity variations. On the Cr surfaces, the CN stretch is even more intense relative to the other vibrational modes than on the Ni surfaces.

It is possible to explain the intensity variations of the CN stretch on the basis of simple geometrical ideas. Figure 5(a) shows a schematic of surface CH_3NH_2 with the lone pair oriented perpendicular to the surface. The dynamical dipole moment, $d\mu/dr$, of the CN stretch is coaxial with the CN bond and has a normal component proportional to sin θ (the parallel component is screened by the surface in dipole scattering). The intensity of a transition is proportional to $\sin^2\theta$, and for small θ, only small changes in θ are required to effect large intensity differences. For the orientation in Fig. 5(a), $\theta \sim 19^\circ$, assuming the gas phase geometry for CH_3NH_2. The lesser intensity of the CN stretch on Ni(100) can be explained by a value of $\theta \sim 11^\circ$ and the greater intensity on Cr(100) by $\theta \sim 25^\circ$. These orientations are illustrated in Fig. 5(b-d). A larger angle on Cr(100) is consistent with a lesser interaction of the CN bond with this surface, as mentioned in the discussion of the narrow linewidth of the CN stretch on Cr(100). These angles are proposed for explaining why intensity differences occur and are not meant to be structural determinations. On any surface, a range of angles is probably present (as evidenced by broad peaks when the angles are small) and would have to be taken into account before more accurate angular determinations can be made.

Other peak intensities in the spectra are consistent with the

above ideas. Other symmetric modes such as ν_3 and ν_6 should show intensity variations like the CN stretch but do not because they overlap with the asymmetric modes ν_2 and ν_5, and also with modes of A" symmetry, ν_{11} and ν_{12}, which gain intensity through impact scattering. The presence of these other overlapping peaks inhibits drastic intensity changes. Much higher resolution would be needed in order to resolve these peaks and observe their intensity variations.

When the CN bond angle with the surface is increased on Cr(100), the NH bond angles with the surface are decreased. The amplitude of the NH_2 wag may then be suppressed because of the closer proximity of the NH_2 group with the surface. This possibility is consistent with the lower intensity of the NH_2 wag observed in the spectra on Cr(100).

5. Comparison Between Ni and Cr

In the introduction, the large differences in reactivity between Ni and Cr surfaces toward CO were mentioned. In the present chapter, we find the somewhat surprising conclusion that a substantial quantity of CH_3NH_2 is <u>undissociated</u> on Cr surfaces at 300 K, in contrast to the results for CO, where no undissociated species exist at 300 K. Two possibilities to explain this are as follows: Carbon or nitrogen atoms of initially dissociated CH_3NH_2 can partially passivate the surface and still allow subsequent molecular adsorption, while the presence of oxygen atoms from dissociated CO more totally passivates the surface and would do the same to subsequent exposure to

CH_3NH_2. Alternatively, CO could have a lower energy transition state for dissociation, perhaps because of back donation to the π^* orbitals, or perhaps for other reasons. Future experiments to determine the effect of preadsorbed C, N, and O on the adsorption of both CO and CH_3NH_2 would be useful. In a similar study on W(100), a c(2x2)-N overlayer was found to inhibit dissociation of NH_3.[52] The above results point to the possibilities of selective chemistry on W and Cr surfaces, which could someday find new uses in catalysis.

E. SUMMARY

A saturation coverage of CH_3NH_2 has been studied on the (100) and (111) surfaces of Ni and Cr at 300 K using EELS. Molecular CH_3NH_2 bonded through the nitrogen lone pair has been identified on each of the above surfaces. On the Cr surfaces, a substantial quantity of dissociation also occurs. CH may be present on Ni(100) but not in substantial amounts on the other surfaces. Other molecular fragments such as CH_2, NH_2, and NH are not detectable by EELS in the presence of CH_3NH_2. The CN stretch is inhomogeneously broadened on the Ni surfaces, and its intensity varies dramatically on the four surfaces. These observations have been explained by a model that takes different CN bond angles with the surface into account.

REFERENCES

*This chapter is based on experiments performed in collaboration with M.A. Schulz, and D.A. Shirley, to be submitted to J. Chem. Phys. for publication.

1. J.L. Gland and E.B. Kollin, Surf. Sci. 104, 478 (1981); J.L. Gland and E.B. Kollin, J. Vac. Sci. Technol. 18, 604 (1981).
2. B.A. Sexton and G.E. Mitchell, Surf. Sci. 99, 523 (1980).
3. M. Grunze, F. Bozso, G. Ertl, and M. Weiss, Appl. Surf. Sci. 1, 241 (1978).
4. M. Weiss, G. Ertl, and F. Nitschké, Appl. Surf. Sci. 2, 614 (1979).
5. G. Ertl, Surf. Sci. 47, 86 (1975).
6. D.H. Winicur, J. Hurst, C.A. Becker, and L. Wharton, Surf. Sci. 109, 263 (1981).
7. T.H. Lin and G.A. Somorjai, Surf. Sci. 107, 573 (1981).
8. M.A. Barteau, E.I. Ko, and R.J. Madix, Surf. Sci. 102, 99 (1981).
9. H. Papp, Surf. Sci. 129, 205 (1983).
10. P.A. Thiel, E.D. Williams, J.T. Yates Jr., and W.H. Weinberg, Surf. Sci. 84, 54 (1979).
11. K. Horn, M. Hussain, and J. Pritchard, Surf. Sci. 63, 244 (1977).
12. H. Pfnür, P. Feulner, and D. Menzel, J. Chem. Phys. 79, 4613 (1983).
13. J.N. Allison and W.A. Goddard III, Surf. Sci. 115, 553 (1982) and references therein.

14. G. Brodén, T.N. Rhodin, C. Brucker, R. Benbow, and Z. Hurych, Surf. Sci. 59, 593 (1976).

15. H. Kato, Y. Sakisaka, T. Miyano, K. Kamei, M. Nishijima, and M. Onchi, Surf. Sci. 114, 96 (1982).

16. E.G. Keim, F. Labohm, O.L.J. Gijzeman, G.A. Bootsma, and J.W. Geus, Surf. Sci. 112, 52 (1981) and references therein.

17. Z. Murayama, I. Kojima, E. Miyazaki, and I. Yasumori, Surf. Sci. 118, L281 (1982) and references therein.

18. R.W. Sheets and G. Blyholder, J. Catal. 67, 308 (1981).

19. Yung-Fang Yu Yao, J. Phys. Chem. 67, 2055 (1963); Yung-Fang Yu Yao, ibid. 68, 101 (1964).

20. C. Kemball and F.J. Wolf, Trans. Faraday Soc. 51, 1111 (1966).

21. H. Wolff and H. Ludwig, J. Chem. Phys. 56, 5278 (1972).

22. A.P. Gray and R.C. Lord, J. Chem. Phys. 26, 690 (1957).

23. K. Tamagake, M. Tsuboi, and A.Y. Hirakawa, J. Chem. Phys. 48, 5536 (1968).

24. S.L. Miles, S.L. Bernasek, and J.L. Gland, Proceedings of the 1982 third International Conference on Vibrations at Surfaces, J. Electron Spectrosc. Related Ph. 29, 239 (1983).

25. K. Christmann and J.E. Demuth, J. Chem. Phys. 76, 6308 (1982).

26. B.A. Sexton, Surf. Sci. 88, 299 (1979).

27. C.J. Purnell, A.J. Barnes, S. Suzuki, D.F. Ball, and W.J. Orville-Thomas, Chem. Phys. 12, 77 (1976).

28. G.W. Watt, B.B. Hutchinson, and D.S. Klett, J. Am. Chem. Soc. 89, 2007 (1967).

29. J.R. Durig, S.F. Bush, and F.G. Baglin, J. Chem Phys. 49, 2106 (1968).

30. H. Ibach and D.L. Mills, Electron Energy Loss Spectroscopy and Surface Vibrations (Academic Press, New York, 1982).

31. C.M. Friend and E.L. Muetterties, J. Am. Chem. Soc. 103, 773 (1981).

32. J.E. Demuth, H. Ibach, and S. Lehwald, Phys. Rev. Lett. 40, 1044 (1978).

33. F.P. Netzer and T.E. Madey, Surf. Sci. 119, 422 (1982).

34. G.B. Fisher, Chem. Phys. Lett. 79, 452 (1981).

35. C. Benndorf and T.E. Madey, Surf. Sci. 135, 164 (1983).

36. T.E. Madey, J.E. Houston, C.W. Seabury, and T.N. Rhodin, J. Vac. Sci. Technol. 18, 476 (1981).

37. R.J. Purtell, R.P. Merrill, C.W. Seabury, and T.N. Rhodin, Phys. Rev. Lett. 44, 1279 (1980); C.W. Seabury, T.N. Rhodin, R.J. Purtell, and R.P. Merrill, Surf. Sci. 93, 117 (1980).

38. G.B. Fisher and G.E. Mitchell, Proceedings of the 1982 third International Conference on Vibrations at Surfaces, J. Electron Spectrosc. Related Ph. 29, 253 (1983).

39. W. Erley and H. Ibach, Surf. Sci. 119, L357 (1982).

40. P.M. George, N.R. Avery, W.H. Weinberg, and F.N. Tebbe, J. Am. Chem. Soc. 105, 1393 (1983).

41. J.E. Demuth and H. Ibach, Surf. Sci. 78, L238 (1978).

42. A.G. Baca, M.A. Schulz, and D.A. Shirley, unpublished results.

43. H. Conrad, G. Ertl, J. Küppers, and E.E. Latta, Surf. Sci. 57, 475 (1976).

44. A.M. Bradshaw and F.M. Hoffmann, Surf. Sci. 72, 513 (1978).

45. G. Ertl, M. Neumann, and K.M. Streit, Surf. Sci. 64, 393 (1977).

46. M.E. Bridge, C.M. Comrie, and R.M. Lambert, Surf. Sci. 67, 393 (1977).

47. P.A Thiel, E.D. Williams, J.T. Yates Jr., and W.H. Weinberg, Surf. Sci. 84, 54 (1979).

48. E.D. Williams and W.H. Weinberg, Surf. Sci. 82, 93 (1979); G.E. Thomas and W.H. Weinberg, J. Chem. Phys. 70, 1437 (1979).

49. W. Ho, R.F. Willis, and E.W. Plummer, Phys. Rev. Lett. 40, 1463, (1978).

50. C. Egawa, S. Naito, and K. Tamaru, Surf. Sci. 131, 49 (1983).

Table 1

Vibrational frequencies (cm^{-1}) of CH_3NH_2 in a) the gas phase, b) an argon matrix, c) cis-$[Pt(CH_3NH_2)_2Cl_2]$, d) solid crystalline CH_3NH_2 and adsorbed on e) Ni(100), f) Ni(111), g) Cr(100), and h) Cr(111).

Mode		gas[a]	Ar[b]	cis-$[Pt(CH_3NH_2)_2Cl_2]$[c]	Solid[d]	Ni(100)	Ni(111)	Cr(100)	Cr(111)
A'									
ν_1	NH_2 sym. stretch	3360	3352	3270,3240,3140	3260	3255	3240	3290	3285
ν_2	CH_3 asym. stretch	2962	2967	3016,3000,2952	2899,2881,2865	2960	2960	2960	2960
ν_3	CH_3 sym. stretch	2820	2819	2928,2896	2808,2793	2820	2820	2820	2820
ν_4	NH_2 deformation	1623	1623	1596,1581,1575	1651,1636	1570	1570	1595	1545
ν_5	CH_3 asym. def.	1474	1464	1465,1453	1467	1445	1485	1465	1445
ν_6	CH_3 sym. def.	1430	1450	1429,1417,1405	1441				
ν_7	CH_3 rock	1130	1140	990	1182	1220	1195	1185	1190
ν_8	CN stretch	1044	1052	1037,1017	1048	1030	1010	1000	1020
ν_9	NH_2 wag	780	796	740	955,913	750	730	-	-

Table 1 (continued)

Mode		gas[a]	Ar[b]	cis-$[Pt(CH_3NH_2)_2Cl_2]$[c]	Solid[d]	Ni(100)	Ni(111)	Cr(100)	Cr(111)
A"									
ν_{10}	NH_2 asym. stretch	3424	3415	-	3332,3330	3320	3305	3350	3340
ν_{11}	CH_3 asym. stretch	2985	2991	-	2963,2942,2918	2985	2985	2985	2985
ν_{12}	CH_3 asym. def.	1485	1481	-	1500	-	-	-	-
ν_{13}	NH_2 twist	-	-	-	1353	-	-	-	-
ν_{14}	CH_3 rock	(1195)	-	-	1182	-	-	-	-
ν_{15}	torsion	265	-	-	-	-	-	-	-

a) Refs. 23-25

b) Ref. 30.

c) Ref. 31. The designations A' and A" as well as the mode assignments do not apply.

d) Ref. 32. The designations A' and A" do not apply.

Table 2

The boiling point and desorption temperatures (in degrees Kelvin) of a multilayer are given for a number of polar molecules adsorbed on the indicated surfaces. Where available the desorption temperature of a second adsorbed layer is also indicated.

	boiling point of pure adsorbate	desorption temperature of multilayer	desorption temperature of 2nd layer
H_2S	212	<110[a]	<110[a]
NH_3	240	100-115[b-d]	130-150[b-d]
CH_3NH_2	267	-	-
CH_3OH	338	140-165[e-g]	140-165[e-g]
H_2O	373	150-170[h-l]	180[h]

a) H_2S/Ni(100). A.G. Baca, M.A. Shulz, and D.A. Shirley, J. Chem. Phys. 81, xxxx (1984).

b) NH_3/Ni(111). Ref. 35.

c) NH_3/Pt(111). Ref. 36.

d) NH_3/Ru(001). Ref. 37.

e) CH_3OH/Mo(100), Ref. 26.

f) CH_3OH/Pd(100), Ref. 27.

g) CH_3OH/Pt(111). B.A. Sexton, Surf. Sci. 102, 271 (1981).

Table 2 (continued)

h) H_2O/Ru(001). P.A. Thiel, F.M. Hoffmann, and W.H. Weinberg, J. Chem. Phys. 75, 5556 (1981); T.E. Madey, and J.T. Yates, Jr., Chem. Phys. Lett. 51, 77 (1977).

i) H_2O/Rh(111). J.J. Zinck and W.H. Weinberg, J. Vac. Sci. Technol. 17, 188 (1980).

j) H_2O/Pt(111). G.B. Fisher and J.L. Gland Surf. Sci. 94, 446 (1980).

k) H_2O/Ir(110). T.S. Wittrig, D.E. Ibbotson, and W.H. Weinberg, Surf. Sci. 102, 506 (1981).

l) H_2O/Pt(100). H. Ibach and S. Lehwald, Surf. Sci. 91, 187 (1980).

Figure Captions

Figure 1. EEL spectra for a saturation coverage of CH_3NH_2 on Ni(100) at 300 K. E_0 = 2.50 eV, $\theta_i = \theta_s = 45°$. I_0 = 44 KHz for Ni(100) and I_0 = 58 KHz for Ni(111).

Figure 2. EEL spectra for a saturation coverage of CH_3NH_2 on Cr(100) and Cr(111) at 300 K. E_0 = 2.45 eV, $\theta_i = \theta_s = 45°$. I_0 = 58 KHz for Cr(100) and I_0 = 41 KHz for Cr(111).

Figure 3. EEL spectra of (a) c(2x2)-N/Cr(100) surface, E_0 = 2.01 eV, (b) 2.0 L of CO/Cr(100), E_0 = 2.12 eV, and (c) a saturation coverage of CH_3NH_2/Cr(100), E_0 = 2.45 eV. All spectra were taken at 300 K with $\theta_i = \theta_s = 45°$.

Figure 4. Logarithmic plots of the CH_3 and NH_2 stretching regions for CH_3NH_2 adsorbed on Ni(100), Ni(111), Cr(100), and Cr(111). The lines through the data are the result of a smoothing procedure, not a best fit.

Figure 5. Possible orientations of adsorbed CH_3NH_2 which are consistent with the intensity of the CN stretch on the different surfaces. (a) The nitrogen lone pair is perpendicular to the surface and the CN bond is at an angle θ from the surface. (b) The CN bond is more parallel to the Ni(100) surface, (c) less parallel on Ni(111), and (d) tilted further away on Cr(100). This figure is meant to illustrate orientations of CH_3NH_2 and does not imply site or structure determinations.

Figure 6. Assessing the contribution of impact scattering in the spectra of Fig. 1 by comparing to (a) a Ni(100) surface exposed to 20 times the saturation coverage of CH_3NH_2, E_o = 2.50 eV, $\theta_i = \theta_s = 45^\circ$, I_o = 8.6 KHz and (b) off specular EELS of a saturation coverage of CH_3NH_2/Ni(111) with E_o = 2.50 eV, $\theta_i = 45^\circ$, $\theta_s = 60^\circ$, I_o = 8.6 KHz.

CH_3NH_2: Ni(100), Ni(111)

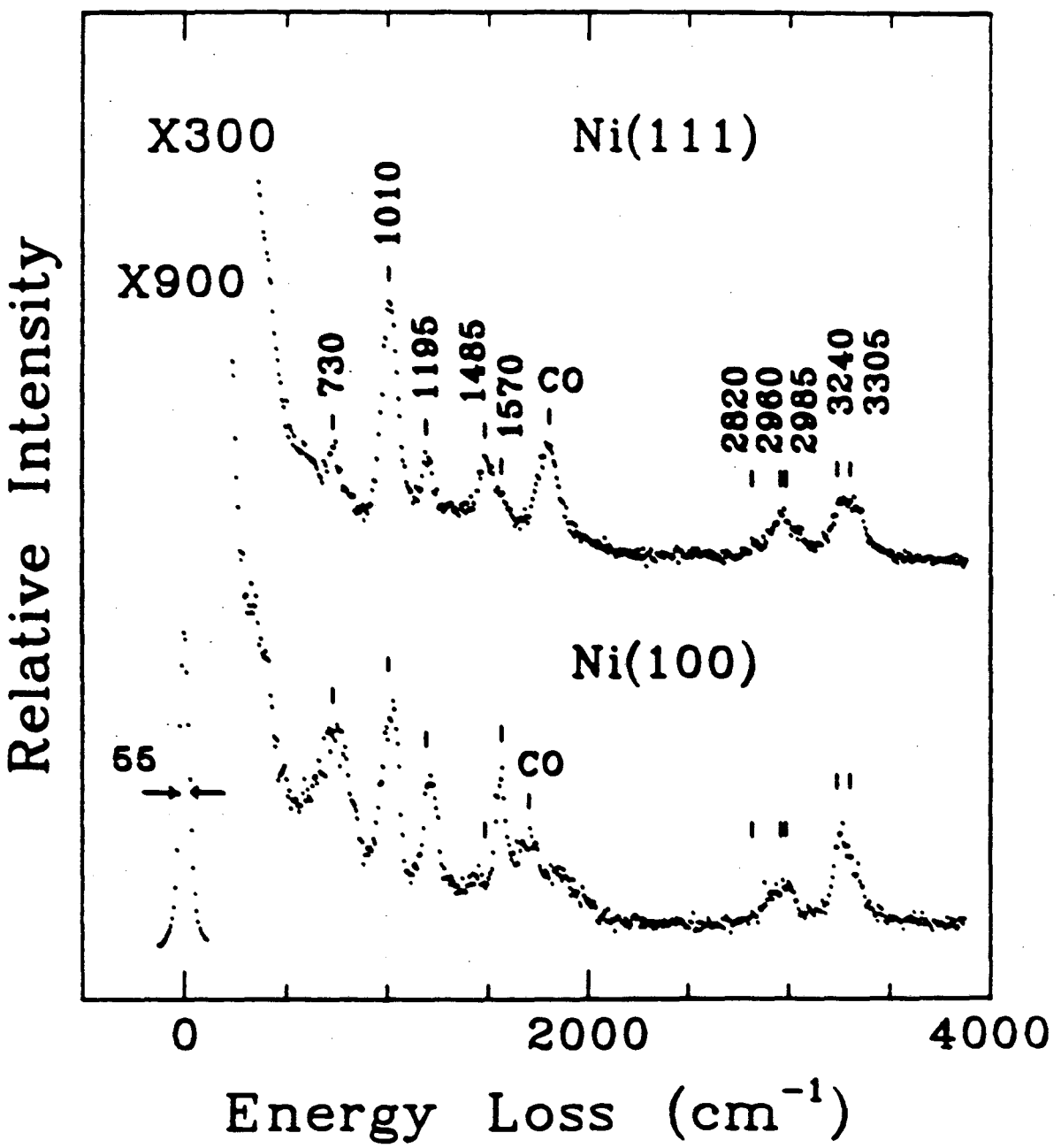

XBL 8412-5206

Figure 1

CH_3NH_2: Cr(111), Cr(100)

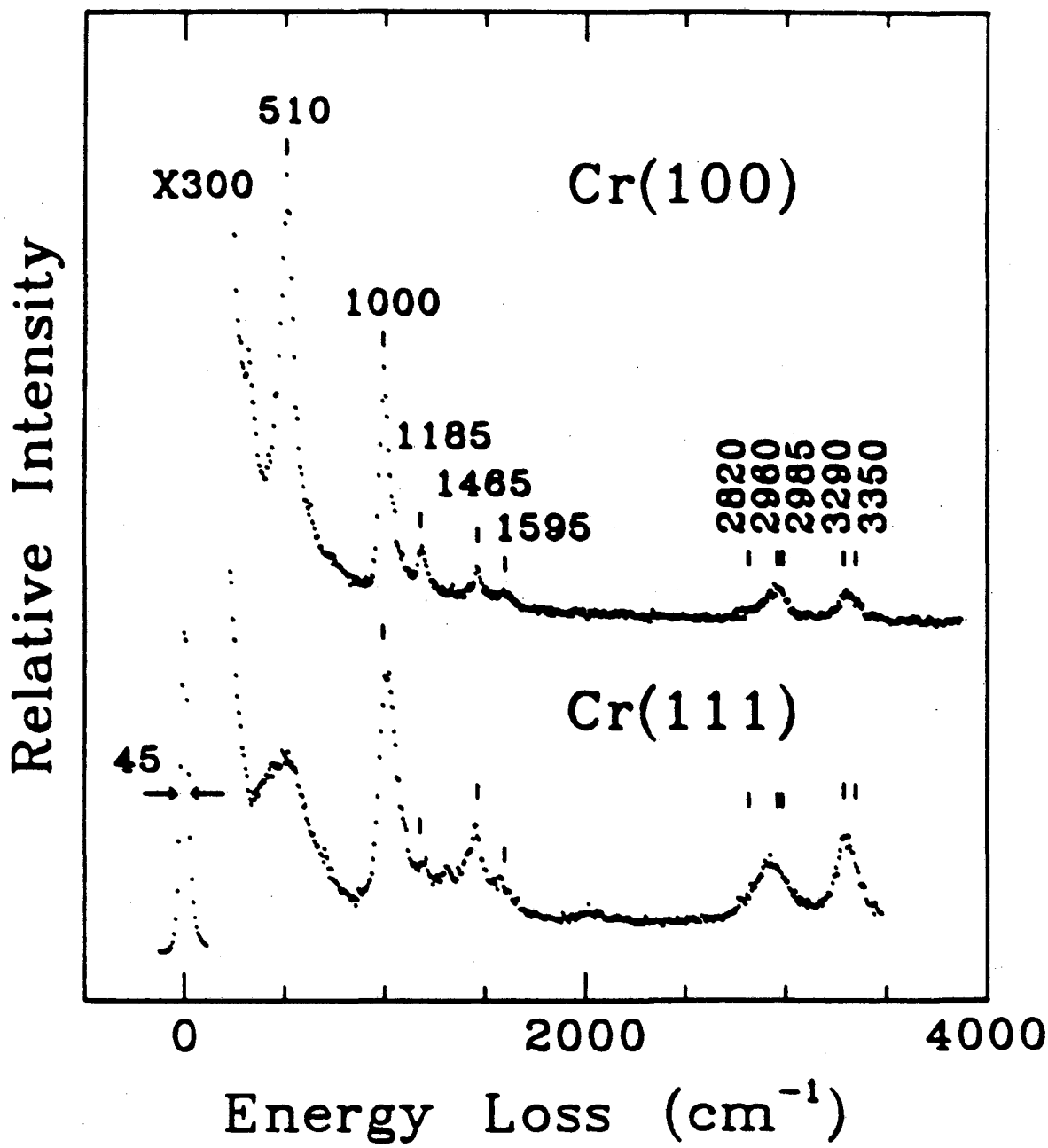

XBL 8412-5208

Figure 2

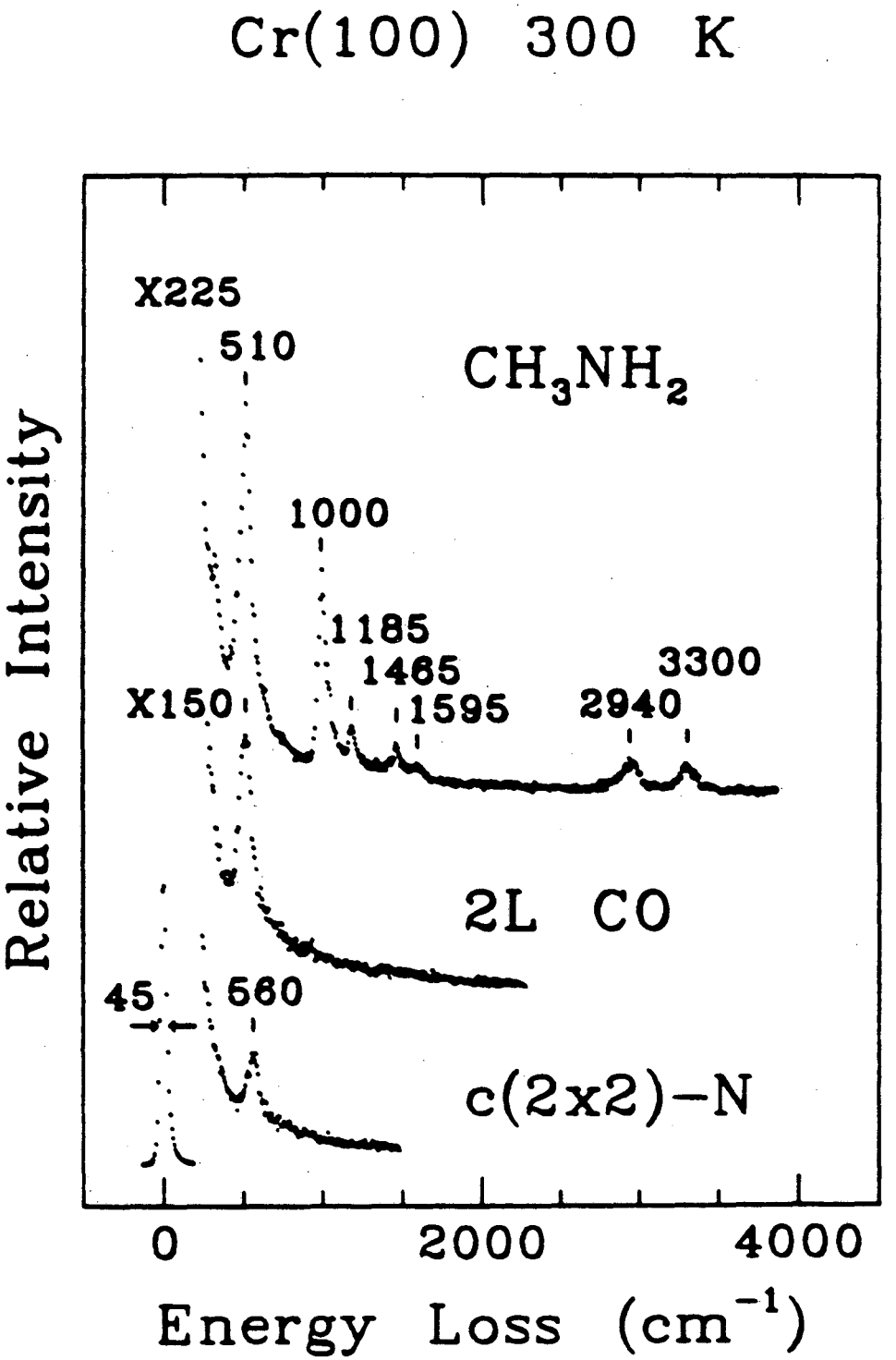

XBL 8412-5209

Figure 3

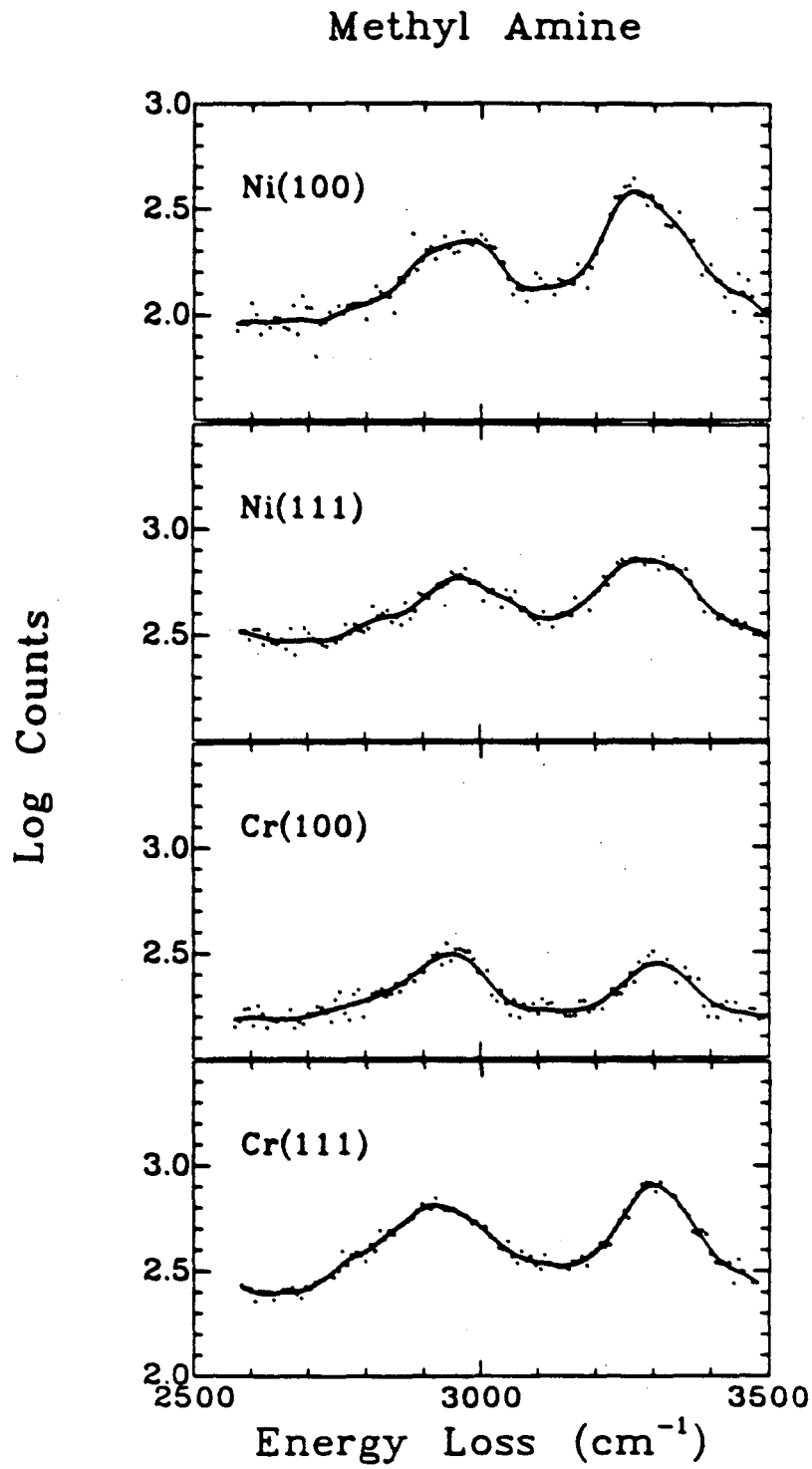

XBL 851-1060

Figure 4

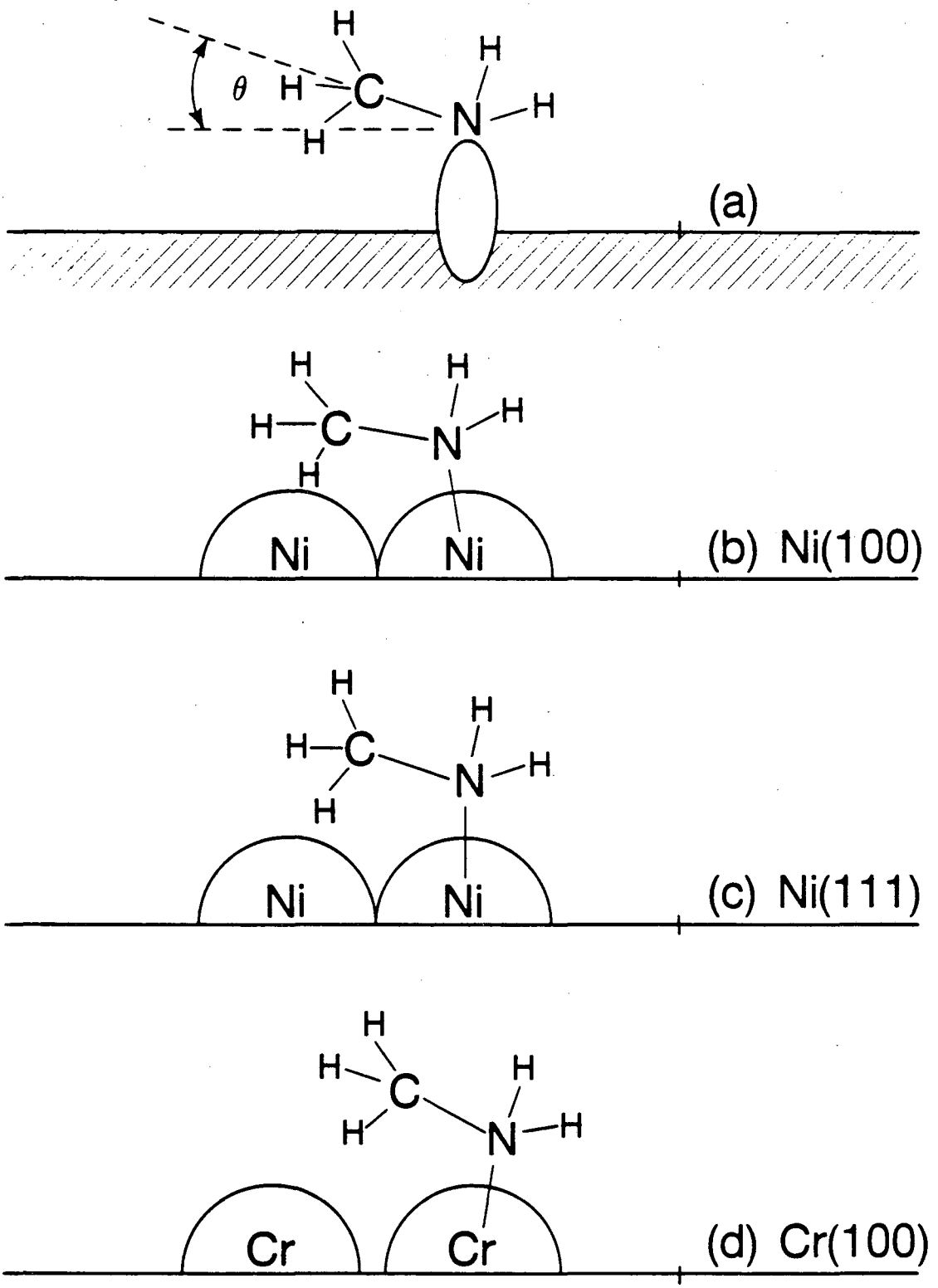

XBL 8412-5383

Figure 5

CH_3NH_2: Ni(100), Ni(111)

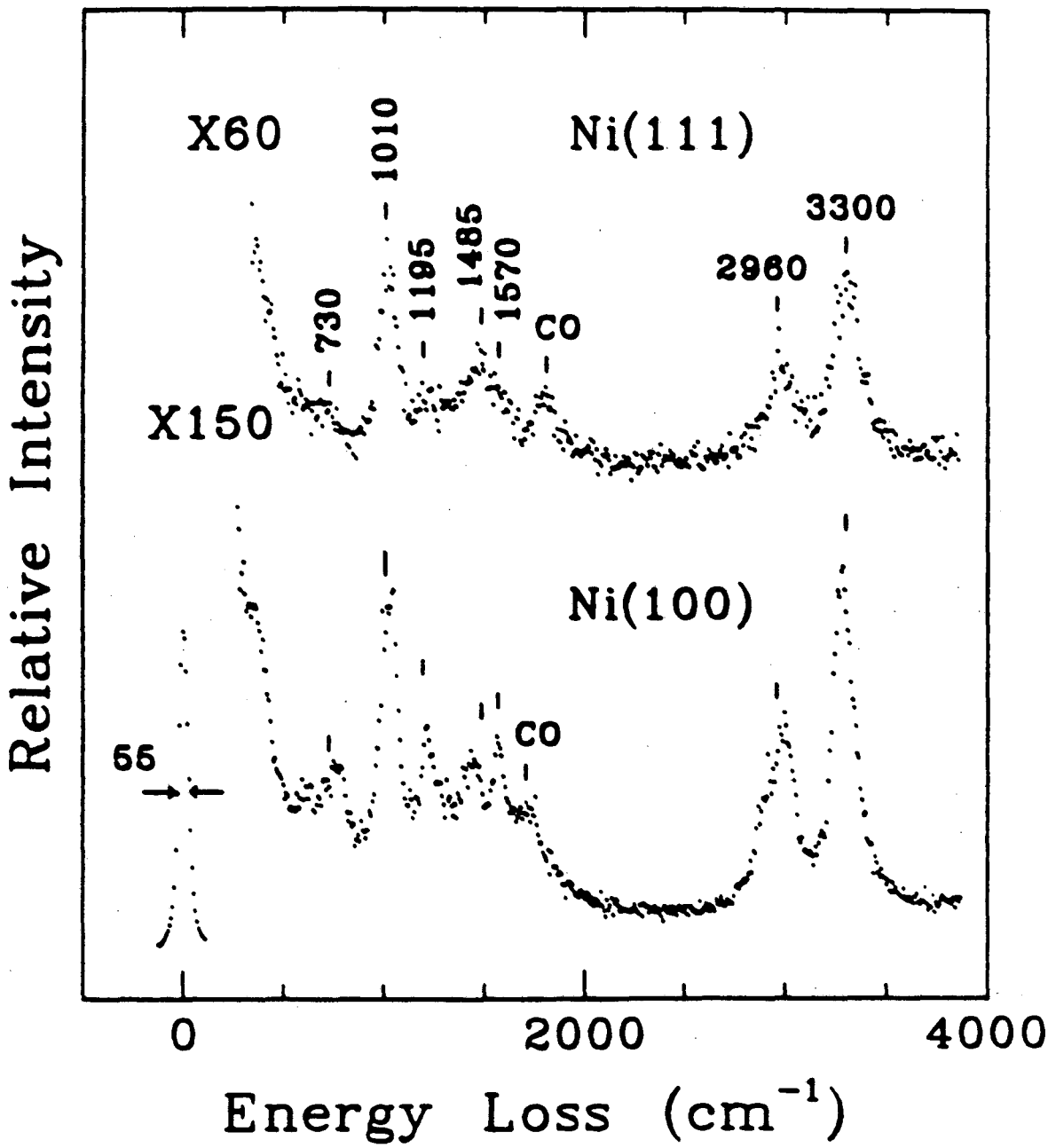

XBL 8412-5207

Figure 6

V. THE INITIAL OXIDATION OF Cr(100)*

A. INTRODUCTION

It is well known that chromium-containing surfaces form a protective oxide layer which makes them extremely stable against corrosion. It is thought that the stability of the oxide Cr_2O_3 plays a major role, and for this reason a number of studies of the oxidation of chromium metal have been carried out. Low energy and reflection high energy electron diffraction (LEED and RHEED)[1-3] as well as scanning transmission electron microscopy micro-diffraction (STEM-MD)[4] have been used to follow the progression from two dimensional order in chemisorption to three dimensional order in Cr oxides. Auger electron spectroscopy and x-ray photoelectron spectroscopy (XPS) have been used to determine the thickness of oxide layers and to follow the kinetics of oxide growth at various temperatures.[5] Studies using work function measurements[6,7] have attempted to identify the various stages of a model of low temperature oxidation proposed by Mott and Fehlner.[8] All of the above studies observe the growth of a thin oxide layer that is common to many metals, but many details of the mechanism of the oxidation are missing, especially in the early stages. This study addresses the chemisorption and initial oxidation of Cr(100) in the temperature range 300-1175 K using LEED, Auger, and EELS.

Several workers using vibrational EELS have observed high frequency modes[9-11] that have been ascribed to subsurface sites of oxygen which are proposed to be precursors of oxidation, with metal

atoms maintaining the registry of the pure metal.[12] In an electronic EELS study of the oxidation of Cr(110), a proposed step in the oxidation can be considered consistent with the vibrational EELS model.[13] As yet there has been no detailed study of such proposed subsurface sites on any metal and their relation to subsequent oxide growth. In the present EELS study, a model of initial oxide domain growth and its relation to subsurface oxygen at different temperatures is presented which lends credence to the previously proposed idea of subsurface sites as precursors to oxidation. The model sheds light on the initial transition from the chemisorbed to the oxide state that is lacking in the review of Mott and Fehlner.[8]

B. EXPERIMENTAL

Chromium is a very reactive metal and most studies of Cr(100) did not achieve satisfactory surface cleanliness.[2,3,6,14] Clean Cr(100) was once thought to exhibit a c(2x2) LEED pattern,[14] but recent studies of the truly clean surface show (1x1) LEED patterns.[15-17] The Cr(100) crystal used in this study showed a (1x1) LEED pattern, which emerged after several weeks of the treatment described in Chapter II and was found to be a sensitive indicator of the surface cleanliness.

Both ambient and effusive beam dosing were used for O_2 exposures. Coverages that were formed by effusive beam dosing are indicated in the data figures. When effusive beam dosing was used for O_2 exposures, approximate values in langmuirs were estimated using

Auger intensities. LEED and Auger measurements were made with LEED optics. Some surfaces were annealed using electron beam heating to a given temperature for approximately five minutes, and temperatures were calibrated with an optical pyrometer. All EEL spectra were taken at 300 K, with an impact energy of 2.06 eV. Both the angles of incidence and scattering were 55° for all spectra.

C. RESULTS

Previous workers have observed some or all of the LEED pattern sequence (1x1) → c(2x2) → (1x1) with increasing O_2 exposure.[1-3,6,14,15] EELS measurements are reported here at coverages where these LEED patterns occur. The coverage dependent EEL spectra of O_2 adsorption on Cr(100) at 300 K are shown in Fig. 1. For a 0.7 L exposure a very weak feature is seen at 545 cm^{-1}. This and the absence of an intense O=O stretching frequency at ~ 800-1000 cm^{-1} in all further spectra are indicative of dissociative chemisorption of oxygen, which is very characteristic of oxygen on metals in this temperature range. At this coverage, a c(2x2) LEED pattern, which was once thought to be characteristic of the clean surface,[14] is visible. The weak intensity of the Cr-O stretch as well as the Auger intensity seems to indicate that there need not be very much oxygen on the surface at a coverage where a c(2x2) LEED pattern is observed. A 1.5 L exposure gives an EEL spectrum similar in intensity and frequency to the 0.7 L exposure. As the exposure of oxygen is increased to ~ 5 L, the sticking coefficient increases, the Cr-O stretch becomes much more

intense, the LEED pattern changes to (1x1), and the mean Cr-O stretching frequency shifts to 520 cm^{-1}. The peak becomes broad and asymmetric compared with the relatively narrow c(2x2) peak, and an envelope of weaker features grows in at the high energy side. As the exposure is increased further to ~ 60 L, the peak grows broader first, and then narrows considerably as a strong peak emerges at 635 cm^{-1}. At this point the Auger ratio O(KLL)/Cr(L,$M_{2,3}M_{4,5}$) is nearly saturated. Diffraction studies of Cr(100) show that a thin layer of rhombohedral Cr_2O_3 forms at room temperature,[1-4] which suggests assigning the 635 cm^{-1} peak as the stretching frequency of the oxide Cr_2O_3. All of the spectra in Fig. 1 except for the 0.7 L exposure are inhomogeneously broadened beyond the experimental resolution of 55 cm^{-1}. The initial broadening of the spectra followed by narrowing suggests a high defect density associated with the initial formation of the oxide; as the oxide layer thickens, the Cr_2O_3 becomes more ordered.

The results of Fig. 1, described above, are for room temperature exposures. A different way of adding O_2 to the crystal with thermal processing steps between exposures is described now. When Cr(100) is exposed to ~ 3 L of O_2 and the surface is heated for 5 minutes to 625 K, the spectrum (a) in Fig. 2 is obtained. A single frequency at 495 cm^{-1} is observed, downshifted from 520 cm^{-1} where the room temperature peak would be expected. When the surface is then annealed to 1175 K, spectrum (b) is obtained. There is essentially no change in the spectrum other than an increase in intensity. Auger spectra

show that there is approximately the same amount of oxygen on the surface for both (a) and (b). A c(2x2) LEED pattern is observed for the samples (a) and (b). Addition of ~ 1 L more of O_2 and a brief heating of the surface to 625 K results in the surface characterized by spectrum (c). Three additional features at 630, 755, and 960 cm^{-1} are observed. The 630 cm^{-1} shoulder was shown above to be characteristic of the oxide. The 755 cm^{-1} and 960 cm^{-1} peaks are never observed on samples prepared at room temperature and not heated. Upon heating the sample to 1175 K all features disappear except the 495 cm^{-1} Cr-O stretch of chemisorbed oxygen. Auger spectra show an increase of oxygen from (b) to (c) and no change in going to (d). Further addition of ~ 1 L O_2 and heating first to 625 K and then to 1175 K (spectra (e) and (f)) repeat the trends found in (c) and (d). The 625 K anneal produces metastable peaks at 630, 755, and 960 cm^{-1} which are removed by a 1175 K anneal. The LEED pattern for (c-f) reverts to (1x1). Auger intensities were measured after each EEL spectrum in Fig. 2 and are plotted in Fig. 3. The sensitivity factors for oxygen and chromium which are needed to calibrate the oxygen coverages were determined by choosing a saturation coverage of CO dissociated on Cr(110) as a reference compound (Chapter VI), for which it is believed that there is 0.5 monolayer of oxygen.

The vibrational modes corresponding to the 755 cm^{-1} and 960 cm^{-1} peaks have a distinct temperature behavior. They are prominent after a 625 K anneal but not at room temperature nor a higher

temperature anneal (1175 K). In order to put forward a hypothesis to explain this, the EELS and Auger intensities will be compared for each sample (a-f) described in Fig 2. To do this, it will be assumed that the EELS intensity is proportional to the number of surface oxygen atoms. That this is not exactly correct can be seen by comparing traces (a) and (b) and also in the discussion of CO intensities on Cr(100) and Cr(110) in Chapter VI. However, for different exposures at a given temperature this assumption should be more reasonable, and in any case, this is the best method available for comparing oxygen in the first atomic layer to that in the first several layers. As can be seen in Fig. 4, the EELS intensity of the 495 cm^{-1} peak after 1175 K anneals remains relatively flat above a coverage of 0.6 monolayer, while the Auger intensity (proportional to total coverage on and below the surface) increases with exposure and is nearly the same for anneals to 625 K and 1175 K. Because of the short screening length in metals, EELS is sensitive primarily to atoms above the surface, while Auger is sensitive to several atomic layers deep, a region which we'll call the "near surface" layer. The results shown in Figs. 3-4 are consistent with the interpretation that ~ 0.6-0.7 monolayer of oxygen is stable on the surface at 1175 K and that any extra oxygen diffuses into the near surface layer, with ~ 10-20% diffusing into the bulk each time a 5 min. anneal at 1175 K is carried out. Presumably, longer anneals will result in more of the oxygen leaving the near surface layer, but this is not central to these conclusions. The data provide evidence for competition between diffusion into the bulk

(favored at high temperature) and oxide nucleation and growth (favored at room temperature).

The situation is most interesting for the 625 K anneals. The oxide (625 cm^{-1} shoulder) is less pronounced than at room temperature. Diffusion at 625 K should be intermediate between that at 300 K and 1175 K. Enhanced diffusion of oxygen at 625 K relative to 300 K can reduce the domain size of Cr_2O_3. The activation energy needed for place exchange of oxygen and Cr atoms, which presumably is the second step (after chemisorption) in oxide formation,[8,18] is more readily available at 625 K than at 300 K. A model consistent with these ideas and the experimental data is proposed and developed in the rest of this section.

It is proposed that oxide growth occurs primarily through expansion of domain size at 300 K, while frequent creation of new, smaller domains occurs at 625 K. The 960 cm^{-1} and possibly also the 755 cm^{-1} peaks are attributed to oxygen in subsurface sites that are precursors to oxide formation. The model is illustrated in Fig. 5. No particular size or shape of the domains are deduced from the data, and none are implied in Fig. 5.

The above ideas are consistent with the experimental data. If a smaller number of oxide domains are present at 300 K, then fewer precursor subsurface sites should have been formed. This is consistent with a lower intensity at 960 cm^{-1} in the 5 L exposure of Fig. 1 compared to spectra (c) and (e) of Fig. 2. The disappearance of the 960 cm^{-1} peak by ~ 8 L implies some coalescence of the room

temperature domains. In the spectra of Fig. 2, (c) and (e) are qualitatively similar yet quantitatively different in a way that supports the above model. The same treatment was carried out in going from (b) → (c) as from (d) → (e). The only difference in the prepared surfaces is that (d) contains oxygen in the near surface layer and (b) does not. The oxygen in the near surface layer is available to form oxide when an oxide domain nucleates in (e) but not in (c). This is manifested by a greater relative intensity at 630 cm^{-1} in spectrum 2(e) compared to 2(c) and a lesser intensity at 960 cm^{-1} in 2(e) vs. 2(c).

The short screening length in metals is responsible for screening the dipole fields generated by vibrating oxygen atoms in the near surface layer and below if this layer remains metallic in character. When the near surface area is largely oxidized, as in the 60 L exposure of Fig. 1, the Cr atoms are no longer effectively screened, and the intensity of the resulting Cr-O stretch at 635 cm^{-1} increases dramatically. For spectrum (f) of Fig. 2, where Auger analysis shows that there are ~ 15-20% as many oxygen as Cr atoms in the near surface layer, compared with 60-70% in the first layer, the near surface layer is largely metallic and EELS is insensitive to oxygen below the surface. These ideas are consistent with the above model.

Although the proposed model is plausible, intuitively appealing, and self-consistent, it is also possible that bridge and atop sites are responsible for the 755 and 960 cm^{-1} peaks. The main arguments

against such an interpretation are as follows: It is difficult to explain why the presence of 15% oxygen in the near surface layer, a layer which remains predominantly metallic in character according to the previous discussion, should affect the populations of the bridge and atop sites. These populations are noticeably different in spectra (c) and (e) of Fig. 2. The arguments previously presented for the intensity differences in 2(c) and 2(e) are more persuasive, although the alternative possibility of bridge and atop sites cannot be ruled out.

D. DISCUSSION

Fehlner and Mott in 1970 reviewed the oxidation of metals and proposed a model of low temperature oxidation[8] (room temperature and below) that revised the earlier ideas of Mott[19] and Cabrera and Mott.[20] Since then, much has been learned about chemisorption, adding new detail to the first stage of oxidation. Several workers have studied the transition from the chemisorption of oxygen on Cr surfaces to the oxide. Since most of these workers examine the ideas of Fehlner and Mott in relation to their respective works, a brief review of the Fehlner and Mott model is given below, followed by a discussion of previous oxidation results on Cr surfaces.

Room temperature oxidation begins rapidly and the kinetics of oxygen uptake are linear. The oxidation then slows down to logarithmic kinetics and a limiting oxide thickness usually less than 25 Å is reached. The logarithmic growth can have a second stage in

which ion transport may occur through channels such as grain boundaries that depend on the structure of the oxide. The mechanism for oxide growth is explained as follows: Oxygen ions formed on the surface of the thin oxide film interact with an image charge formed in the metal. This image force lowers the activation energy for a process called place exchange in which a Cr ion changes place with an oxygen ion. If the oxide film is thin enough, the image energy may be comparable to the binding energy of a Cr atom and place exchange can occur spontaneously. Linear kinetics are then observed. If the oxide layer is thicker, a density of oxygen ions on the surface produces a voltage across the film, which can either lower the activation barrier for continued slower place exchange or oxygen transport through the oxide film, if suitable channels in the film are present. Such channels could be present in some types of amorphous, glassy oxides or at the grain boundaries of crystallites. Eventually the oxide thickness becomes large enough that negligible lowering of the activation barrier occurs and further oxidation can only occur at elevated temperatures. The concept of place exchange is a modification of Eley and Wilkinson[18] to the earlier ideas of Cabrera and Mott.[20]

There is general agreement from diffraction studies that rhombohedral Cr_2O_3 is formed on Cr(100) with high O_2 exposures, although there is conflict about the orientation.[1-4] The STEM-MD study also proposes a spinel-like oxide that precedes the rhombohedral Cr_2O_3. This proposal is not in conflict with the vibrational EELS

data, as a great broadening in the spectra of Fig. 1 is observed before the Cr_2O_3 oxide is fully developed which could be because of initial growth of the spinel-like structure and the transition to rhombohedral Cr_2O_3.

Allen et al.[5] studied the oxidation on Cr metal using Auger and XPS. They observed a saturation of the O(KLL) Auger signal above ~ 10 L and a gradual growth of the oxide through the core level shifted Cr 2p peaks. At 600 K thicker layers of oxide can be grown. They obtained information about the kinetics of oxide growth at various temperatures and compared this to expressions derived by Fehlner and Mott,[8] but the limited resolution of XPS is not suited to uncovering the details of initial oxide growth.

Peruchetti et al.[6] studied the initial oxidation of Cr(100). They assumed that oxygen chemisorbed above the surface will produce a work function change and oxygen incorporated into the surface will not. Using these assumptions, they concluded that rapid linear oxidation occurs between 0-4 L and that no oxygen is observed above the surface. Between 4-6 L, they concluded that oxygen adsorbs on top and that a limiting surface coverage of $\theta = 0.25$ is attained. Place exchange was proposed to occur between 0-4 L, adsorption on the surface between 4-6 L, and continued slow oxidation between 6-30 L. These proposals are inconsistent with the EELS data and with commonly held ideas of chemisorption. A Cr-O frequency at ~ 520 cm^{-1} characteristic of chemisorption and a gradual transition towards the oxide above ~ 5 L is observed in this work. The EELS data after 625 K

and 1175 K anneals indicate that ~ 0.6 monolayer of chemisorbed oxygen above the surface is very stable.

Sakisaka et al.[13] studied the initial oxidation of Cr(110) using electronic EELS. They described the process in four steps: (1) dissociative adsorption below 2 L, (2) incorporation of oxygen below the surface between 2-6 L, (3) rapid oxidation between 6-15 L, and (4) slow thickening of the film. The latter two stages are consistent with the model of Fehlner and Mott, while step (2) is consistent with the model proposed here. Steps (3) and (4) are not addressed here.

This model implies that the kinetics of place exchange are different for the initial nucleation of an oxide domain and for place exchange occurring in an already existing domain. No attempt will be made to analyze the kinetics, but some observations can be made. The model seems to imply that at least in the case of Cr(100) place exchange at room temperature is an activated process. However, it is possible that place exchange on Cr(100) is unactivated. If such is the case, then at 300 K subsurface sites are populated instantaneously as soon as the surface coverage is high enough, and therefore, while O_2 is still being exposed. During the 625 K anneals, no O_2 was being exposed. The different kinetics observed at 300 K and 625 K can then be rationalized by proposing different sticking coefficients and/or atom mobilities on parts of the surface above oxide domains at 300 K. Clearly, further experiments are needed to determine whether the model developed in this chapter is general to oxidation or specific to the sequence of experiments presented here.

If the model proposed in this chapter is general, then it must be incorporated into the model of low temperature oxidation. The concept of place exchange is not challenged here, but the details of its occurrence can be made more explicit and the energetics rationalized. The energetics of a general place exhange mechanism are readily supplied because an oxide is thermodynamically more stable than a metal and bond energies of weakly chemisorbed atoms which are adsorbed at high coverages are small. In that case, the activation energy of place exchange is more important than the energetics and according to Fehlner and Mott,[8] it is supplied by the image charge initially and by the Cabrera-Mott field at greater oxide thicknesses. However, the energetics may be different and more important for the first occurrence of place exchange which creates a nucleus for oxide growth. It is difficult to say what kind of an oxide can be formed initially, how many of the neighboring Cr atoms have oxide character, and if so how much. Oxide character implies Cr-O bond lengths that are oxide-like, and for the first subsurface oxygen atom this would imply weaker metal-metal bonds which may or may not be energetically favorable overall. On the other hand, initial place exchange to create a subsurface interstitial site is virtually guaranteed to be energetically favorable by virtue of not having to break any metal-metal bonds, and this at the same time rationalizes the high frequency ascribed to the site.[12]

E. SUMMARY

The chemisorption and initial oxidation of Cr(100) has been studied by EELS, Auger, and LEED. Chemisorption leads to Cr-O stretching frequencies between 495-545 cm^{-1}. The sticking coefficient between 0-1.5 L, coverages at which a c(2x2) LEED pattern is observed, is lower than that between 1.5-8 L. A Cr-O stretching frequency at 635 cm^{-1}, probably due to rhombohedral Cr_2O_3, is observed to emerge strongly by ~ 60 L. Based on a sequence of O_2 exposures at 300 K and after 625 K and 1175 K anneals, a model of the initial oxidation of Cr(100) is proposed. Subsurface oxygen in interstitial sites with Cr atoms maintaining bulk positions is proposed to act as a nucleus for subsequent oxide growth. Oxide growth at 300 K is proposed to occur primarily through domain expansion, while frequent creation of new domains is observed at 625 K. At elevated temperatures competition between domain growth and diffusion into the bulk is observed.

REFERENCES

*This chapter is based on experiments performed in collaboration with L.E. Klebanoff, M.A. Schulz, E. Paparazzo, and D.A. Shirley, to be submitted to Surface Science for publication.

1. P. Michel and C. Jardin, Surf. Sci. 36, 478 (1973).
2. S. Ekelund and C. Leygraf, Surf. Sci. 40, 179 (1973).
3. H.M. Kennett and A.E. Lee, Surf. Sci. 33, 377 (1972).
4. F. Watari and J.M. Cowley, Surf. Sci. 105, 240 (1981).
5. G.C. Allen, P.M. Tucker, and R.K. Wild, JCS Faraday Trans. II, 74, 1126 (1978).
6. J.C. Peruchetti, G. Gewinner, and A. Jaéglé, Surf. Sci. 88, 479 (1979).
7. G. Gewinner, J.C. Peruchetti, A. Jaéglé, and A. Kalt, Surf. Sci. 78, 439 (1978).
8. F.P. Fehlner and N.F. Mott, Oxidation of Metals, 2, 59 (1970).
9. G. Dalmai-Imelik, J.C. Bertolini, and J. Rousseau, Surf. Sci. 63, 67 (1977).
10. J.L. Gland, B.A. Sexton, and G.B. Fisher, Surf. Sci. 95, 587 (1980).
11. W. Erley and H. Ibach, Solid State Comm. 37, 937 (1981).
12. H. Ibach and D.L. Mills, Electron Energy Loss Spectroscopy and Surface Vibrations (Academic Press, New York, 1982) pp. 282-284.
13. Y. Sakisaka, H. Kato, and M. Onchi, Surf. Sci. 120, 150 (1982).
14. G. Gewinner, J.C. Peruchetti, A. Jaéglé, and R. Riedinger, Phys. Rev. Lett. 43, 935 (1979).

15. G. Gewinner, J.C. Peruchetti, and A. Jaéglé, Surf. Sci. 122, 383 (1982).

16. J.S. Foord, and R.M. Lambert, Surf. Sci. 115, 141 (1982).

17. L.E. Klebanoff, S.W. Robey, G. Liu, and D.A. Shirley, Phys. Rev. B 30, 1048 (1984).

18. D.D. Eley and P.R. Wilkinson, Proc. Roy. Soc. (London) Sec. A 254, 327 (1960).

19. N.F. Mott, Trans. Faraday Soc. 35, 1175 (1939); ibid. 36, 472 (1940); ibid. 43, 429 (1947).

20. N. Cabrera and N.F. Mott, Rept. Prog. Phys. 12, 163 (1948-1949).

FIGURE CAPTIONS

Figure 1. Coverage dependence of EEL spectra for O_2 exposed to clean Cr(100) at 300 K. Exposures made in this way lead toward the oxide Cr_2O_3. The 8 L and 60 L exposures were made with effusive beam dosing. $\theta_i = \theta_s = 55°$. $E_o = 2.06$ eV.

Figure 2. EEL Spectra for O_2/Cr(100) exposures performed in the following ways: (a) A ~ 3 L exposure annealed at 625 K for 5 min., (b) annealed to 1175 K for 5 min., (c) a sequential addition of ~ 1.8 L at 300 K and annealed to 625 K for 5 min., (d) followed by an anneal to 1175 K for 5 min., (e) a sequential addition of ~ 1.8 L at 300 K and annealed to 625 K for 5 min., and (f) followed by an anneal to 1175 K for 5 min. The LEED patterns observed were c(2x2 for (a-c) and (1x1) for (d-f). All O_2 exposures used effusive beam dosing. $\theta_i = \theta_s = 55°$. $E_o = 2.06$ eV.

Figure 3. Oxygen coverage vs. O_2 exposure as determined by Auger peak to peak heights in the derivative mode using a saturation coverage of CO/Cr(110) as a reference compound to determine the sensitivity factors of Cr and O.

Figure 4. Intensity of the Cr-O stretch at 495 cm^{-1} vs. total coverage, including oxygen below the surface, for EEL spectra taken after 1175 K anneals.

Figure 5. A model of the oxidation and diffusion occurring at 300 K and during the sequence of O_2 exposures described in

Fig. 2. o represents oxygen atoms of chemisorbed oxygen and Cr_2O_3, and • represents oxygen in the proposed subsurface sites. The solid lines represent the Cr surface, the straight dotted lines represent the boundary of the near surface layer which, of course, is not actually sharp, and the curved dotted lines represent the oxide boundary. In (a) oxidation proceeds by domain growth at 300 K, and in (b) diffusion competes with domain growth and domain creation.

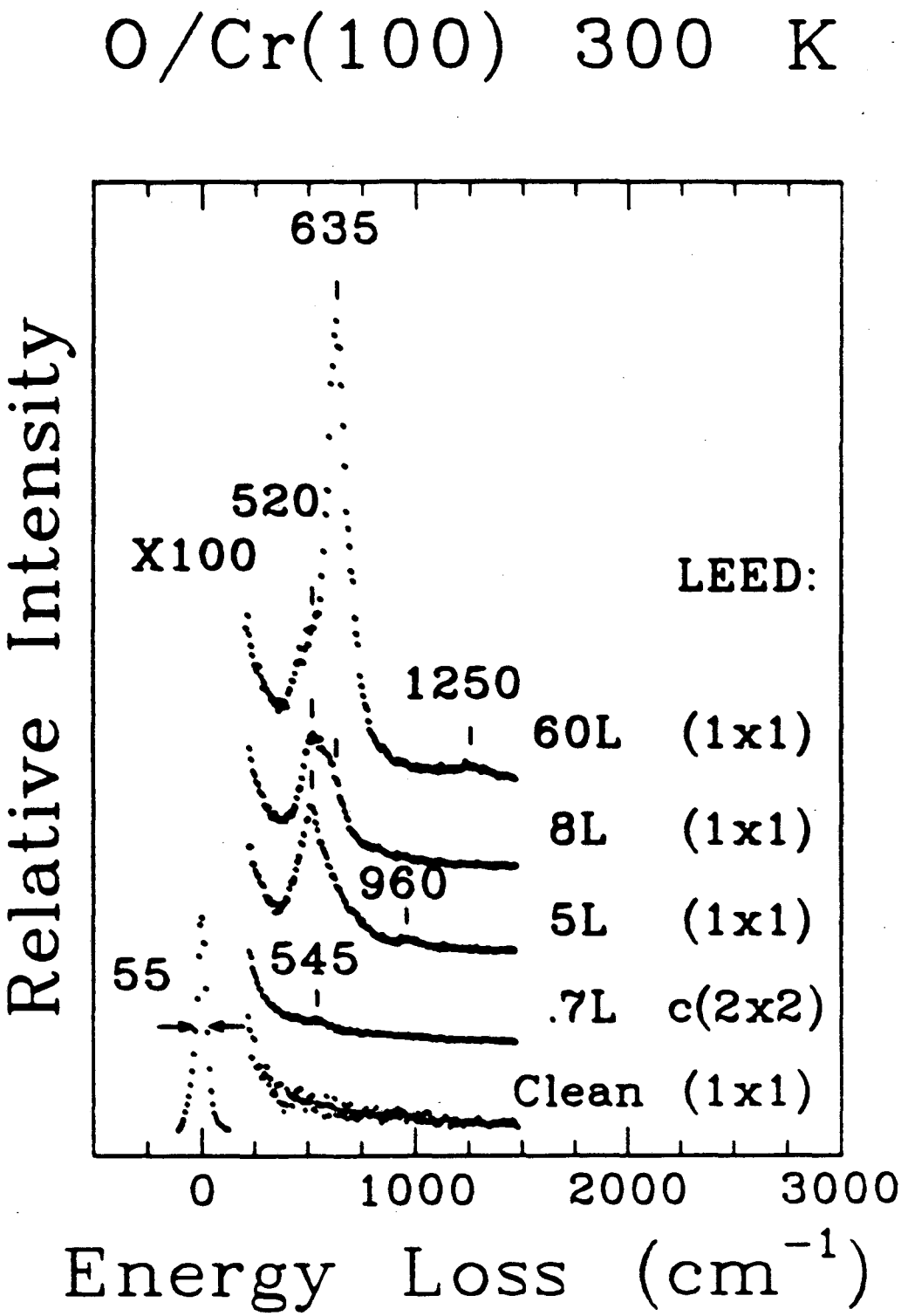

XBL 851-776

Figure 1

O/Cr(100)

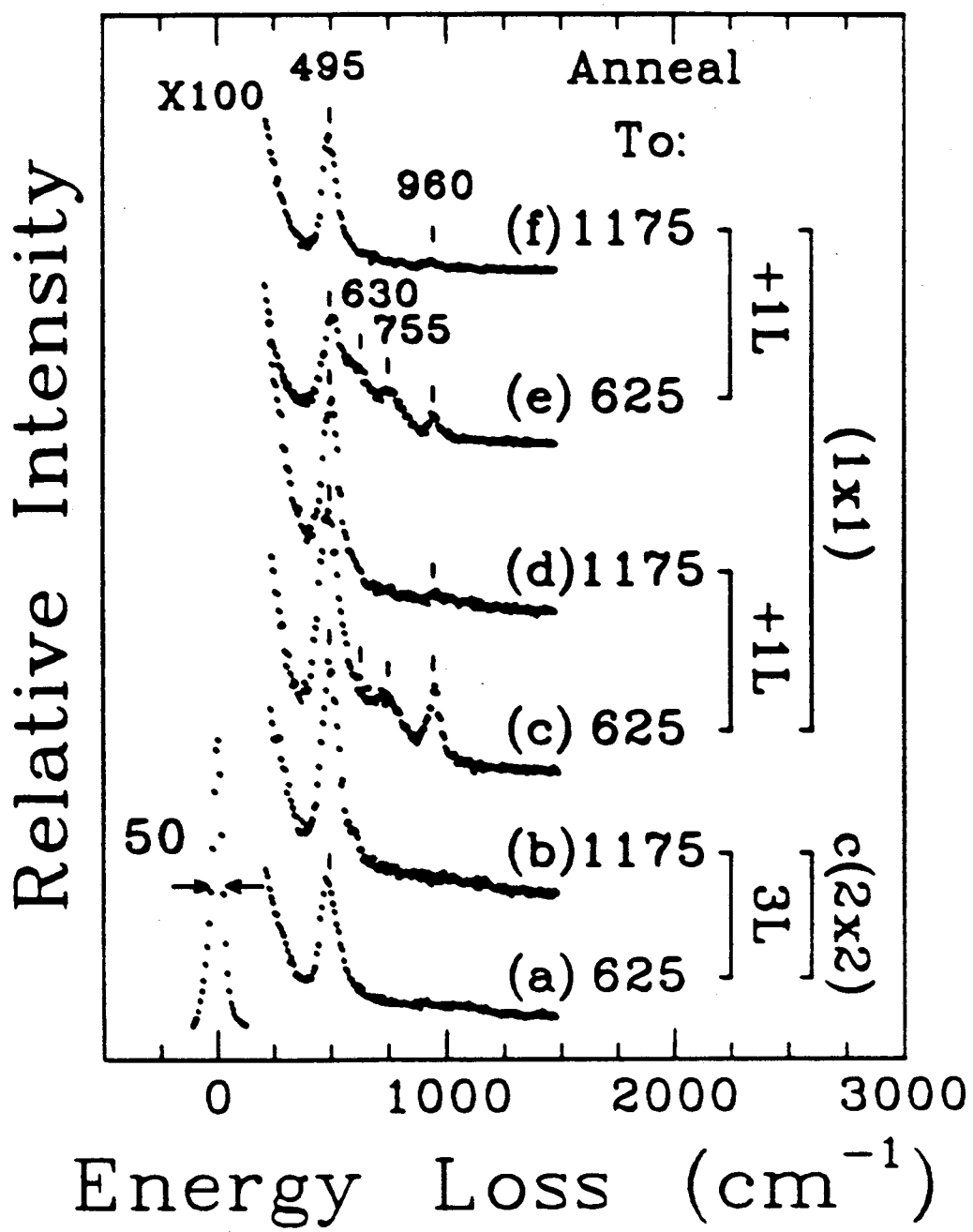

XBL 851-778

Figure 2

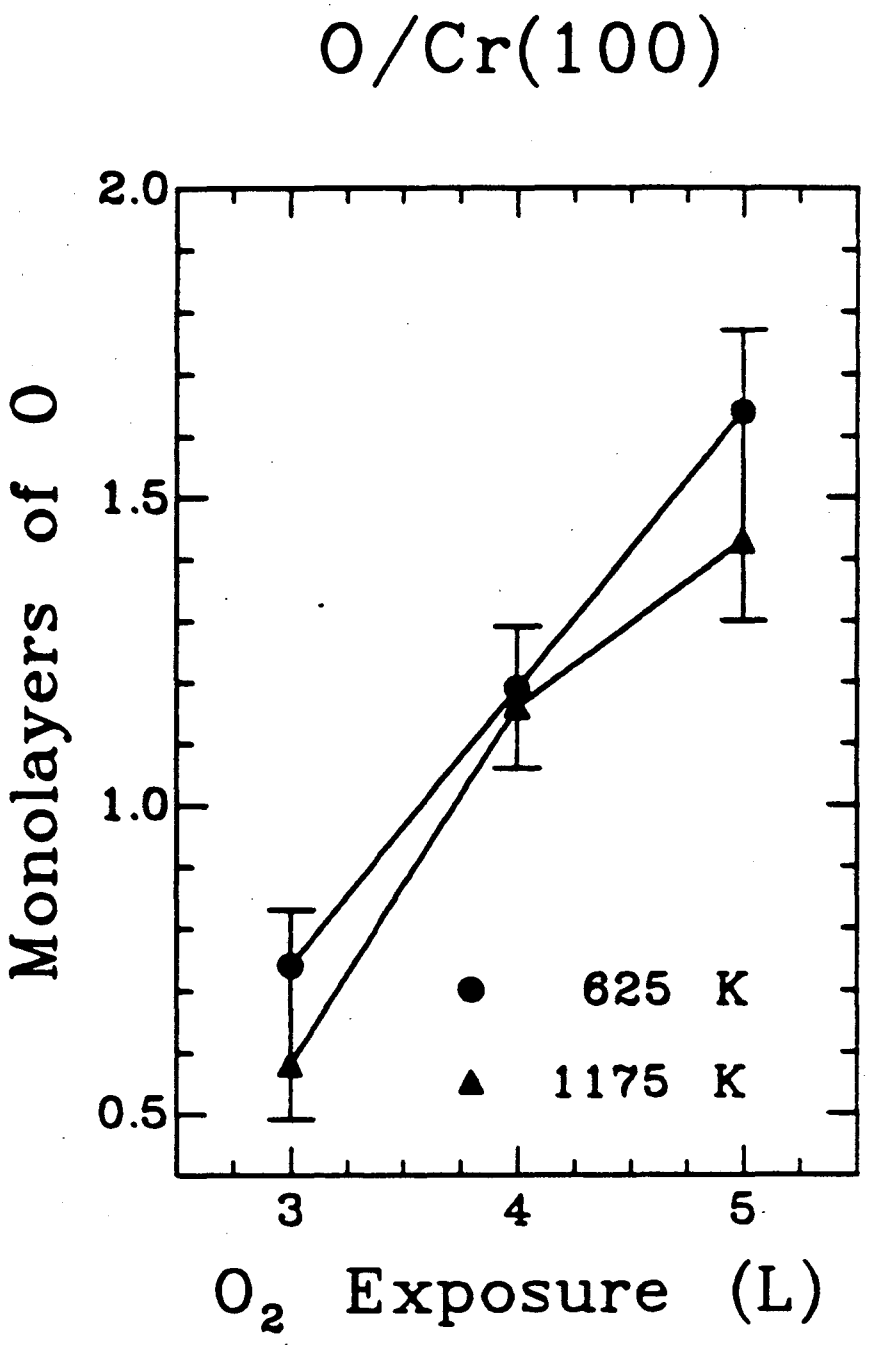

XBL 851-1059

Figure 3

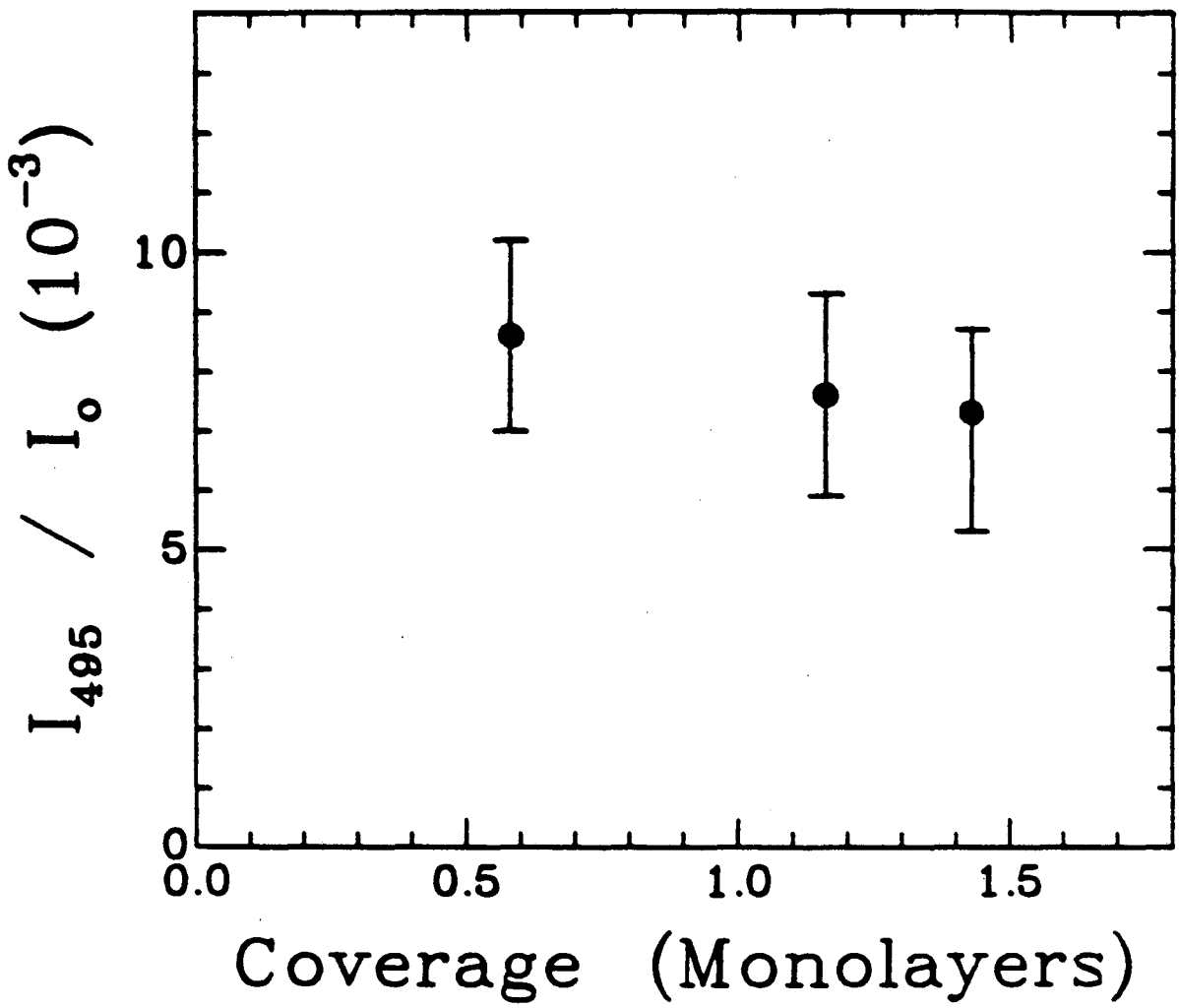

XBL 851-1058

Figure 4

300 K Oxidation

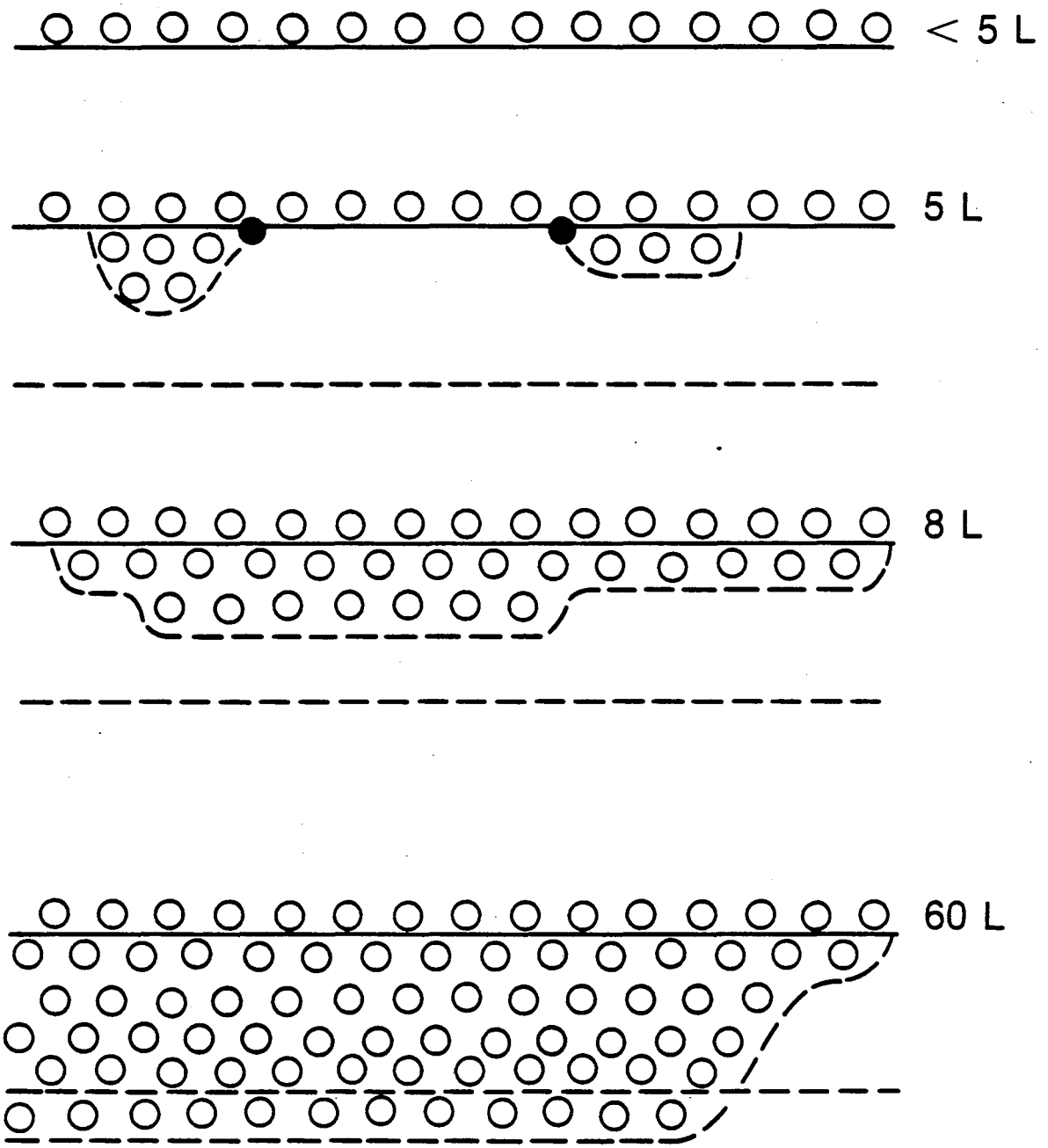

XBL 851-9715

Figure 5(a)

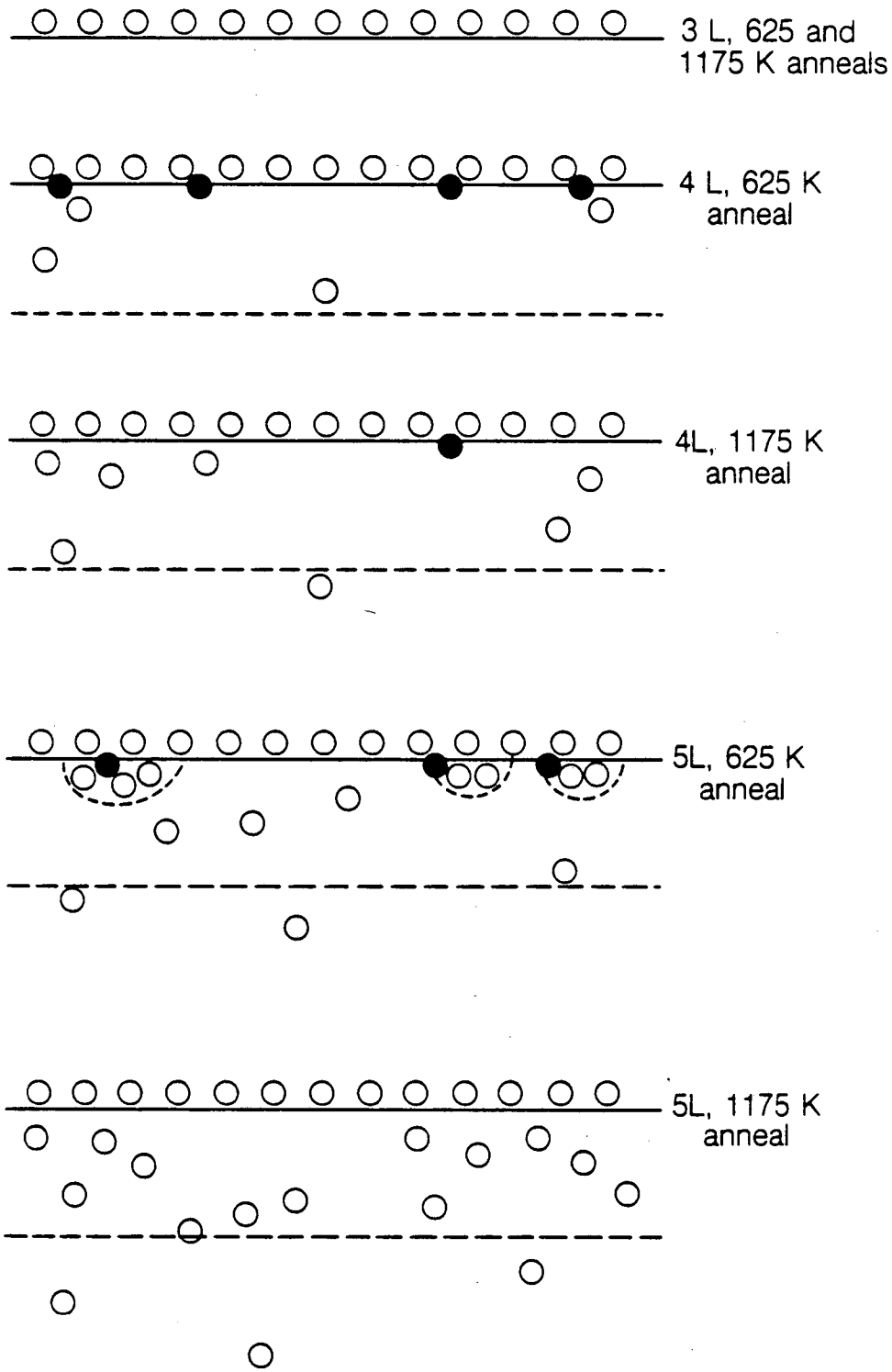

XBL 851-772

Figure 5(b)

VI. DISSOCIATIVE ADSORPTION OF CO AND O_2 ON Cr(100), Cr(110), AND Cr(111) IN THE TEMPERATURE RANGE 300-1175 K*

A. INTRODUCTION

Brodén *et al*. reviewed the adsorption of CO on a number of transition metal surfaces and found a correlation between the separation Δ of the 4σ and 1π orbitals of CO and the tendency of CO to dissociate.[1] The parameter $\Delta(1\pi-4\sigma)$, larger for surfaces with a greater tendency to dissociate CO, was found to vary in a systematic way across the Periodic Table. Elements further left and higher up the transition metal series dissociate CO more readily than those to the right or bottom.[1] The results from the review, which are summarized below, are for the low index surfaces at 300 K. CO completely dissociates on Mo, partly dissociates on W and Fe, and is completely molecular on Ru, Ir, Ni, Pd, and Pt.[1] Results published since then on Re,[2] Rh,[3] and Co[4] have been largely in agreement with the trends found by Brodén *et al*.

Of the voluminous literature about CO on transition metal surfaces there are only two studies of chromium surfaces. Shinn and Madey[5] observed molecular CO at 120 K on Cr(110) and Kato *et al*.[6] used low resolution (electronic transitions) EELS to find that CO dissociates on Cr(110) at 300 K and that dissociated CO gives the same spectrum as chemisorbed oxygen. Because the electronic EELS study used an electron beam with primary energies (60-250 eV) and currents (.4 $\mu A/mm^2$) sufficient to induce dissociation and/or desorption of molecular CO, it was felt that independent confirmation using high

resolution vibrational EELS would be useful. This study confirms their observation on Cr(110) and is extended to the other low index surfaces of chromium. The results show complete dissociation of CO on all three surfaces at room temperature and above, in agreement with the trend proposed by Brodén et al. The dissociative adsorption of CO and oxygen are fully characterized in this chapter and are presented together because the results show great similarities.

B. EXPERIMENTAL

Chromium is the most reactive transition metal for which clean surfaces have been studied. As mentioned in Chapter V, Cr surfaces have often proven difficult to clean in the past. In particular, the LEED patterns observed on Cr(100) are very sensitive to the surface cleanliness. In preparation for the present study, the (110) and (111) surfaces of Cr have been cleaned in the same way required to produce the clean (100) surface.

The Cr surfaces were exposed to CO by ambient dosing and to O_2 by effusive beam dosing. When effusive beam dosing was used, approximate values in langmuirs were estimated using Auger intensities. LEED and Auger measurements were made with LEED optics after EEL spectra were taken, so as not to induce dissociation. Some surfaces were annealed by electron beam heating to a given temperature for approximately five minutes, and temperatures were calibrated with an optical pyrometer. All EEL spectra were taken at 300 K, and impact energies as well as angles of incidence and scattering are given in

each figure. The impact energies ranged between 2.0 and 2.5 eV, while the incident current was ~ $2x10^{-11}$ A. Linewidths for most spectra are reported in Table 1.

C. OXYGEN ADSORPTION

Oxygen chemisorption results on the (110) and (111) surfaces of Cr are presented here. Chemisorption results of O/Cr(100) were presented in Chapter V. These data are needed to assign the spectra for the dissociative adsorption of CO on these surfaces. Because of the similarities of the results for both oxygen and CO adsorption on all three surfaces, the discussion of the site assignments will be presented together in section E.

1. O/Cr(110)

The coverage dependent spectra for O/Cr(110) at 300 K are shown in Fig. 1. At low coverages (~ 1.6 L) a Cr-O stretching frequency is observed at 555 cm^{-1}. The width of the peak is ~ 80 cm^{-1} FWHM. As more O_2 is added the frequency shifts upward to 570 and then 585 cm^{-1} for ~ 3 L and ~ 4 L exposures, respectively. No evidence for molecular O_2 is observed at any coverage. A small unidentified feature at 1205 cm^{-1} is observed in the high exposure spectrum. The upward shift of 30 cm^{-1} of the Cr-O stretch is in contrast to what is observed on Cr(100) where the initial Cr-O frequency at 545 cm^{-1} appears to shift downward with coverage. The spectra are broadened relative to instrumental resolution, but not in the way that was

observed on Cr(100), where asymmetric broadening due to the onset of oxidation became apparent during the completion of the chemisorption phase. On Cr(110), all Cr-O stretches are symmetrically broadened up to 4 L exposure. The highest coverage studied here was ~ 0.6 monolayer.

When the lowest coverage surface (1.6 L) is heated to 825 K (Fig. 2), the Cr-O stretching intensity becomes stronger but no shift in frequency is observed. For the highest coverage (4 L) surface (Fig. 3), an 825 K anneal also results in no shift of the Cr-O frequency. An extra feature at 440 cm^{-1} is observed while the 1205 cm^{-1} peak has disappeared. Again, this is in contrast to the 25 cm^{-1} downward shift on Cr(100) for a 625 K anneal.

2. O/Cr(111)

Oxygen adsorption on Cr(111) leads to considerably broader features, as can be seen in Fig. 4. At an exposure of ~ 0.6 L, trace (b), there is a peak at ~ 580 cm^{-1} and a broad envelope of peaks centered at 440 cm^{-1}. Heating to 625 K, trace (c), gives essentially the same spectrum. Further addition of ~ 0.9 L, trace (d), smears out the spectra. Annealing to 625 K and 1175 K, (e-f), further broadens the spectra. A (1x1) LEED pattern is observed at all coverages and temperatures. In contrast to O/Cr(100) and O/Cr(110), temperature treatments do not lead to greater order. The highest coverage studied here is ~ 0.8 monolayer. The sticking coefficient is much larger for Cr(111) than for the other two surfaces, in agreement

with previous reports.[7,8]

D. CO ADSORPTION

1. CO/Cr(100)

The coverage dependence of CO adsorption on Cr(100) at 300 K is shown by the EEL spectra in Fig. 5. One stretching frequency at 520 cm^{-1} is observed which does not shift appreciably in any of the spectra shown. The width of this peak is narrow at 0.2 L and broadens to ~ 80 cm^{-1} at 1.0 L. At 0.2 L, a c(2x2) LEED pattern is observed, while a (1x1) LEED pattern is reestablished by 1.0 L. Further increases in CO exposure do not lead to further changes in the EEL spectra. The absence of a feature in the range 1700-2100 cm^{-1}, which would be indicative of molecular CO, contrasts with CO adsorption on W(100),[9] where molecular adsorption is observed at the highest coverages at 300 K and dissociation occurs at lower coverages. A small peak at 930 cm^{-1} is similar in frequency and intensity to a peak at 960 cm^{-1} for O/Cr(100) which was assigned to subsurface oxygen. The 30 cm^{-1} shift of this peak is probably due to the perturbation of coadsorbed carbon.

Annealing the spectra in Fig. 5 to 825 K leads to large intensity changes in the EEL spectra. Typical of these anneals is the 0.2 L CO exposure, shown in Fig. 6. The increase in intensity after the 825 K anneal is thought to be due to an increase in the surface order since a c(2x2) LEED pattern is observed for the 0.2 L exposure which becomes much sharper on annealing. A small downward frequency shift from 520

cm^{-1} to 505 cm^{-1} is observed with annealing. Annealing after 0.5 L and 1.0 L exposures shows the same frequency shift and less dramatic intensity increases. The peak at 930 cm^{-1} disappears with annealing. Finally, a nearly clean spectrum is observed after flashing to ~ 1175 K, as observed in previous work on W(100)[9] where TDS has shown CO desorption at high temperatures due to recombination of adsorbed carbon and oxygen.

The EEL spectra of CO/Cr(100) are similar to those of low coverages of O/Cr(100). The room temperature frequency is 545-520 cm^{-1} for oxygen and 520 cm^{-1} for dissociated CO. Annealing to higher temperatures shifts the frequency to 495 cm^{-1} for oxygen and 505 cm^{-1} for dissociated CO. Auger spectra show clearly that carbon is present and this agrees with the fact that flashing to 1175 K cleans the carbon and oxygen covered surface and not the oxygen covered surface. In Chapter IV it was shown that Cr-O and Cr-C frequencies are nearly degenerate on Cr(100). The spectral broadening at the 1.0 L exposure is likely to be due to different coverage dependences of coadsorbed carbon and oxygen stretching frequencies. The narrow peak at 0.2 L exposure coupled with the small peak at 930 cm^{-1} may indicate that oxygen initially assumes subsurface sites in the presence of carbon.

2. CO/Cr(110)

The coverage dependence of CO adsorption at 300 K on the Cr(110) surface is shown in Fig. 7. For a 0.2 L exposure a loss is observed

at 560 cm^{-1}. At 0.5 L and 0.75 L a second loss is seen at 420 cm^{-1}. The higher energy feature shifts upward in frequency with increasing coverage from 560 to 590 cm^{-1}, while the lower energy feature does not appear to shift. For all three coverages shown in Fig. 7, a (1x1) LEED pattern is observed. Again, no evidence for molecular CO is observed.

Figure 8 shows the effect of annealing the 0.75 L exposure to 825 K. Again some differences in intensity are observed, as was the case on Cr(100). Annealing the 0.2 L and 0.5 L surfaces show similar results. The high energy peak becomes more intense after an 825 K anneal at 0.5 L and 0.75 L, while the low energy peak decreases. In addition, the high energy peak is shifted back to 560 cm^{-1} at all coverages. On Cr(110) after an 825 K anneal, the 0.5 L and 0.75 L exposures show spectra with a 55 cm^{-1} FWHM, essentially instrumental resolution. Auger spectra show no substantial decrease in carbon or oxygen signal after either anneal.

Similarities to O/Cr(110) are apparent and differences, though present, are slight. The coverage dependence of the high frequency peak is virtually identical. When the dissociated CO overlayer is annealed, the frequency shifts back to 560 cm^{-1}, and its FWHM narrows. When the oxygen overlayer is annealed, no shift occurs and no narrowing occurs. When dissociated CO is annealed, the 420 cm^{-1} peak decreases, but when the 4 L O_2 exposed surface is annealed, a 440 cm^{-1} peak appears.

There is a quite dramatic effect on the LEED patterns after an

825 K anneal. These are shown schematically in Fig. 9. At 0.2 L streaks begin to appear in one direction. At 0.5 L spots appear on either side of the (1x1) spots. By 0.75 L a (6x1) LEED pattern is observed. These LEED patterns correspond to the spectra where sharp features are observed in EELS at 560 cm^{-1} for both 0.5 L and 0.75 L exposures. They will be discussed further in section E.2.

3. CO/Cr(111)

The coverage dependent spectra of CO/Cr(111)at 300 K are seen in Fig. 10. In contrast with the other two surfaces, but similar to oxygen adsorption on Cr(111), the spectra here are extremely broad. Two stretching frequencies are observed, at 565 and 440 cm^{-1}. The frequency at 440 cm^{-1} is especially broad and may correspond to more than one mode. The absence of a higher frequency indicates that CO dissociates on Cr(111). Both frequencies are very nearly the same as observed on Cr(110). This suggests that similar sites are being populated on each surface. For the 1.0 L exposure (Fig. 11), annealing to 625 K and 825 K sharpens up the spectra somewhat but no appreciable changes are observed in the frequencies. For the 0.5 L exposure, annealing to 625 K and 825 K gives qualitatively similar results, but the spectra are broader than in Fig. 11. When the surface is heated to 1175 K, over 90% of the carbon and oxygen atoms are removed, as is observed on Cr(100) and Cr(110).

4. Comparison Between Surfaces

Several similarities and trends common to these three chromium surfaces are noted. It is found that CO dissociates at room temperature on all three surfaces and that the spectra on all three surfaces resemble those for the oxygen covered surfaces. In Chapter IV, it was shown that Cr-O and Cr-C stretching frequencies on Cr(100) are nearly degenerate, and they are also of comparable intensity. This was determined by comparing CO/Cr(100), N/Cr(100), and CH_3NH_2/Cr(100) (partly dissociated). A similar conclusion holds for Cr(110)[10] and can be expected for Cr(111).

V. DISCUSSION

1. Site Assignments

It was noted above that Cr-O and Cr-C stretching frequencies are nearly degenerate. This conclusion forms the basis for the ensuing discussion, where it will be argued that different peaks correspond to separate adsorption sites and <u>not</u> different atomic species. This assertion is supported by the similar frequencies but different intensity variations with temperature for CO/Cr(110) and O/Cr(110), which are most easily explained by differences in site populations vs. temperature. The site population distributions are slightly different for CO and O_2 adsorption.

A discussion of the sites responsible for the Cr-O and Cr-C stretching frequencies on the three surfaces, illustrated in Fig. 12, will now be made. The (100) surface has 4-fold symmetry. A hollow

site on this surface does not have the same meaning as it would on a more densely packed face-centered cubic (fcc) surface with 4-fold symmetry. On the body-centered cubic (bcc) surface, the spacing between the chromium atoms is so large that a 4-fold coordinated site in the hollow with Cr-O or Cr-C bond lengths typical of known compounds cannot be attained. For an adatom in the hollow, 5-fold coordination occurs and the bond to the second layer Cr atom can be .1-.2Å shorter than the other bonds. In keeping with the convention established by previous workers, this site will be referred to as the 4-fold hollow site, rather than atop to the second layer, even though the greatest bond strength may come from the second layer Cr atom. It is also possible for the adatom to bond to two first layer Cr atoms and one second layer atom in a 3-fold coordinated site on a (110) plane of the (100) surface. The sites we need to consider are atop to the first layer, bridge, 3-fold, or the 4-fold hollow. On the (110) surface the possible sites are atop, short bridge, long bridge, or 3-fold. The (111) surface (Fig. 12c), being the least densely packed, has three layers of chromium atoms exposed. Each surface chromium atom is the peak of an isolated hill and three neighboring surface atoms define a "pocket" where most of the available adsorption sites are. The possible sites are atop to the first, second, and third layer atoms, bridge between first and second layer atoms (short bridge), between first and third layer atoms (long bridge), and between second and third layer atoms (short bridge), and 3-fold to a first, second, and third layer atom. In all, there are seven standard

adsorption sites on Cr(111). This plethora of sites may explain why the spectra are so broad on Cr(111) for both oxygen adsorption and CO adsorption.

A comparison of the sites available on these three surfaces show some interesting similarities. All of the available 3-fold sites on each surface lie in (110) planes. The only difference among the sites is the coordination number of the oxygen-bonded chromium atoms, i.e., the number of their chromium nearest neighbors. The bridge sites available on Cr(111) and Cr(110) are the long and short bridge sites on the (110) plane.

The low coverage frequency of the Cr-O stretch is 560 and 580 cm^{-1} at 300 K on the (110) and (111) surfaces, respectively. This suggests that the site for this peak is the same on both surfaces, allowing for differences in average chromium coordination number. A second peak near 420-440 cm^{-1} is observed on Cr(110) and Cr(111) surfaces. Again, the similar frequency suggests a similar site on both surfaces. The lower frequency suggests a higher coordinated site. The assignments of a 3-fold site for the peaks at 420-440 cm^{-1} and a long bridge site for the 560-580 cm^{-1} peaks are favored. Such assignments were made using EELS for O/W(110)[11] where vibrational frequencies at 580 and 380 cm^{-1} were observed. An assignment of long and short bridge sites for the low and high frequency peaks, respectively, would not allow the formation of the (6x1) LEED pattern at θ=1 and will be discussed further in section 2.

On Cr(100), vibrational frequencies between 520 and 545 cm^{-1}

are observed. The frequencies are higher than what would be expected for a 4-fold hollow site where no bonding to second layer atoms can occur, e.g. in (100) surfaces of fcc metals. For bcc metals, bonding to the second layer is likely to be stronger than bonding to the first layer, according to the discussion in the previous paragraph. This will raise the vibrational frequency by an indeterminate amount since it is not known a priori what the relative strengths of the bonds are. The EELS data alone cannot distinguish between 3-fold and 4-fold hollow sites on Cr(100), but there are structural measurements on the similar surfaces of Mo and W which bear on this question.[12-14] None of the structural measurements have found dissociated CO, O, or N to be in 3-fold sites on Mo(100)[12] or W(100),[13,14] and we are hesitant to make such an assignment on Cr(100).

2. Cr(110) LEED Patterns

The LEED patterns that result from high temperature (875 K) anneals of CO/Cr(110) are shown in Fig. 9. For a 0.2 L CO exposure, streaks are apparent along the [10] direction. The streaks are probably caused by both a mixture of unit cells such as (5,1), (6,1), (7,1), etc. and a small domain size associated with low coverage, which will cause uncertainty broadening of the spots. Two extra spots equally spaced about the (1x1) spots emerge for the 0.5 L exposure. A mixture of unit cells can adequately explain the patterns since the first extra spots at the ends are less affected than spots in the middle: e.g. 1/5 is very close to 1/6 and 4/5 to 5/6, but 1/3, 2/5,

and 1/2 are further apart. At 0.75 L, the full (6x1) LEED pattern becomes very sharp. A model of the surface consistent with the 3-fold and long bridge sites proposed in section 1 is shown in Fig. 13. It should be noted that a (1x6) domain is inequivalent on the (110) surface and is not observed. It is emphasized that this model is not necessarily unique. The population ratios of the sites are not necessarily known. It may be possible to propose incommensurate overlayers which are consistent with the EELS data. Such a model would require that the EELS frequencies do not shift with the ordering that occurs after an 825 K anneal and that the 560 cm^{-1} peak is narrower after the anneal. Long rows in the [01] direction would also have to be retained.

Another possibility is surface reconstruction. Compression of the outer layer of Cr atoms to form a close-packed layer would eliminate the long bridge site and affect the EEL spectra, but other types of reconstructions may be possible. One type that is common to Cr(110) surfaces, faceting, can be ruled out. Faceting is known to occur at high temperature in the presence of oxygen and is evidenced by streaks along one direction and the presence of rectangular spots due to (100) planes.[15-17] Here, the observed streaks disappear when the (6x1) LEED pattern is fully developed and no evidence of (100) spots is present.

A saturation coverage of approximately one monolayer of carbon and oxygen atoms ($\theta \sim 0.5$ for oxygen and $\theta \sim 0.5$ for carbon) is postulated, and this assumption is used to quantify the Auger spectra

used in Chapter V. A saturation coverage of $\theta \sim 0.83$ (a missing row or incommensurate adlayer to explain the (6x1) LEED pattern) would not significantly affect the results. If the model of Fig. 13 is not correct, any other explanation would involve adlayer interactions suggestive of a crowded surface.

An assignment of long and short bridge sites for the low and high frequency EELS peaks, respectively, would not allow the formation of an unreconstructed (6x1) LEED pattern at $\theta=1$. One would be left to propose $\theta=.83$ or less in order to make every sixth row different.

F. SUMMARY

Dissociative chemisorption of O_2 and CO has been characterized on Cr(100), Cr(110), and Cr(111). No evidence of molecular CO was observed on any of the surfaces studied at 300 K and above. Dissociated CO and O give very similar EEL spectra on all surfaces. The EEL spectra are broader on Cr(111) than on Cr(100) or Cr(110), indicative of multiple sites on this very open surface. For O_2 exposures on Cr(110) and at low coverages on Cr(111), similar Cr-O stretching frequencies at ~ 560-580 cm^{-1} and 420-440 cm^{-1} are suggestive of similar sites for both surfaces. These sites are proposed to be the long bridge and 3-fold sites on (110) planes of the two surfaces. No site determinations based on EELS frequencies can be made for the Cr(100) surface, although a 4-fold hollow site is a likely candidate and is consistent with the EELS data. Both O/Cr(110) and CO/Cr(110) show an increase in frequency with coverage at 300 K,

but no change in frequency with coverage for CO/Cr(100). High temperature anneals of CO/Cr(110), CO/Cr(100), and O/Cr(100) result in downward shifts in EELS frequencies, but no shifts for O/Cr(110). A (6x1) LEED pattern is observed after an 825 K anneal for a 0.75 L exposure of CO/Cr(110) and a model consistent with the LEED pattern and sites based on EELS data is presented. A summary of all frequencies and linewidths is reported in Table 1.

REFERENCES

*This chapter is based on experiments performed in collaboration with L.E. Klebanoff, M.A. Schulz, E. Paparazzo, and D.A. Shirley, to be submitted to Surface Science for publication.

1. G. Brodén, T.N. Rhodin, C. Brucker, R. Benbow, and Z. Hurych, Surf. Sci. 59, 593 (1976).
2. W. Braun, G. Meyer-Ehmsen, M. Neumann, and E. Schwarz, Surf. Sci. 89, 354 (1979).
3. J.T. Yates, Jr., E.D. Williams, and W.H. Weinberg, Surf. Sci. 91, 562 (1980) and references therein.
4. H. Papp, Surf. Sci. 129, 205 (1983).
5. N.D. Shinn and T.E. Madey, Phys. Rev. Lett. 53, 2481 (1984).
6. H. Kato, Y. Sakisaka, T. Miyano, K. Kamei, M. Nishijima, and M. Onchi, Surf. Sci. 114, 96 (1982).
7. J.C. Peruchetti, G. Gewinner, and A. Jaéglé, Surf. Sci. 88, 479 (1979).
8. G. Gewinner, J.C. Peruchetti, A. Jaéglé, and A. Kalt, Surf. Sci. 78, 439 (1978).
9. H. Froitzheim, H. Ibach, and S. Lehwald, Surf. Sci. 63, 56 (1977).
10. A.G. Baca, M.A. Schulz, and D.A. Shirley, unpublished results.
11. N.J. DiNardo, G.B. Blanchet, and E.W. Plummer, Surf. Sci. 140, L229 (1984).
12. S.H. Overbury, Nucl. Inst. Methods Phys. Research B2, 448 (1984).
13. N.R. Palmer and D.A. King, Phys. Scripta T4, 122 (1983).

14. K. Griffiths, D.A. King, G.C. Aers, and J.B. Pendry, J. Phys. C: Solid State Phys. 15, 4921 (1982).

15. P. Michel and C. Jardin, Surf. Sci. 36, 478 (1973).

16. S. Ekelund and C. Leygraf, Surf. Sci. 40, 179 (1973).

17. H.M. Kennett and A.E. Lee, Surf. Sci. 33, 377 (1972).

Table 1

A summary of all vibrational frequencies (in cm^{-1}) for the dissociative adsorption of CO and O_2 on Cr(100), Cr(110), and Cr(111) from Chapters V and VI. Where available, the linewidths in cm^{-1} are given in parenthesis.

		Anneal To:			
	Exposure	300 K	625 K	825 K	1175 K
O/Cr(100)	0.75 L	545(60)	-	-	-
	5 L	520(150)	-	-	-
	8 L	(520,635)(~ 170)	-	-	-
	60 L	520,625(85),1250	-	-	-
	3 L	-	495(90)	-	495(90)
	4 L	-	495,630,755,960	-	495,960
	5 L	-	495,630,755,960	-	495,960
O/Cr(110)	1.6 L	555(90)	-	555(80)	-
	3 L	570(80)	-	-	-
	4 L	585(80),1205	-	440,585(80)	-
O/Cr(111)	0.6-1.5 L	440,580(55)	440,580	-	440,580(v. broad)

Table 1 (continued)

	Exposure	Anneal To: 300 K	625 K	825 K	1175 K
CO/Cr(100)	0.2 L	520(55)	-	505(90)	-
	1.0 L	520(90)	-	510(160)	-
	2.0 L	520(80),930	-	-	-
CO/Cr(110)	0.2 L	420,560(95)	-	555(75)	-
	0.5 L	420,585(80)	-	555(60)	-
	0.75 L	420,590(75)		425,560(60)	-
CO/Cr(111)	0.2-1.0 L	440,565(v. broad)	440,560	440,570	-

FIGURE CAPTIONS

Figure 1. Coverage dependence of EEL spectra for O_2 exposed to Cr(110) at 300 K. E_0 = 2.50 eV. $\theta_i = \theta_s = 55°$.

Figure 2. EEL spectra of the 1.6 L O_2 exposure to Cr(110) annealed to 825 K for 5 min. The lowest spectrum is of the clean surface. Spectra were collected at 300 K. E_0 = 2.50 eV. $\theta_i = \theta_s = 55°$.

Figure 3. EEL spectra of the 4 L O_2 exposure to Cr(110) annealed to 825 K for 5 min. The lowest spectrum is of the clean surface. Spectra were collected at 300 K. E_0 = 2.50 eV. $\theta_i = \theta_s = 55°$.

Figure 4. EEL spectra of O_2 exposed to the Cr(111) surface taken after the following treatments: (b) A 0.6 L exposure at 300 K, (c) annealing to 625 K for 5 min., (d) further addition of 0.9 L at 300 K, (e) annealing to 625 K for 5 min., and (f) annealing to 825 K for 5 min. E_0 = 2.20 eV. $\theta_i = \theta_s = 55°$.

Figure 5. Coverage dependence of EEL spectra for CO exposed to clean Cr(100) at 300 K. E_0 = 2.20 eV. $\theta_i = \theta_s = 55°$.

Figure 6. EEL spectra of the 0.2 L exposure of CO to Cr(100) annealed to 825 K for 5 min. The lowest spectrum is of the clean surface. Spectra were collected at 300 K. E_0 = 2.20 eV. $\theta_i = \theta_s = 55°$.

Figure 7. Coverage dependence of EEL spectra for CO exposed to

Cr(110) at 300 K. E_0 = 2.20 eV. $\theta_i = \theta_s = 55°$.

Figure 8. EEL spectra of the 0.75 L exposure of CO to Cr(110) annealed to 825 K for 5 min. The lowest spectrum is of the clean surface. Spectra were collected at 300 K. E_0 = 2.20 eV. $\theta_i = \theta_s = 55°$.

Figure 9. LEED patterns observed for CO exposures to Cr(110) after anneals to 825 K for 5 min. (x) denotes the substrate spots and (•) denotes the overlayer spots. For the 0.2 L and 0.5 L exposures, streaks are observed in the [10] direction.

Figure 10. Coverage dependence of EEL spectra for CO exposed to Cr(111) at 300 K. E_0 = 2.20 eV. $\theta_i = \theta_s = 55°$.

Figure 11. EEL spectra of the 1.0 L exposure of CO to Cr(111) annealed to 625 K and 825 K for 5 min. The lowest spectrum is of the clean surface. Spectra were collected at 300 K. E_0 = 2.20 eV. $\theta_i = \theta_s = 55°$.

Figure 12. Models of the Cr surfaces. (a) Cr(100). Dotted circles are the second layer atoms. (b) Cr(110). (c) Cr(111). Three layers of atoms are exposed in this very open surface.

Figure 13. A model of the Cr(110) surface consistent with both the (6x1) LEED pattern and the EELS data. The LEED pattern is observed after annealing a 0.75 L CO exposure to 825 K for 5 min.

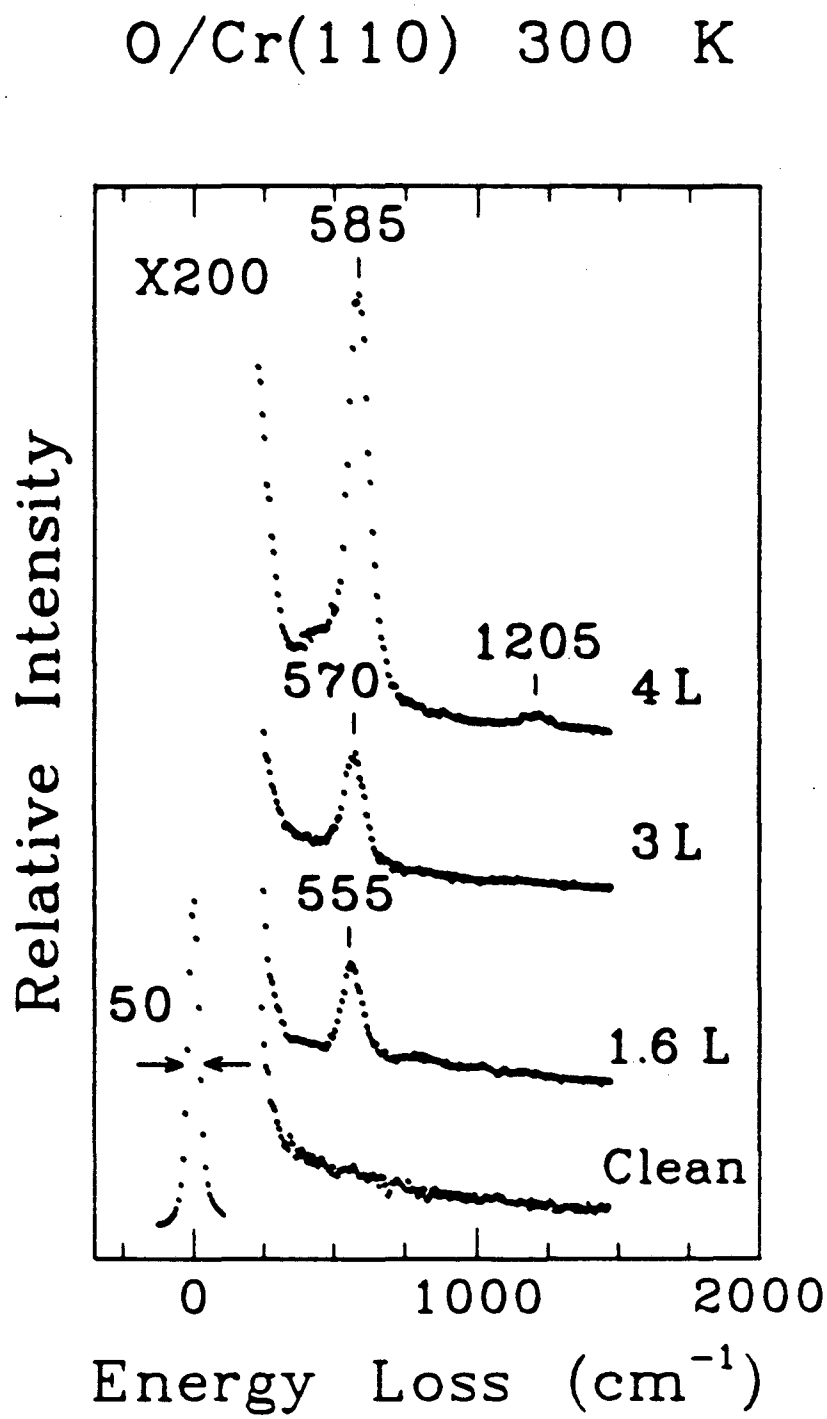

XBL 851-821

Figure 1

O/Cr(110) Low Coverage

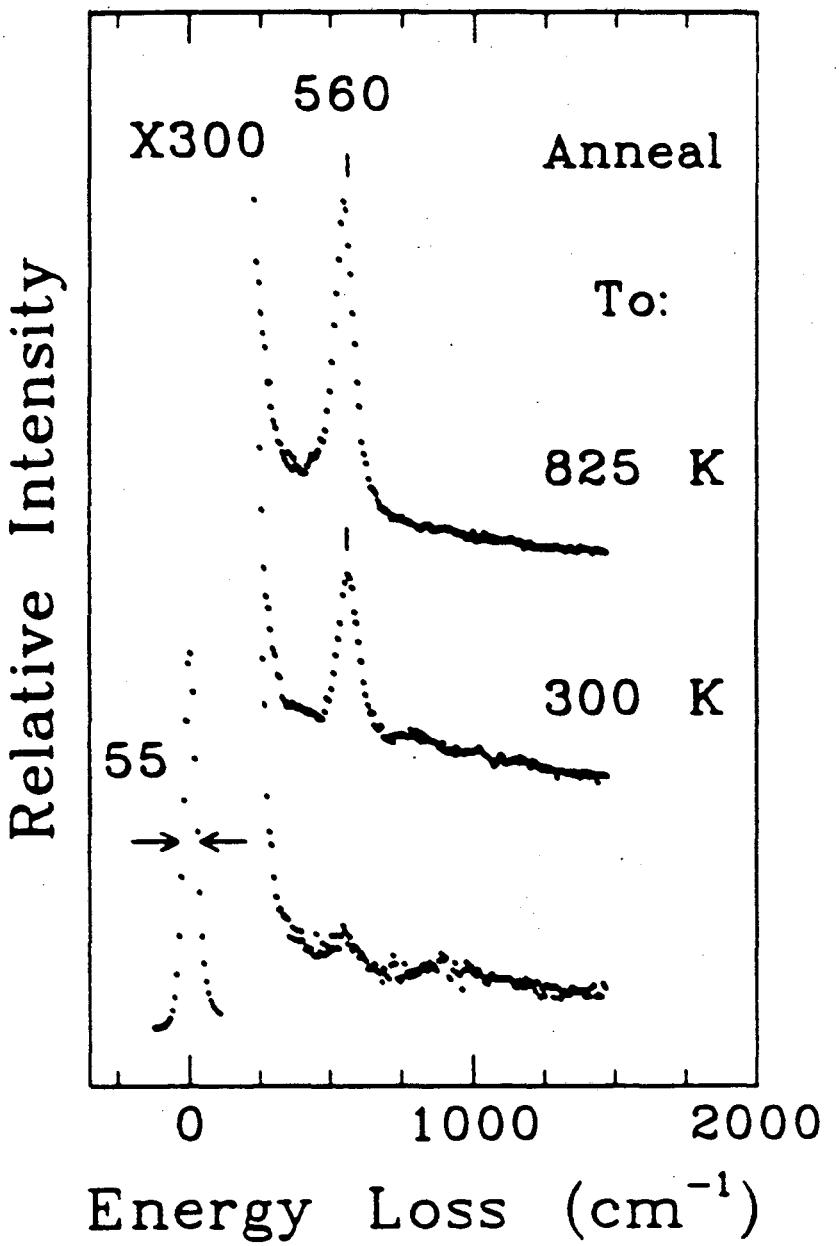

XBL 851-888

Figure 2

O/Cr(110) High Coverage

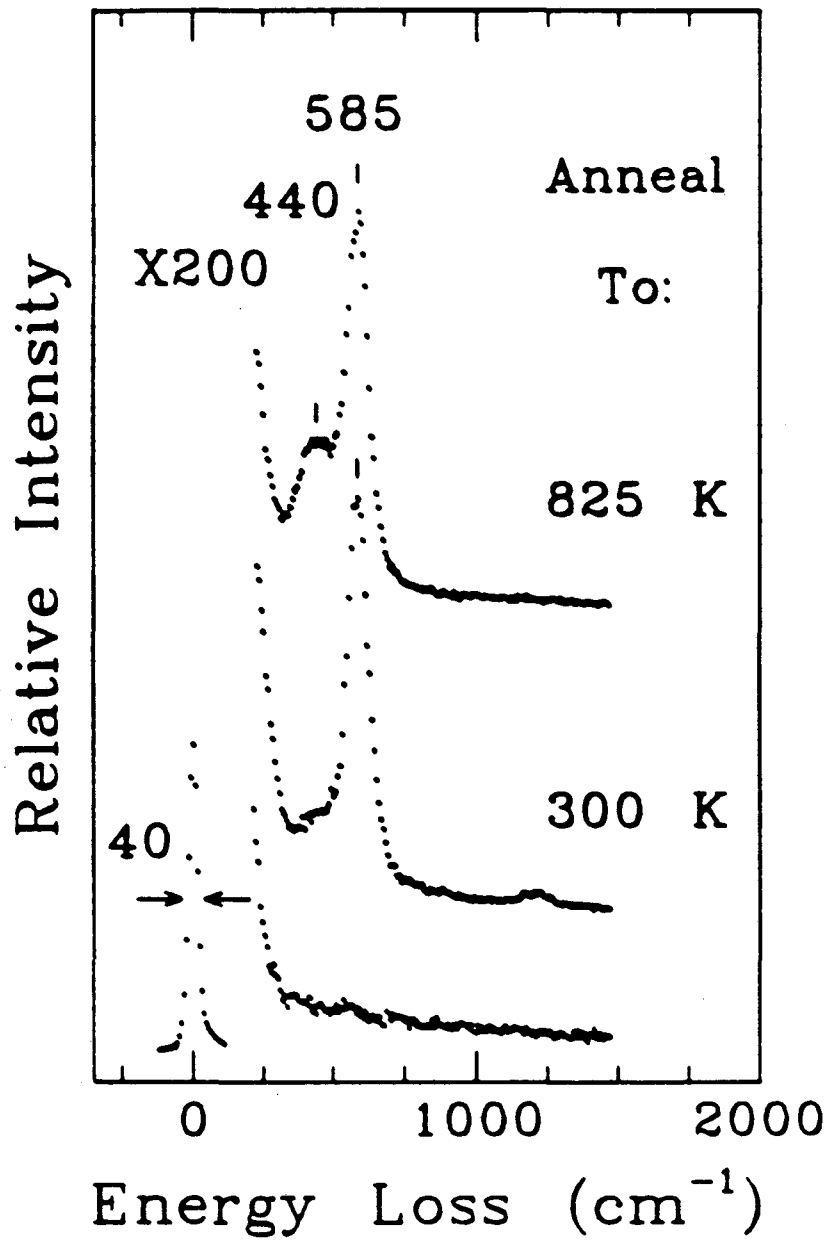

XBL 851-822

Figure 3

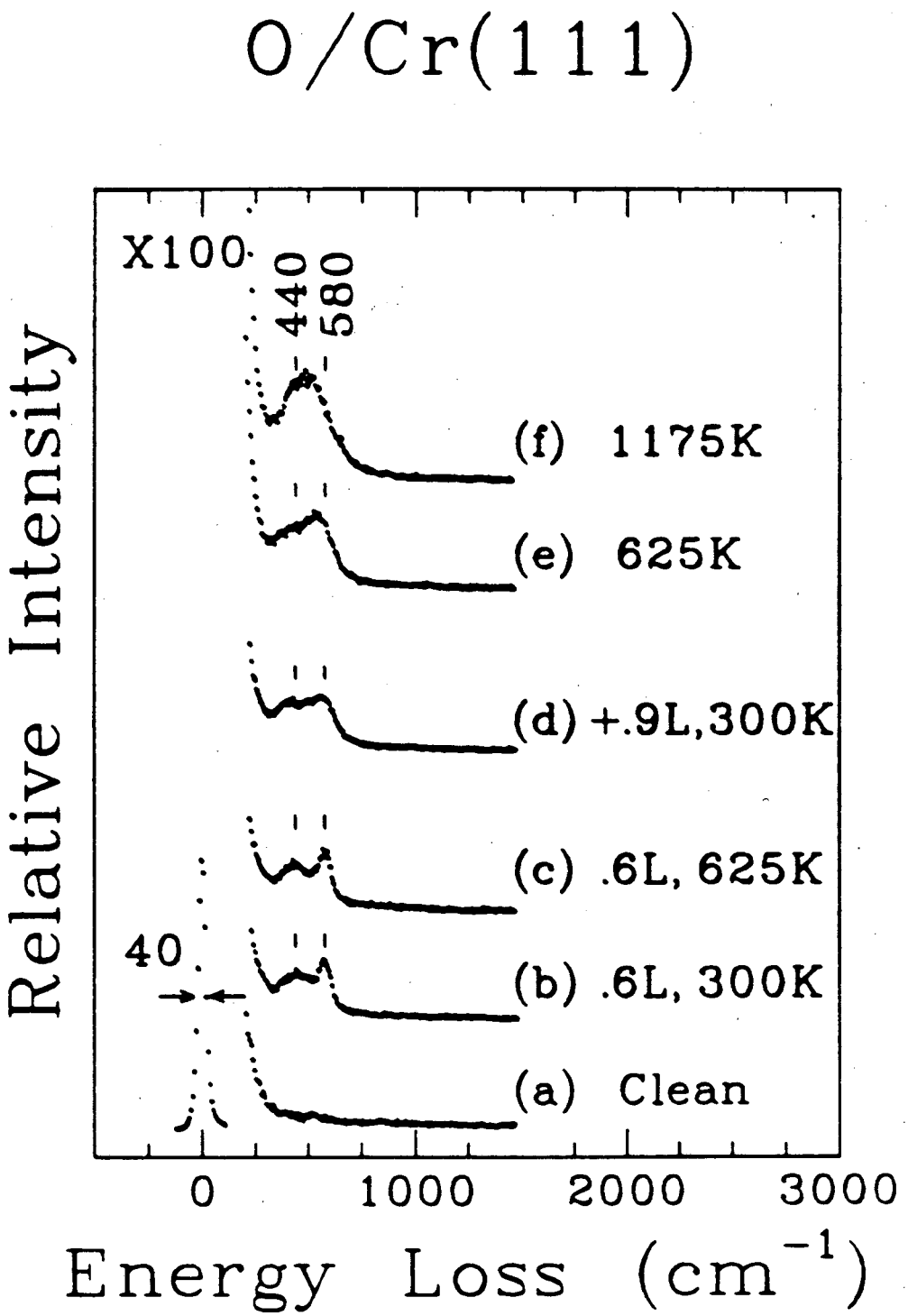

XBL 851-820

Figure 4

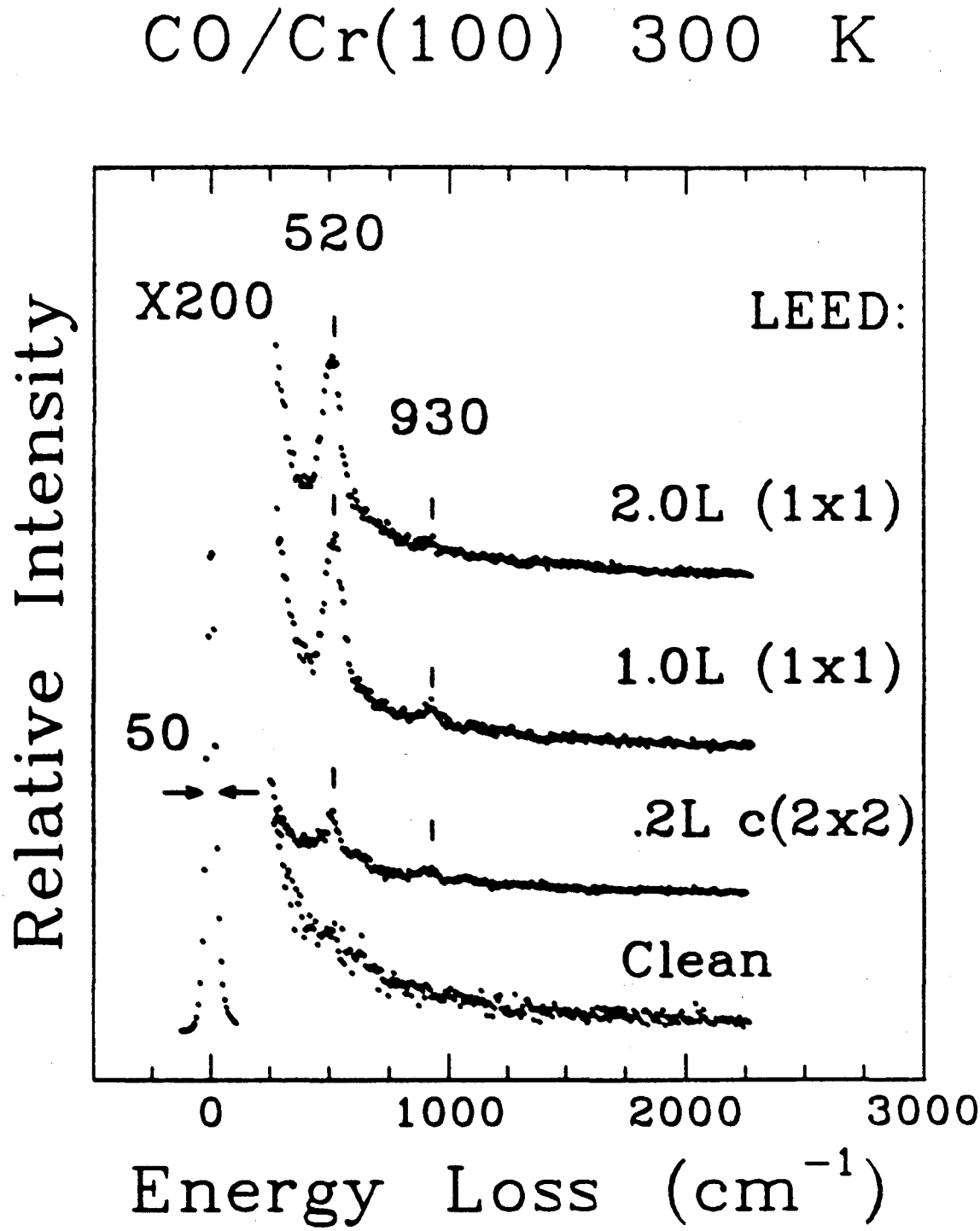

XBL 8412-5466

Figure 5

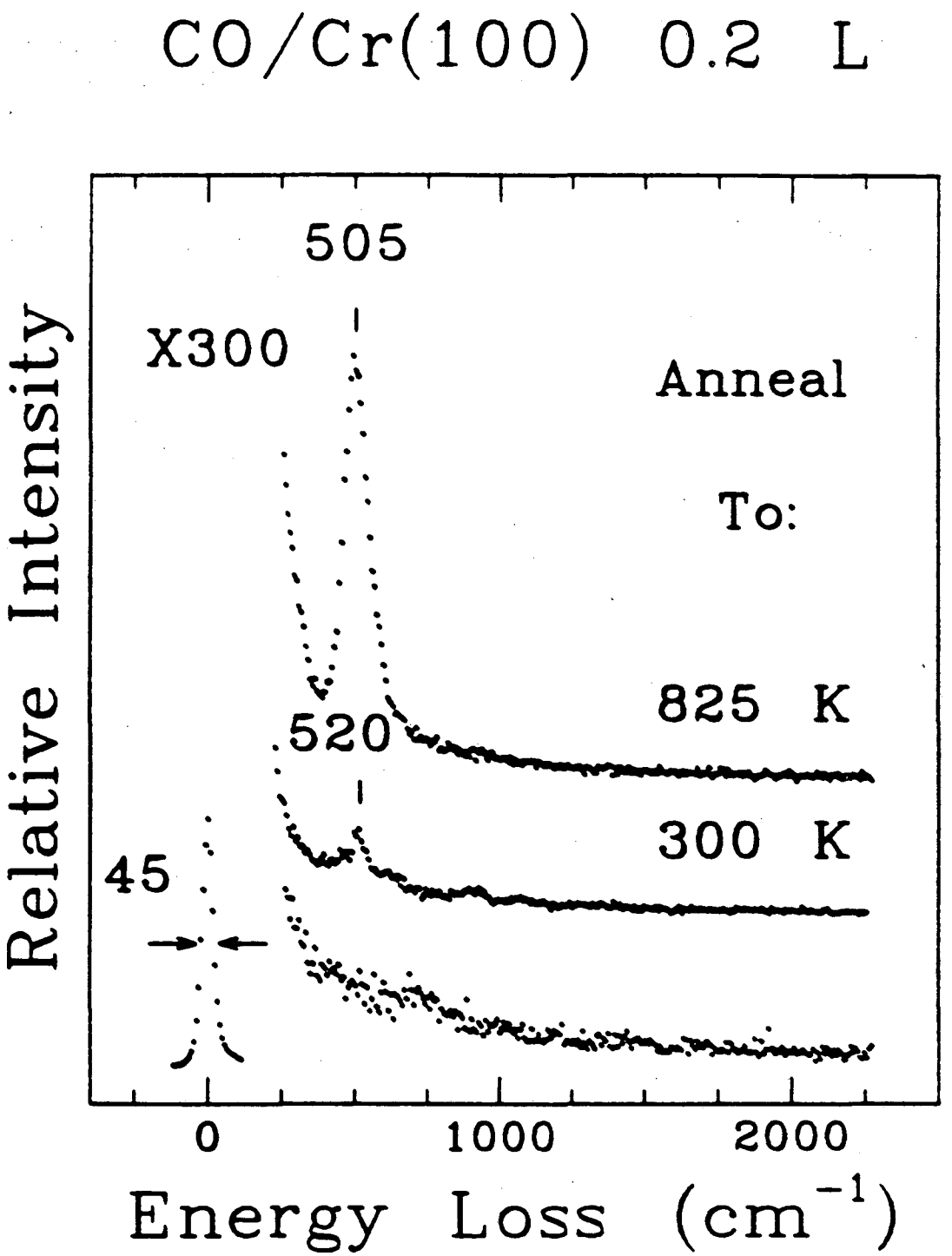

XBL 8412-5463

Figure 6

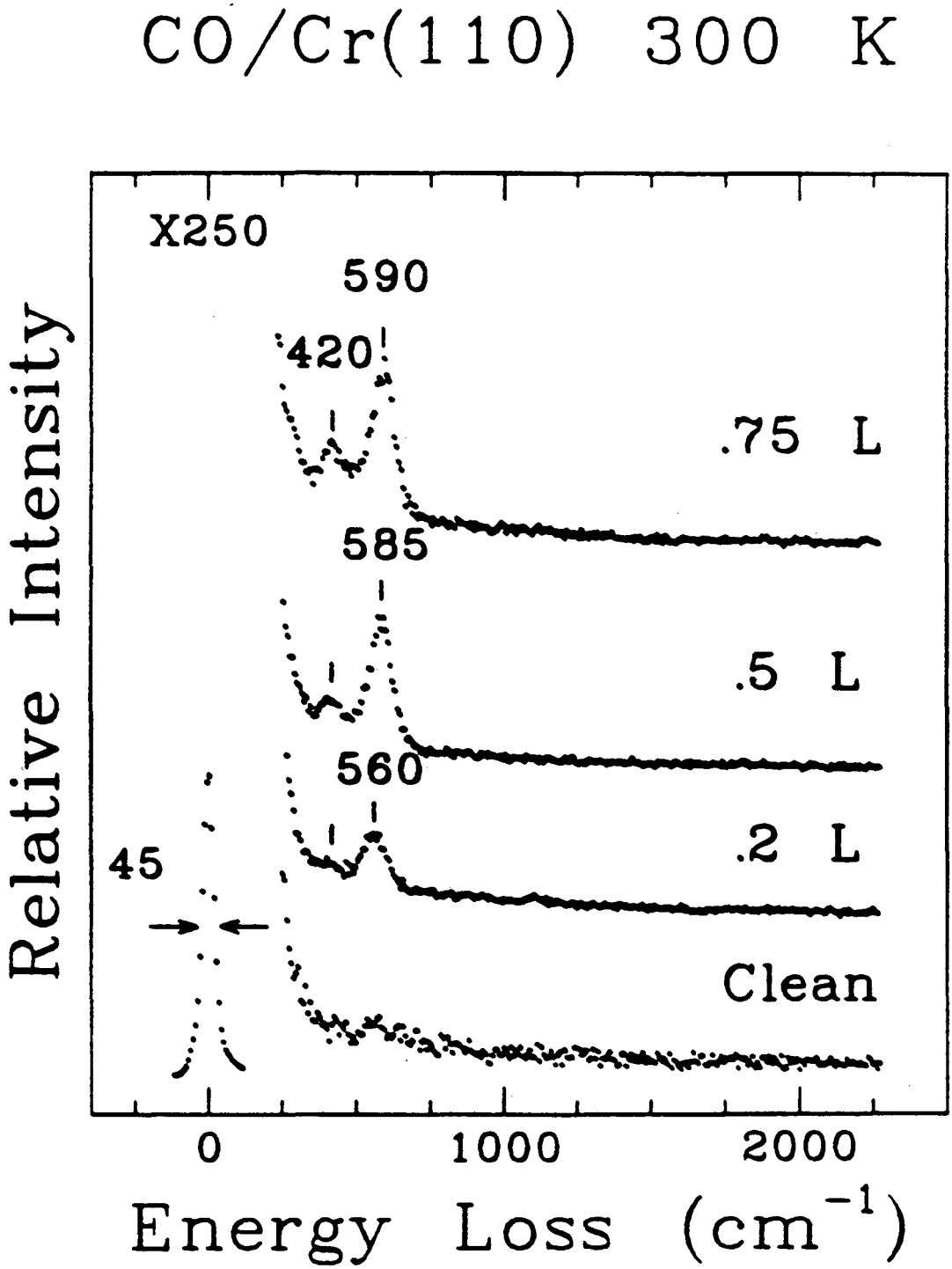

XBL 8412-5473

Figure 7

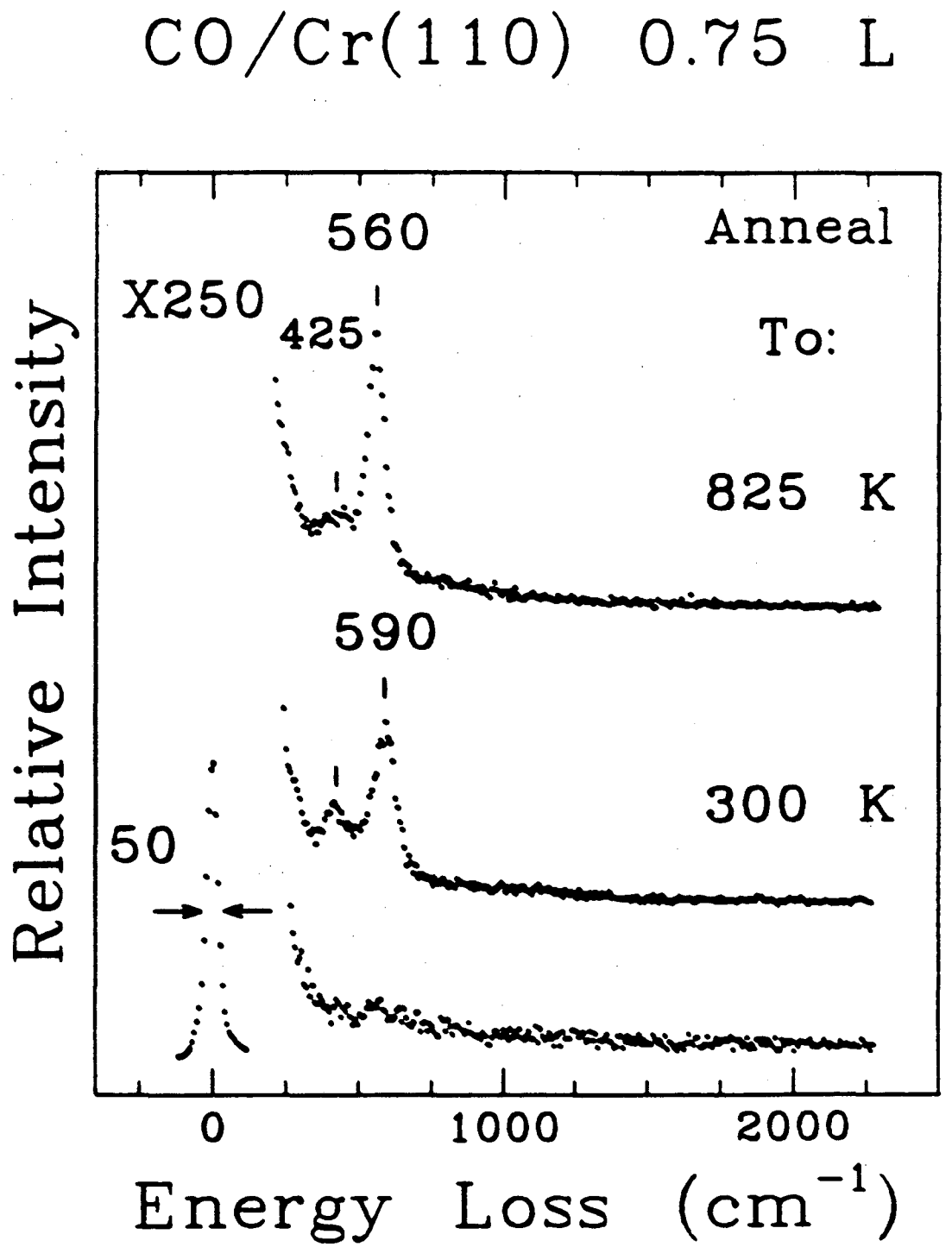

XBL 8412-5462

Figure 8

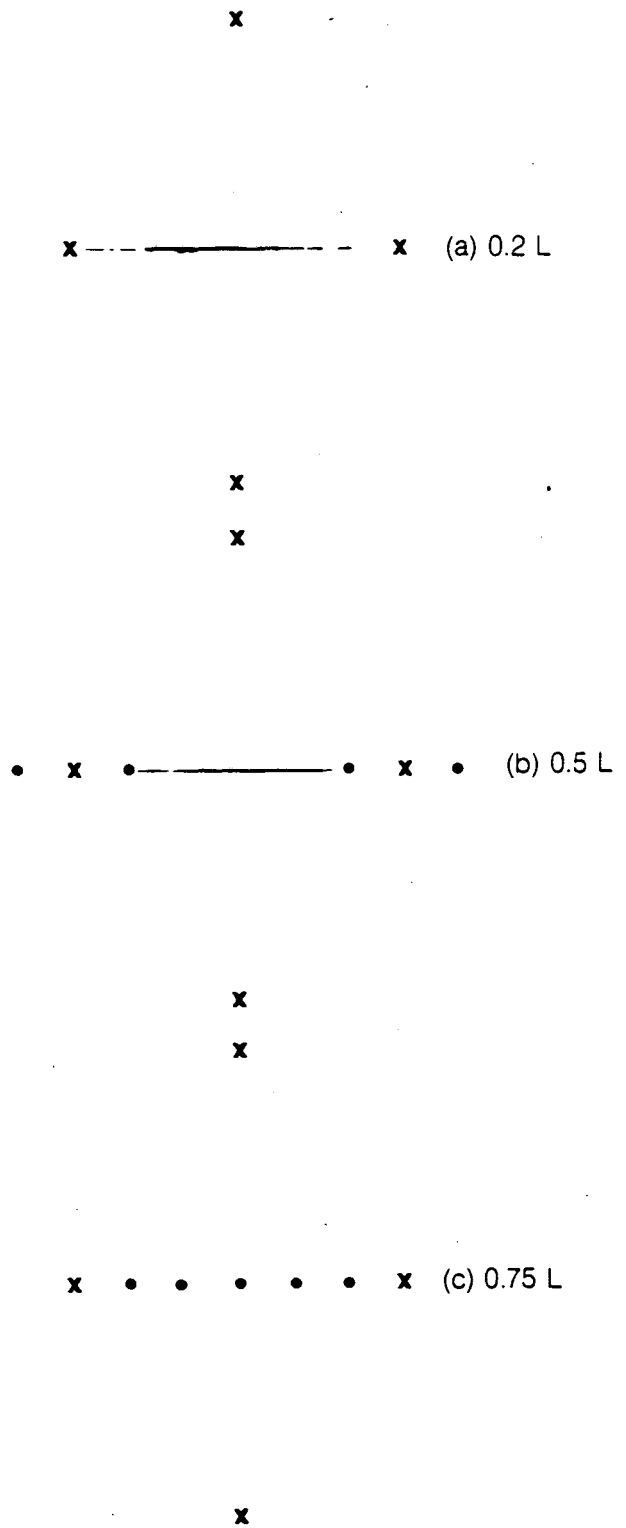

XBL 851-777

Figure 9

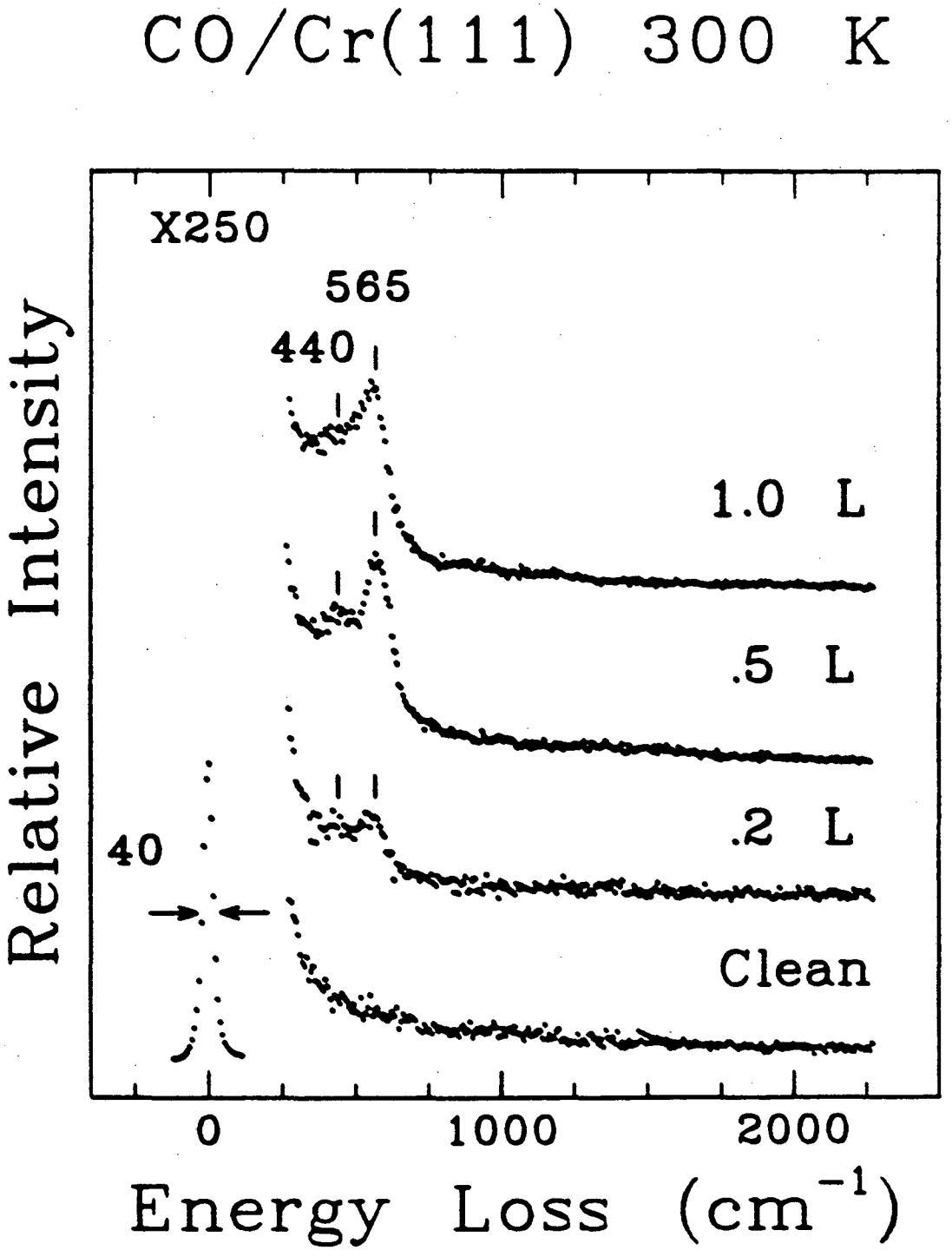

XBL 8412-5474

Figure 10

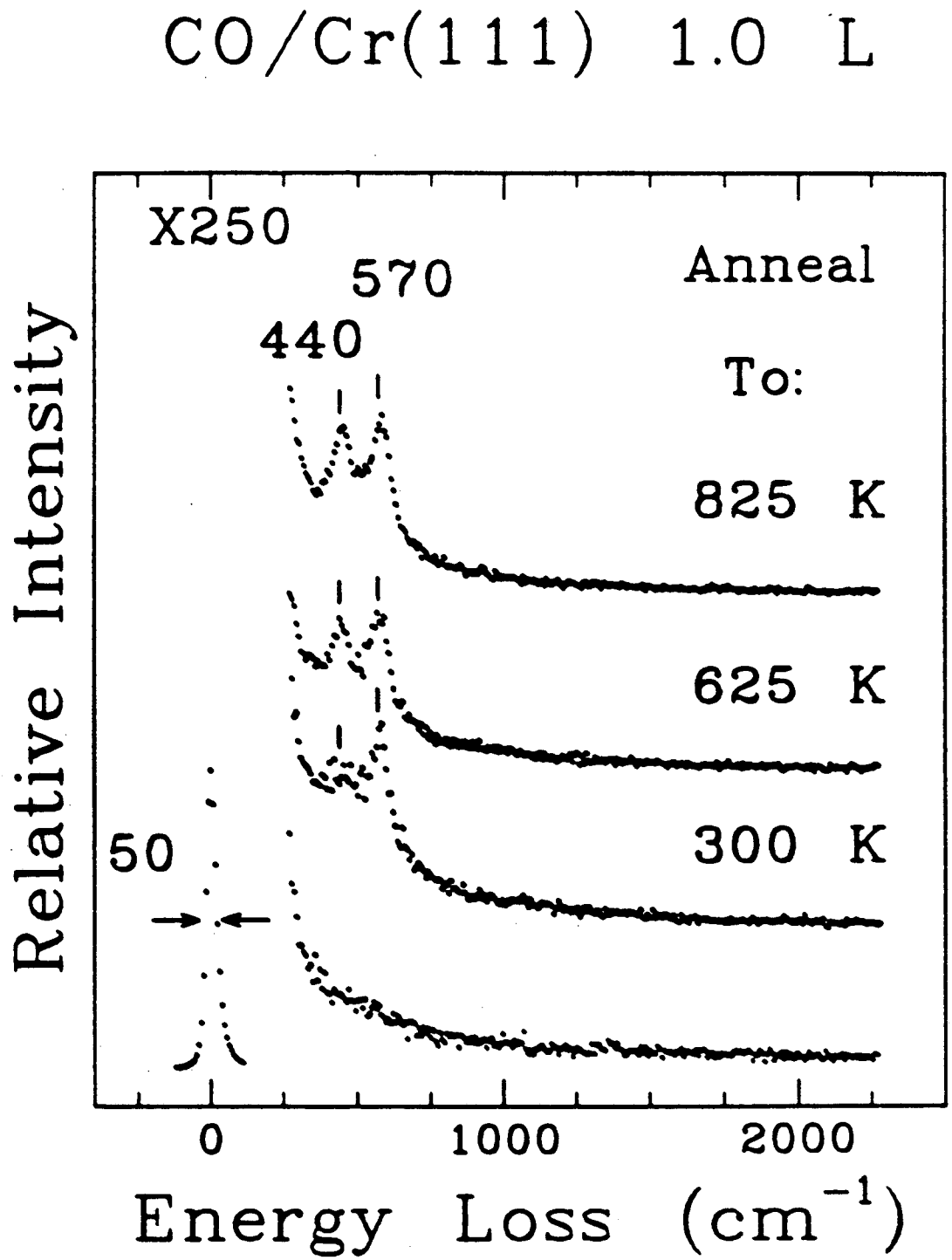

XBL 8412-5469

Figure 11

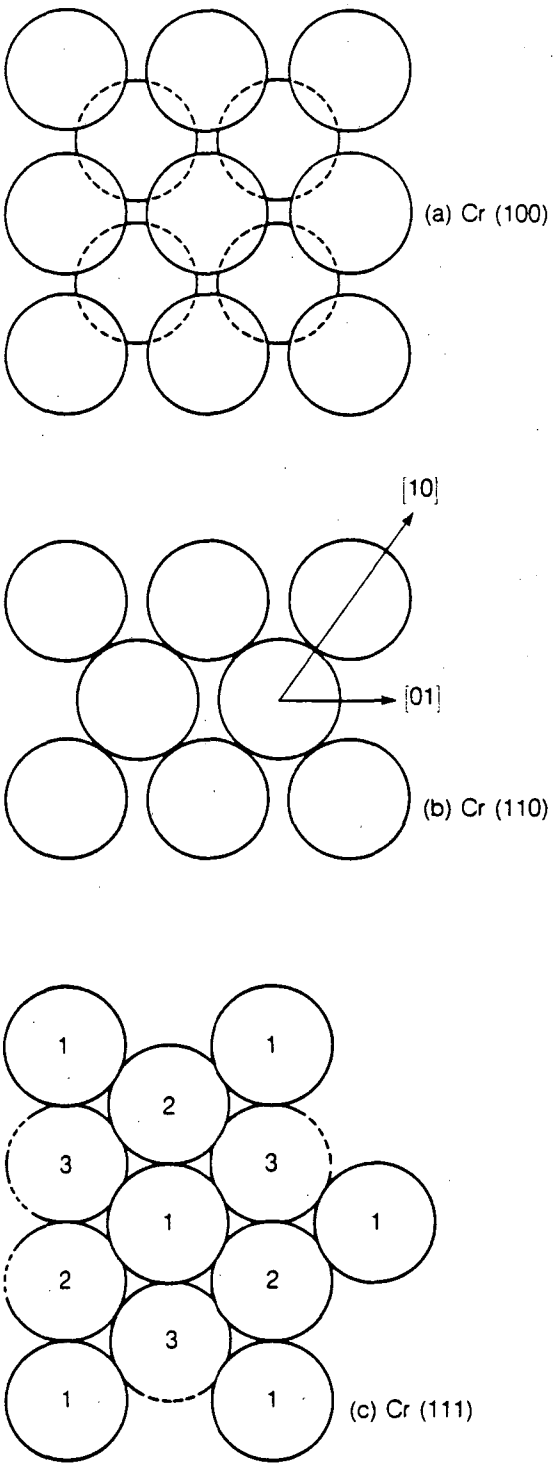

Figure 12

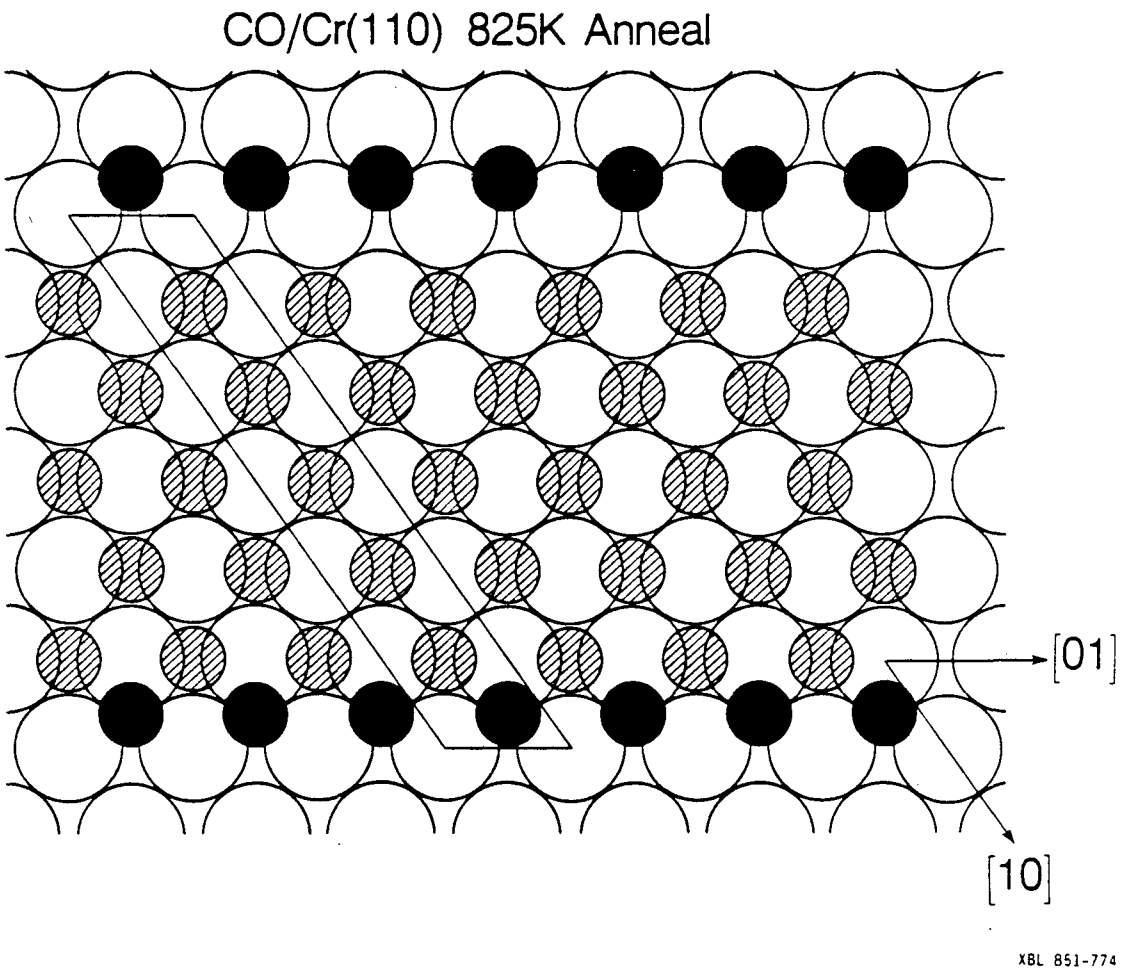

Figure 13

ACKNOWLEDGEMENTS

First, I wish to thank my family for the support and encouragement they have given me these past five years, and the twenty two years before then. My father Alfonso, my mother Nina, and my grandmother Tila provided me the environment that made this education possible. The strong friendship of Carolyn has helped me develop the emotional strength to complete this project.

My research director Dave Shirley gave me the independence I needed to develop critical thought. Danny Rosenblatt taught me to perform and design experiments. We went through the lows and highs together in the development of the EELS project. His patience and respect for me is deeply appreciated.

My other collaborators in the EELS project were Margaret Schulz, Lennie Klebanoff, and Ernesto Paparazzo. We participated together in the famous "Berkeley run" that produced over half of the data in my thesis. Margaret has been tremendously helpful in all of the experiments I performed. Her enthusiasm and motivation spurred me on.

The other members of the Shirley group have been my friends and coworkers. I'll always remember the few but enjoyable bike rides with Phil Heimann. I thank Dennis Trevor, Paul Kobrin, Chris Parks, Dennis Lindle, John Barton, Steve Robey, Janice Reutt, Charlie Bahr, Trish Ferrett, Novella Piancastelli, Lou Terminello, Alexis Schach, Laisheng Wang, and Tong Leung for friendship and helpful discussions.

The support staff at LBL have been very helpful to me. I wish to thank Wini Heppler, Barbara Moriguchi, Joe Katz, Don Malone, Ed

Vronin, John Anderson, Tom Gee, Charlie Taylor, Tony Moscarelli, Larry Ornelas, and Maria Garcia for performing essential services.

My friends at I House and in Berkeley have made this place special. They include Ernesto, Rodolfo, Mario, Senyo, Prabir, and especially Bal, who introduced me to the wonders of Indian cooking.

Finally, I thank AT&T Bell Laboratories for giving me a graduate fellowship and Lou Brus, my mentor at Bell Labs.

This report was done with support from the Department of Energy. Any conclusions or opinions expressed in this report represent solely those of the author(s) and not necessarily those of The Regents of the University of California, the Lawrence Berkeley Laboratory or the Department of Energy.

Reference to a company or product name does not imply approval or recommendation of the product by the University of California or the U.S. Department of Energy to the exclusion of others that may be suitable.

TECHNICAL INFORMATION DEPARTMENT
LAWRENCE BERKELEY LABORATORY
UNIVERSITY OF CALIFORNIA
BERKELEY, CALIFORNIA 94720